

©2015

Allison Marie Faig

ALL RIGHTS RESERVED

DESIGN, SYNTHESIS, AND CHARACTERIZATION OF BIOACTIVE
AMPHIPHILES FOR THERAPEUTIC APPLICATIONS

by

ALLISON MARIE FAIG

A dissertation submitted to the

Graduate School-New Brunswick

Rutgers, The State University of New Jersey

In partial fulfillment of the requirements

For the degree of

Doctor of Philosophy

Graduate Program in Chemistry and Chemical Biology

Written under the direction of

Dr. Kathryn E. Uhrich

And approved by

New Brunswick, New Jersey

OCTOBER, 2015

ABSTRACT OF THE DISSERTATION

Design, synthesis, and characterization of bioactive
amphiphiles for therapeutic applications

by ALLISON MARIE FAIG

Dissertation Director:

Kathryn E. Uhrich

Amphiphilic molecules are comprised of hydrophobic and hydrophilic domains. These molecules possess diverse chemical structures, which govern their physicochemical and biological properties, and these properties dictate amphiphiles' use in various applications. This dissertation focuses on the design, synthesis, and characterization of amphiphiles for biomedical applications.

Amphiphilic macromolecules (AMs), comprised of an acylated sugar backbone conjugated to a hydrophilic poly(ethylene glycol), were investigated as atherosclerosis treatments. Atherosclerosis is characterized by the accumulation and macrophage-mediated uptake of oxidized low-density lipoprotein (oxLDL). Previous studies indicate that AMs competitively inhibit oxLDL uptake through interacting with macrophage scavenger receptors, which contain hydrophobic and/or basic residues near their binding domains. Using knowledge of

scavenger receptor binding domains, two AM series – termed ether- and alkyl-AMs – were designed to elucidate whether hydrogen-bonding or hydrophobic-hydrophobic interactions more significantly influenced bioactivity, respectively. Upon successful synthesis of each series, AM physicochemical and biological properties were assessed. More hydrophobic AMs, possessing longer and/or alkyl-terminated (i.e., alkyl-AMs) acyl arms, exhibited enhanced oxLDL uptake inhibition and thus improved bioactivity. These studies demonstrated that hydrophobic interactions significantly influence anti-atherosclerotic activity.

Biscationic tartaric acid-based amphiphiles were also investigated for antimicrobial applications. Cationic amphiphiles exhibit unique membrane-disrupting bactericidal mechanisms via a combination of electrostatic and hydrophobic-hydrophobic interactions. This work explored the specific impact of charge location on cationic amphiphiles' antimicrobial and membrane activity. Two series of analogous cationic amphiphiles were synthesized, termed gemini-like and bola-like, which differed only in their charge location. After successful synthesis, antimicrobial activity was assessed and lead compounds identified. Bola-like amphiphiles exhibited preferential activity against gram-positive bacteria, while gemini-like amphiphiles were more active against gram-negative bacteria. Biophysical experiments indicated that the lead gemini-like amphiphile interacted with model membranes via electrostatic interactions, whereas the lead bola-like amphiphile relied on a combination of electrostatic and hydrophobic interactions. These studies demonstrate the significant influence of charge location on cationic amphiphile antimicrobial and membrane activity.

PREFACE

*“So Lyra and her daemon turned away from the world they were born in, and
looked toward the sun, and walked into the sky.”*

-Philip Pullman

DEDICATION

This work is dedicated to my parents, Diane and Stephen Faig, my siblings, Jonathan and Stephen, and especially my rock, Brent Bouma, who has continuously supported my endeavors over the past seven years.

ACKNOWLEDGEMENTS

I am extremely thankful for the mentors, teachers, family, and friends who have guided me throughout this journey and thereby contributed to this dissertation. Your insight, advice, and company have made this work possible.

With special thanks to:

Kathryn Uhrich, Evan Mintzer, Larry Romsted, Ralf Warmuth, Prabhas Moghe, Bill Welsh, Michael Chikindas, Susan Skelly, Joel Freundlich, Stuart Palmer, Shan Wan, Jerry Kukor, Brent Ruben, Barbara Bender, Susan Lawrence, Kim Manning, Michelle Morano, Roselin Rosario-Meléndez, Dawanne Poree, Li Gu, Sabrina Snyder, Latrisha Petersen, Adam York, Timothy Arthur, Connie Yu, Nick Stebbins, Joanna Zhang, Jennifer Chan, Jonathan Faig, Alysha Moretti, Stephan Bien-Aime, Ning Wang, Dania Davie, Richa Rana, Kervin Smith, all other past and present Uhrich and Moghe group members, Stern College for Women, Bryan Langowski, Kristina Wetter, Karen Fowler, Allison Larkin, Kristin Render, S. Bruce King, Patricia Dos Santos, Julie Reisz, Jenna DuMond, Grant McAllister, Heiko Wiggers, Alyssa Howards, all other Wake Forest University Chemistry Department and German Department faculty, and all past and present Chemistry Graduate Student Association members. I would also like to thank the National Institutes of Health, U.S. Department of Education, McCoy Family Fellowship, and Rutgers University for financial support. For those not mentioned, please know that your help has not gone unnoticed.

TABLE OF CONTENTS

ABSTRACT OF THE DISSERTATION	ii
PREFACE	iv
DEDICATION	v
ACKNOWLEDGEMENTS	vi
TABLE OF CONTENTS	vii
LIST OF TABLES	xii
LIST OF ILLUSTRATIONS.....	xiii
LIST OF ABBREVIATIONS	xvii
1. INTRODUCTION	1
1.1. Amphiphilic Molecules	1
1.2. Amphiphile Classifications	2
1.3. Amphiphile Applications	5
1.4. Specific Projects	7
1.4.1. Amphiphilic Macromolecules for Atherosclerosis Treatment: Impact of Hydrophobic Chain Composition.....	8
1.4.2. Biscationic Tartaric Acid-Based Amphiphiles: Charge Location Impacts Antimicrobial Activity.....	9
1.5. Summary.....	11
1.6. References.....	11

2. AMPHIPHILIC MACROMOLECULES FOR ATHEROSCLEROSIS

TREATMENT: IMPACT OF HYDROPHOBIC CHAIN COMPOSITION 13

2.1. Introduction 13

2.2. Results and Discussion 18

2.2.1. Synthesis..... 18

2.2.2. Physicochemical Characterization 23

2.2.3. Biological Activity 26

2.3. Conclusion 36

2.4. Experimental 37

2.4.1. Materials..... 37

2.4.2. Characterization 38

2.4.3. Synthesis of Ether-AMs..... 39

2.4.4. Synthesis of Alkyl-AMs..... 45

2.4.5. Critical Micelle Concentration Measurements..... 48

2.4.6. Dynamic Light Scattering Measurements 49

2.4.7. Cell Culture 49

2.4.8. Cell Viability Studies..... 50

2.4.9. OxLDL Uptake by Macrophages 50

2.4.10. Statistical Analysis 51

2.5. References..... 52

3. BISCATIONIC TARTARIC ACID-BASED AMPHIPHILES: CHARGE

LOCATION IMPACTS ANTIMICROBIAL ACTIVITY 57

3.1. Introduction 57

3.2. Results and Discussion	61
3.2.1. Synthesis and Characterization	61
3.2.2. Antimicrobial Activity	66
3.2.3. Biophysical Assessment	72
3.3. Conclusion	81
3.4. Experimental	82
3.4.1. Materials.....	83
3.4.2. Characterization	83
3.4.3. Synthesis of Bola-like Amphiphiles	84
3.4.4. Synthesis of Gemini-like Amphiphiles	88
3.4.5. Antimicrobial Screening	92
3.4.6. Broth Microdilution Assay.....	93
3.4.7. Kinetic Kill Assays	94
3.4.8. Langmuir Monolayer Studies	94
3.4.9. Isothermal Titration Calorimetry	95
3.5. References.....	96
4. APPENDIX: MISCELLANEOUS PROJECTS	100
4.1. Quaternary-Ammonium Containing Amphiphiles for Intracranial Applications	100
4.1.1. Results and Discussion.....	102
4.1.2. Experimental	107
4.1.3. References.....	109
4.2. Cationic Amphiphilic Polymers for Antimicrobial Applications....	110

4.2.1. Results and Discussion.....	112
4.2.2. Experimental	116
4.2.3. References.....	120
4.3. Screening Cationic Amphiphile Activity Against Clinically Relevant Pathogens.....	121
4.3.1. Results and Discussion.....	122
4.3.2. References.....	124
4.4. Investigation into Antimicrobial Amphiphile Critical Micelle Concentrations.....	124
4.4.1. Results and Discussion.....	125
4.4.2. Experimental	126
4.4.3. References.....	127
4.5. Optimized Purification of NHS-Activated Hydrophobe	127
4.5.1. Results and Discussion.....	128
4.5.2. Experimental	129
4.5.3. References.....	130
4.6. Synthesis of Di-<i>tert</i>-Butyl 5-Aminoisophthalate	131
4.6.1. Results and Discussion.....	132
4.6.2. Experimental	134
4.6.3. References.....	136
4.7. Carboxylic Acid Protection of Mucic Acid.....	136
4.7.1. Results and Discussion.....	137
4.7.2. Experimental	140

4.7.3. References.....	141
4.8. General Materials and Methods.....	142
4.8.1. References.....	144
5. FUTURE WORK SUGGESTIONS.....	145
5.1. References.....	148
6. COPYRIGHT PERMISSION	149
6.1. Biomacromolecules.....	149

LIST OF TABLES

Table 2.1. Physicochemical properties of ether- (2.5) and alkyl-AMs (2.7), with 2000 M _w compounds on the left and 5000 M _w compounds on the right.....	24
Table 3.1. MICs and MBCs (μM) of amphiphiles ^a	70
Table 3.2. Time killing (h) of selected strains by amphiphiles ^a	72
Table 4.1. Bola- and gemini-like amphiphiles MIC values (μg/mL) against various bacteria types; Assays with Vero cells demonstrate amphiphile cytocompatibility; ESKAPE pathogens are underlined; MICs highlighted in green and yellow depict very potent and potent treatments, respectively.....	123

LIST OF ILLUSTRATIONS

Figure 1.1. Schematic of an amphiphile with a hydrophilic head (blue) and hydrophobic tail (red) forming a micelle	1
Figure 1.2. Depiction of different amphiphile classes, including conventional amphiphiles (A), gemini amphiphiles (B), bola amphiphiles (C), and polymer amphiphiles (D)	3
Figure 1.3. Common amphiphile uses within the biomedical field, including drug encapsulation and surface modification	6
Figure 1.4. Depiction of AMs' ability to inhibit scavenger receptor-mediated oxLDL uptake	9
Figure 1.5. Depiction of bola-like (left) and gemini-like (right) amphiphiles' potential interactions with gram-positive and gram-negative bacteria, respectively	10
Figure 2.1. Schematic depicting the atherosclerotic cascade; this graphic was adapted from previous Rutgers theses ^{10,11}	14
Figure 2.2. Chemical structure of ether- and alkyl-AMs.....	18
Figure 2.3. Synthetic scheme for ether-AMs; The different alkyl arm lengths investigated are denoted as a, b, and c in order of increasing length; The PEG M_w used is denoted numerically in kiloDaltons as a subscript with x = 45 yielding 2 kDa PEG and x = 113 yielding 5 kDa PEG (e.g., 2.5a₂ signifies an ether-AM containing the shortest alkyl chain length and a 2 kDa PEG tail)....	19
Figure 2.4. ¹ H NMR spectra for 2.5a₂ ether-AM synthesis as an example: 8-methoxyoctanoic acid 2.2a (A), 2,3-bis(8-methoxyoctanoyl) DBT 2.3a (B), 2,3-bis(8-methoxyoctanoyl) TA 2.4a (C), and ether-AM 2.5a₂ (D).....	21
Figure 2.5. Synthetic scheme for alkyl AMs; The different alkyl arm lengths investigated are denoted as a, b, and c in order of increasing length; The PEG M_w used is denoted numerically in kiloDaltons as a subscript with x = 45 yielding 2 kDa PEG and x = 113 yielding 5 kDa PEG (e.g., 2.7a₂ signifies an alkyl-AM containing the shortest alkyl chain length and a 2 kDa PEG tail).....	23

Figure 2.6. CMC curves of representative ether- (2.5c₅) and alkyl- (2.7c₅) AMs, in which the inflection point of the curves corresponds to AM CMC values; Alkyl-AMs continuously exhibited lower CMC values than analogous ether-AMs	25
Figure 2.7. Cell viability screening results for varying concentrations of 5000 M _w (A) and 2000 M _w (B) AMs; AMs with different alkyl arm lengths are grouped between the dashed lines; The cell viability cut-off of 70 % is denoted as a red line on the graph; Compound 2.5a₂ at 10 ⁻⁴ M was included in oxLDL uptake studies although its viability was not assessed, as it was non-toxic at 10 ⁻³ M	28
Figure 2.8. Effect of administering varying concentrations of 5000 M _w (A) and 2000 M _w (B) ether-AMs (dark grey) and alkyl-AM analogs (light grey) on % oxLDL uptake in HMDMs; AMs of specific alkyl lengths are grouped between the dash lines, and the AM treatments not investigated due to cytotoxicity are indicated as text on the graph; Significant deviations from the oxLDL positive control (black) are denoted by asterisks on the graph	31
Figure 2.9. Percent of HMDMs positive for oxLDL after incubation with varying concentrations of 5000 M _w (A) and 2000 M _w (B) ether-AMs (dark grey) and alkyl-AM analogs (light grey); AMs of specific alkyl lengths are grouped between the dash lines, and the AM treatments not investigated due to cytotoxicity are indicated as text on the graph; Significant deviations from the oxLDL positive control (black) are denoted by asterisks on the graph	33
Figure 2.10. Dose response of most efficacious AM treatments.....	35
Figure 3.1. Representation of different amphiphile architectures investigated for antimicrobial applications; Cationic groups are depicted in blue while hydrophobic regions are depicted in red.....	59
Figure 3.2. Chemical structures and representations of bola-like (left) and gemini-like (right) cationic amphiphiles.....	60
Figure 3.3. Synthetic scheme for bola-like amphiphiles; Final amphiphile structures are denoted as B7 , B9 , or B11 depending on the number of methylenes within their hydrophobic domain	61
Figure 3.4. Synthetic scheme for gemini-like amphiphiles; Final amphiphile structures are denoted as G7 , G9 , or G11 depending on the number of methylenes within their hydrophobic domain	63

Figure 3.5. FT-IR spectra showing the carbonyl region for B11 synthesis as an example: 3.4c (A) and B11 (3.5c , B)	64
Figure 3.6. ¹ H NMR spectra for G11 synthesis as an example: 3.8c (A) and G11 3.9c (B)	66
Figure 3.7. Antimicrobial screening of bola-like amphiphiles B7 (top), B9 (middle), and B11 (bottom) against <i>E. coli</i> (left) and <i>S. aureus</i> (right) as determined by a disk diffusion assay; Zones of inhibition (i.e., no bacterial growth) correspond to antimicrobial activity	67
Figure 3.8. Antimicrobial screening of gemini-like amphiphiles G7 (top), G9 (middle), and G11 (bottom) against <i>E. coli</i> (left) and <i>S. aureus</i> (right) as determined by a disk diffusion assay; Zones of inhibition (i.e., no bacterial growth) correspond to antimicrobial activity	68
Figure 3.9. Raw Langmuir monolayer data depicting the surface pressure increase upon injection of B11 (A) or G7 (B) into the aqueous subphase of a trough containing DOPC (black) or DOPG (red) monolayers at initial surface pressures of approximately 25 mN/m.....	74
Figure 3.10. Interaction of B11 (A, triangles) and G7 (B, diamonds) with DOPG (black) or DOPC:DOPG (1:1 mole ratio, light grey) lipid monolayers indicated by change in surface pressure as a function of initial surface pressure.....	76
Figure 3.11. ITC traces obtained from titrating DOPC into B11 (A) and G7 (B); Upper curves depict heat flow as a function of time, whereas lower curves depict the corresponding integrated area of each peak as a function of injection number; Heat flow was negligible for both titrations.....	78
Figure 3.12. ITC traces obtained from titrating DOPC:DOPG (1:1 mole ratio) into B11 (A) and G7 (B); Upper curves depict heat flow as a function of time, whereas lower curves depict the corresponding integrated area of each peak as a function of injection number.....	80
Figure 4.1. Depiction of QA-containing AM NP formulation for intracranial applications	102
Figure 4.2. Synthetic methods investigated to conjugate choline chloride to M12P5	103
Figure 4.3. Proposed synthesis of QA-M12P5 via a QA-M12 intermediate.....	104
Figure 4.4. ¹ H NMR spectra of M12 (A), Boc-M12 (B), and Amine-M12 (C).....	105
Figure 4.5. MS of reaction after 48 h, indicating the presence of Boc-M12 methyl ester, QA-M12 product, and degradation product.....	106
Figure 4.6. Lead antimicrobial amphiphiles, B11 (left) and G7 (right), identified in Chapter 3.....	111

Figure 4.7. Synthetic scheme investigated to generate a B11 -based polyamide via a PCP-activated ester intermediate	113
Figure 4.8. ¹ H NMR spectra of 2,3-bis(12-Bocaminododecanoyl) -DBT (A), -TA (B), and -PCP (C) .	114
Figure 4.9. Synthetic scheme for lipase-catalyzed synthesis of B11 -based polyamide	115
Figure 4.10. ¹ H NMR spectrum of lipase-mediated polymerization product	116
Figure 4.11. Surface pressure increase as a function of B11 concentration; The inflection point corresponds to B11 's CMC	126
Figure 4.12. Synthetic scheme for NHS-M12	128
Figure 4.13. ¹ H NMR spectra of product obtained from conventional (A) and optimized (B) purification methods; Impurities are denoted by red circles	129
Figure 4.14. Chemical structure of 2cbM	131
Figure 4.15. Synthetic scheme for di- <i>tert</i> -butyl 5-aminoisophthalate.....	133
Figure 4.16. ¹ H NMR spectra of di- <i>tert</i> -butyl 5-nitroisophthalate (A) and di- <i>tert</i> -butyl 5-aminoisophthalate (B).....	134
Figure 4.17. Chemical structure of conventional mucic acid-based AM (M12P5).....	137
Figure 4.18. Reaction conditions attempted to generate <i>tert</i> -butyl (left) or benzyl (right) protected mucic acid; The reaction conditions attempted did not result in product formation.....	139
Figure 4.19. Meso DBT backbone modified with dendrimer branch points to enable conjugation to four hydrophobic arms	140
Figure 5.1. Chemical structures of two potential gemini-like amphiphiles possessing shorter aliphatic arms.....	146
Figure 5.2. Depiction of different amine moieties that can be investigated, using G7 's amphiphile structure as an example; Counterions (not shown) will depend on the synthetic methodologies used to synthesize the final structure	147

LIST OF ABBREVIATIONS

[(M+2)/2]	Mass plus two, divided by two	Ar	Aromatic, Argon
		BBB	Blood brain barrier
[M-1]	Mass minus one	BnBr	Benzyl bromide
[M+1]	Mass plus one	BnOH	Benzyl alcohol
[M+23]	Mass plus sodium	Boc	Tert-butyloxycarbonyl
%	Percent	b	Block
°	Degrees	br	Broad
°C	Degrees Celsius	C	Carbon
±	Plus or minus	C=O	Carbonyl
~	Approximately	CD36	Scavenger receptor B
\$	Dollars	CD ₃ OD	Deuterated methanol
¹³ C	Carbon (when describing NMR)	CDCl ₃	Deuterated chloroform
		CFU	Colony forming units
¹ H	Proton (when describing NMR)	CHCl ₃	Chloroform
		cm ⁻¹	Wavenumber units
Å	Angstrom	CMC	Critical micelle concentration
ACN	Acetonitrile		
AET	Aminoethyltartrate	d	Doublet, day
AM	Amphiphilic macromolecule	Da	Dalton
		DBT	Dibenzyl tartrate
AMP	Antimicrobial peptide		

DCC	Dicyclohexyl carbodiimide	E	Times ten raised to the power of
DCM	Dichloromethane	EDCI	1-ethyl-3-(3-dimethyl aminopropyl)carbo diimide
dd	Doublet of doublets		
Dio	3,3'-dioctadecyl oxacarbocyanine	eq	Equivalents
DLS	Dynamic light scattering	ESI	Electrospray ionization
		ET	Diethyl tartrate
DMAP	4-dimethylamino pyridine	FBS	Fetal bovine serum
		FT-IR	Fourier transform infrared spectroscopy
DMF	Dimethylformamide		
DMSO- <i>d</i> ₆	Deuterated dimethyl sulfoxide	<i>g</i> <i>g</i>	<i>g</i> -force Gram
DOPC	1,2-dioleoyl-sn-glycero- 3-phosphocholine	G- G+	Gram-negative Gram-positive
DOPG	1,2-dioleoyl-sn-glycero- 3-phospho-(1'-rac- glycerol)	GPC h	Gel permeation chromatography Hour
DPTS	4-(dimethylamino) pyridinium 4-toluene sulfonate	H H ₂ H ₂ O	Proton Hydrogen gas Water
DSC	Differential scanning calorimetry	H ₂ SO ₄ HCl	Sulfuric Acid Hydrochloric acid

HEPES	4-(2-hydroxyethyl)-1-piperazineethane sulfonic acid	LUV	Large unilamellar vesicle
		M	Molar
HMDM	Human monocyte-derived macrophage	m	Multiplet
		M-CSF	Macrophage colony-stimulating factor
HPLC	High pressure liquid chromatography	<i>m/z</i>	Mass-to-charge ratio
I	Intensity	MBC	Minimum bactericidal concentration
ICAD	Intracranial artery disease	MeI	Methyl Iodide
ITC	Isothermal titration calorimetry	MeOH	Methanol
		MFI	Mean fluorescence intensity
K ₂ CO ₃	Potassium carbonate		
KBr	Potassium bromide	mg	Milligram
kcal	Kilocalories	MgSO ₄	Magnesium sulfate
kDa	Kilodalton	MHz	Megahertz
kg	Kilogram	MIC	Minimum inhibitory concentration
KHSO ₄	Potassium bisulfite		
KOH	Potassium hydroxide	min	Minute
L	Liter	MIP	Maximum insertion pressure
LDL	Low-density lipoprotein		
LPS	Lipopolysaccharide	mL	Milliliter
		mm	Millimeter

mM	Millimolar	PBMC	Peripheral blood
mmol	Millimole		mononuclear cell
mN/m	Millinewton per meter	PBS	Phosphate buffered
mPEG-NH ₂	Monomethoxy-		saline
	poly(ethylene glycol)-	PCP	Pentachlorophenol
	amine	Pd/C	Palladium on carbon
MS	Mass spectrometry	PDI	Polydispersity index
M _w	Weight averaged	PEG	Poly(ethylene glycol)
	molecular weight	PLA	Poly(lactic acid)
N	Nitrogen	ppm	Parts per million
N ₂	Nitrogen gas	PPO	Poly(propylene oxide)
Na ₂ CO ₃	Sodium carbonate	PT	N,N-dipropyl tartramide
NaHCO ₃	Sodium bicarbonate	PTFE	Polytetrafluoroethylene
ng	Nanogram	QA	Quaternary ammonium
NHS	N-hydroxysuccinimide	quin	Quintet
nm	Nanometer	rpm	Revolutions per minute
NMR	Nuclear magnetic	RPMI	Roswell Park Memorial
	resonance		Institute
NP	Nanoparticle	RT	Room temperature
O	Oxygen	s	Singlet, second
oxLDL	Oxidized low-density	SDS	Sodium dodecyl sulfate
	lipoprotein	S _N 2	Nucleophilic
			substitution 2

SOCl ₂	Thionyl chloride	μM	Micromolar
SRA	Scavenger receptor A	μm	Micrometer
t	Triplet		
t-BuOH	Tert-butanol		
TA	Tartaric acid		
TEA	Triethylamine		
TFA	Trifluoroacetic acid		
TLC	Thin layer chromatography		
T _m	Melting temperature		
TMS	trimethylsilane		
TSA	Tryptic Soy Agar		
TSB	Tryptic Soy Broth		
USD	United States dollars		
UV-Vis	Ultraviolet-visible		
vs.	versus		
w/w	Weight by weight		
wt %	Weight percent		
ZnCl ₂	Zinc Chloride		
δ	Chemical shift		
μcal	Microcalories		
μg	Microgram		
μL	Microliter		

1. INTRODUCTION

1.1. Amphiphilic Molecules

Amphiphilic molecules are compounds comprised of hydrophobic and hydrophilic domains.¹⁻⁵ As amphiphilic molecules are generally surface-active agents, the term amphiphile is often used interchangeably with surfactant.⁴⁻⁶ Due to amphiphiles' tendency to accumulate at an interface, these compounds can reduce the surface tension of a liquid or the interfacial tension between two liquids.¹⁻⁵ Furthermore, given their hydrophilic and hydrophobic properties, amphiphiles can self-assemble into various aggregate structures.^{1,5,6}

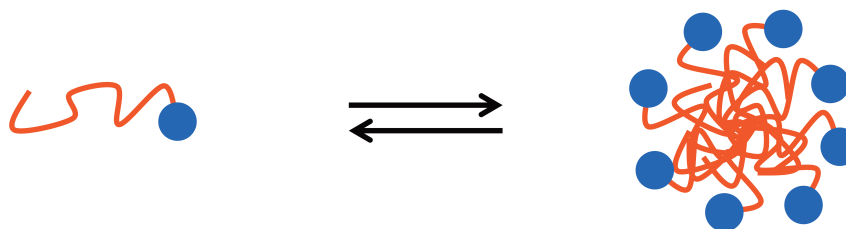


Figure 1.1. Schematic of an amphiphile with a hydrophilic head (blue) and hydrophobic tail (red) forming a micelle

In the presence of water, for instance, amphiphiles may self-assemble into micelles or bilayer structures in which the hydrophobic domains are shielded from water by hydrophilic domains (Figure 1.1).^{1,4,6,7} This assembly process only

occurs above a critical micelle concentration (CMC) and is driven by the hydrophobic effect, in which the displacement of ordered water molecules surrounding the amphiphile hydrophobic domain increases the system's entropy.^{1,2,4,6} Both the CMC value and the type of aggregate structure formed (e.g., spherical micelle, cylindrical micelle, bilayer) are dictated by various parameters, including temperature, the presence of additives (e.g., salts, alcohols), and the amphiphile chemical structure.^{1,4,6} Sodium dodecyl sulfate (SDS, Figure 1.2A) is an example of a conventional amphiphile that forms spherical micelles in water (20-25 °C) and has a CMC value of approximately 8-10 mM.^{2,8} While conventional amphiphiles possess a hydrophilic headgroup attached to a hydrophobic tail,¹ a variety of different amphiphiles exist which can be classified based on their different features.

1.2. Amphiphile Classifications

Amphiphiles are either naturally or synthetically derived. Amphiphilic peptides and phospholipids are naturally occurring compounds capable of self-assembling into biologically relevant structures, including the cell membrane.^{7,9} In contrast, many commercial amphiphiles, including SDS, are produced through chemical synthesis. Given the broad array of possible amphiphile structures, amphiphiles can be classified according to various features, including their type of polar headgroup, number and connection of hydrophobic domains, and molecular weight (Figure 1.2).

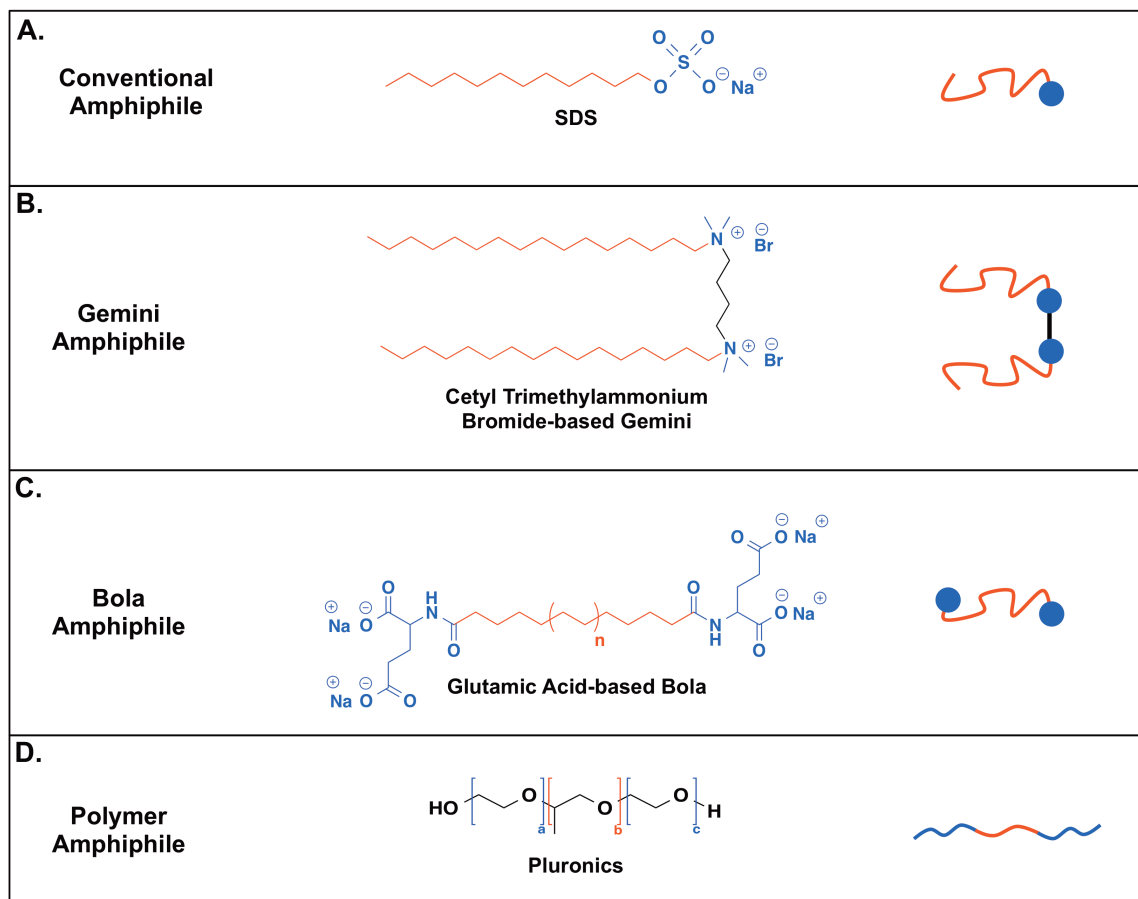


Figure 1.2. Depiction of different amphiphile classes, including conventional amphiphiles (A), gemini amphiphiles (B), bola amphiphiles (C), and polymer amphiphiles (D)

Amphiphiles are most commonly classified as ionic or nonionic.²⁻⁶ Ionic amphiphiles contain one or more charged hydrophilic moieties and therefore may be anionic, cationic, or zwitterionic in nature. Anionic amphiphiles typically possess carboxylate, phosphonate, or sulfate groups, whereas cationic groups generally rely on amines or quaternary ammoniums to impart a positive charge.³⁻

⁶ Zwitterionic compounds contain an equal number of positive and negative charges.⁴ In contrast to ionic amphiphiles' charged headgroups, nonionic amphiphiles usually contain polyether or polyhydroxyl hydrophilic domains.³⁻⁶ As amphiphiles of different polar headgroup classes are often used for different applications, this particular classification can be useful when designing amphiphiles for specific objectives. For instance, anionic amphiphiles are common in many shampoos, while cationic amphiphiles may be used as biocides.^{3,5} Amphiphile applications will be discussed in depth in Section 1.3.

In addition to classifying amphiphiles based on their hydrophilic domain, a second important parameter is the number of hydrophobic components and their connections within the amphiphile. While conventional amphiphiles are depicted as containing one hydrophobic alkyl chain, amphiphiles can contain multiple hydrophobic chains, which may be comprised of different chemical groups (e.g., saturated alkyl chains, unsaturated alkyl chains, and aromatic rings).^{1,2,4} For amphiphiles containing multiple hydrophobic or hydrophilic domains, their connections within the amphiphile structure can vary. Gemini amphiphiles, for instance, are dimeric in nature, consisting of two conventional amphiphiles linked together through a spacer (Figure 1.2B). These amphiphiles are highly surface active and have very low CMC values.^{1,5,6} Bola amphiphiles, comprised of two hydrophilic groups linked via one or two long hydrophobic domains (Figure 1.2C), constitute a second amphiphile class capable of forming a variety of higher-ordered aggregates (e.g., micelles, vesicles, lamella).^{1,10}

While the amphiphiles depicted thus far have centered on small molecular weight compounds, amphiphiles can also be polymeric (Figure 1.2D). Polymer amphiphiles can be described according to the aforementioned classifications; however, they differ from small molecules in that their hydrophobic and hydrophilic components are generally comprised of polymers. Typical polymer amphiphiles are diblock or triblock copolymers consisting of distinct hydrophobic and hydrophilic polymer domains.¹¹ Pluronics, a triblock copolymer comprised of two poly(ethylene glycol) (PEG) and one poly(propylene oxide) (PPO) blocks in an ABA fashion, is one of the most studied polymer amphiphiles.¹² Similar to small molecular weight amphiphiles, polymer amphiphiles form a variety of aggregate structures and can be found in numerous applications.^{11,12}

1.3. Amphiphile Applications

Many amphiphile applications stem from amphiphiles' ability to accumulate at interfaces and self-assemble into aggregates. As amphiphiles form micelle-like structures with a hydrophobic interior, they are capable of solubilizing hydrophobic compounds.^{2,6} Consequently, amphiphiles are employed in various consumer goods, such as mouthwash and detergents, to help solubilize flavors and debris or dirt, respectively.^{2,3}

In addition to consumer applications, amphiphiles are widely used throughout the biomedical field. Given their ability to solubilize compounds within their micelle core, numerous amphiphilic polymers have been investigated

for drug delivery applications (Figure 1.3).¹³⁻¹⁵ For instance, micelles assembled from PEG-block-poly(lactide) (PLA) copolymers or Pluronics have been investigated for the solubilization and delivery of hydrophobic drugs, often enhancing drug efficacy.^{13,14} Using PEG as the hydrophilic block within these amphiphiles provides an added benefit of reducing nonspecific protein adsorption and cell adhesion,^{13,16} thus, potentially enhancing carriers' biological stability. Similar copolymer and amphiphilic peptide systems have been used to solubilize contrast agents and magnetic nanoparticles for biomedical imaging applications.^{9,15,17}

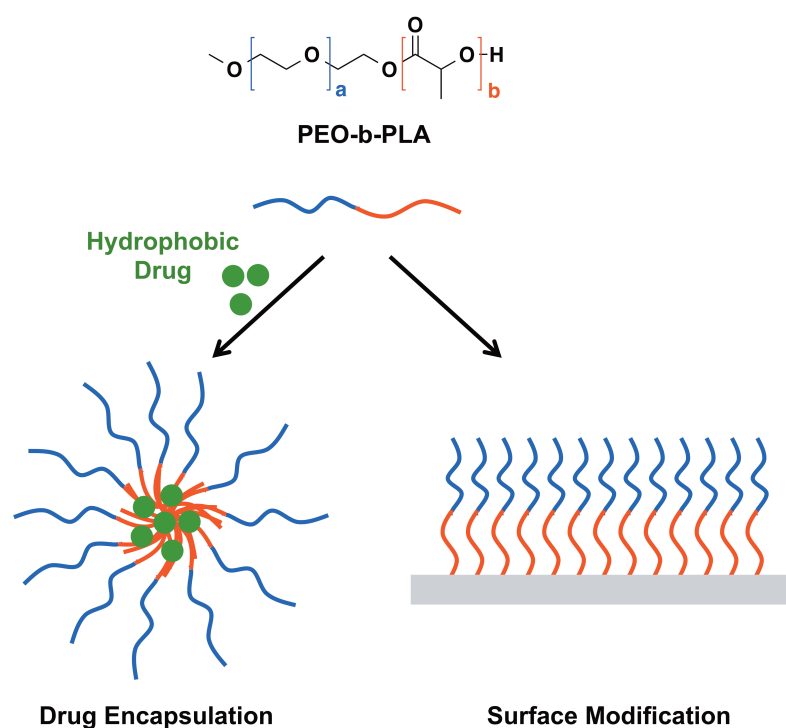


Figure 1.3. Common amphiphile uses within the biomedical field, including drug encapsulation and surface modification

Aside from using amphiphile aggregates as delivery vehicles, other biomedical applications take advantage of amphiphiles' tendency to self-assemble at solid liquid interfaces (Figure 1.3). PEG-block-PLA copolymers, for example, will assemble on PLA surfaces, providing a PEG layer that extends into the aqueous medium and is unlikely to interact with various biological entities.¹³ This surface modification could consequently be useful for designing implantable biomaterials or for tissue engineering applications.

Finally, amphiphiles themselves can possess inherent bioactivity and could therefore serve as therapeutic agents. Perhaps the most widely investigated bioactive amphiphiles are used for antimicrobial applications. Cationic amphiphilic peptides have received attention as antimicrobial therapies, given their unique bactericidal mechanism of interacting with and destabilizing bacterial membranes.¹⁸⁻²¹ In addition to antimicrobial applications, amphiphiles are currently being investigated as antitumor, antiviral, and antiplatelet agents.^{22,23} As a result of their dynamic, interfacial behavior, amphiphilic molecules possess great potential in the biomedical realm. Therefore, this work sought to explore novel amphiphilic molecules possessing inherent therapeutic potential. The design, synthesis, and evaluation of such compounds are presented.

1.4. Specific Projects

1.4.1. Amphiphilic Macromolecules for Atherosclerosis Treatment: Impact of Hydrophobic Chain Composition

Atherosclerosis, a leading cause of cardiovascular disease, is an inflammatory disease characterized by the accumulation of oxidized low-density lipoprotein (oxLDL) in the vascular intima, its uptake by macrophages, and the subsequent formation of foam cells and arterial plaque. Amphiphilic macromolecules (AMs) comprised of sugar backbones modified with branched aliphatic chains and a hydrophilic PEG tail can inhibit macrophage uptake of oxLDL and thereby mitigate the atherosclerotic cascade. Previous studies indicate that AM hydrophobic domains influence this bioactivity through interacting with macrophage scavenger receptors, which can contain basic and/or hydrophobic residues within their binding pockets. In this study, two classes of AMs are compared to investigate their ability to promote athero-protective potency via hydrogen-bonding or hydrophobic interactions with scavenger receptors (Figure 1.4).²⁴ A series of ether-AMs, containing methoxy-terminated aliphatic arms capable of hydrogen-bonding, was synthesized. Compared to analogous AMs containing no ether moieties (alkyl-AMs), ether-AMs showed improved cytotoxicity profiles. Increasing AM hydrophobicity via incorporation of longer and/or alkyl-terminated hydrophobic chains yielded macromolecules with enhanced oxLDL uptake inhibition. These findings indicate that hydrophobic interactions and the length of AM aliphatic arms more significantly influence AM bioactivity than hydrogen-bonding interactions.

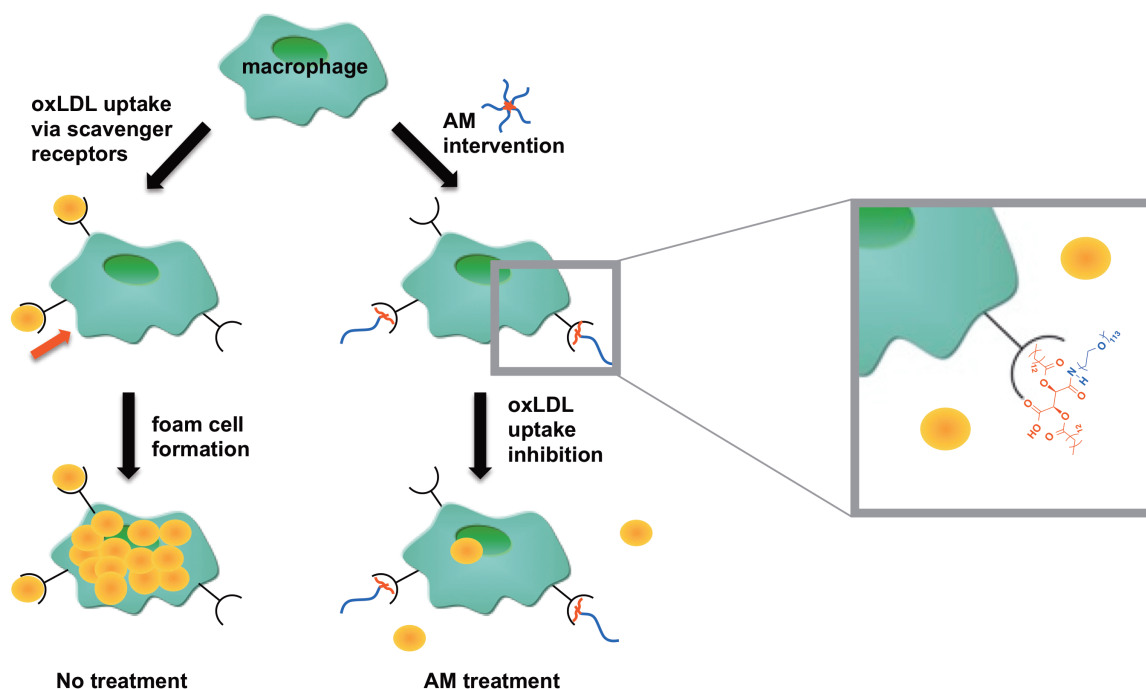


Figure 1.4. Depiction of AMs' ability to inhibit scavenger receptor-mediated oxLDL uptake

1.4.2. Biscationic Tartaric Acid-Based Amphiphiles: Charge Location Impacts Antimicrobial Activity

Increased instances of multidrug resistant bacteria have necessitated the development of new antimicrobial agents. Cationic amphiphiles have received increasing attention as antimicrobials given their unique ability to disrupt bacteria cell membranes. While extensive research has demonstrated that amphiphiles' hydrophobic-to-charge ratio significantly modulates antibacterial activity, less work has focused on elucidating the specific impact of charge location on

amphiphile bioactivity. In this study, two series of cationic amphiphiles, termed bola-like and gemini-like amphiphiles, were synthesized with analogous hydrophobic-to-charge ratios yet differing charge location and their resulting antibacterial activity assessed (Figure 1.5).²⁵ Bola-like amphiphiles exhibited preferential activity against gram-positive bacteria, with activity increasing with increasing hydrophobicity, whereas gemini-like amphiphiles were more active against gram-negative bacteria, with activity decreasing with increasing hydrophobicity. After identifying lead compounds from each amphiphile series (bola- and gemini-like), biophysical experiments indicated that both amphiphiles were membrane-active; notably, the lead gemini-like amphiphile exhibited a strong dependence on electrostatic interactions for membrane interaction. In contrast, the lead bola-like amphiphile exhibited a reliance on both hydrophobic and electrostatic contributions. These results demonstrate that charge location significantly impacts cationic amphiphiles' antibacterial and membrane activity.

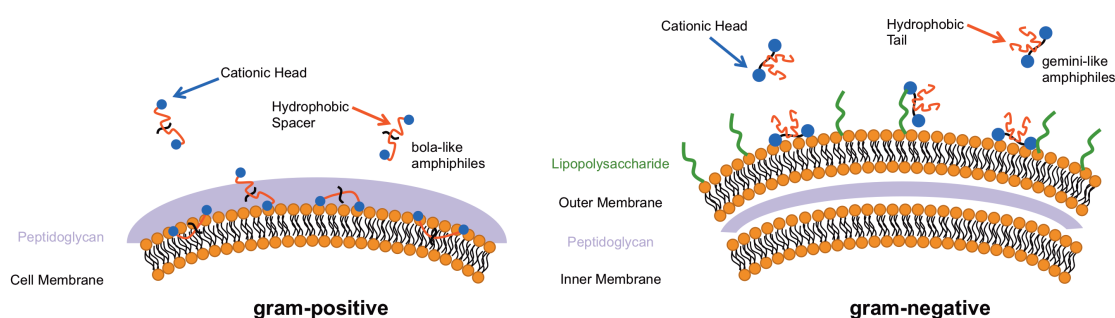


Figure 1.5. Depiction of bola-like (left) and gemini-like (right) amphiphiles' potential interactions with gram-positive and gram-negative bacteria, respectively

1.5. Summary

Amphiphilic molecules' unique properties have implicated their use in various biomedical applications, ranging from drug delivery to surface coatings. Through rationally designing amphiphile structures, bioactive compounds can be generated for various therapeutic applications. By investigating structural modifications of AM hydrophobic domains, key insights into AMs' antiatherosclerotic potency were gained. By altering the location of cationic moieties on hydrophobic backbones, novel antimicrobial agents were developed with varying bioactivity.

1.6. References

1. Sorrenti, A.; Illa, O.; Ortuno, R. M. *Chem. Soc. Rev.* **2013**, 42, 8200.
2. Moulik, S. P. *Current Science* **1996**, 71, 368.
3. Mishra, M.; Muthuprasanna, P.; Prabha, K. S.; Rani, P. S.; Babu, I. A. S.; Chandiran, I. S.; Arunachalam, G.; Shalini, S. *Int J PharmTech Res* **2009**, 1, 1354.
4. Romsted, L. S. *Supramolecular Chemistry: From Molecules to Nanomaterials* **2012**.
5. Holmberg, K.; Jönsson, B.; Kronberg, B.; Lindman, B. *Surfactants and polymers in aqueous solution*; Wiley, 2003.
6. Hill, J. P.; Shrestha, L. K.; Ishihara, S.; Ji, Q.; Ariga, K. *Molecules* **2014**, 19, 8589.
7. Mandal, D.; Shirazi, A. N.; Parang, K. *Organic & Biomolecular Chemistry* **2014**, 12, 3544.

8. Khan, A. M.; Shah, S. S. *Journal of the Chemical Society of Pakistan* **2008**, 30, 186.
9. Hamley, I. W. *Soft Matter* **2011**, 7, 4122.
10. Estroff, L. A.; Hamilton, A. D. *Chemical Reviews* **2004**, 104, 1201.
11. Liu, S. Y.; Armes, S. P. *Current Opinion in Colloid & Interface Science* **2001**, 6, 249.
12. Holder, S. J.; Sommerdijk, N. A. J. M. *Polymer Chemistry* **2011**, 2, 1018.
13. Otsuka, H.; Nagasaki, Y.; Kataoka, K. *Current Opinion in Colloid & Interface Science* **2001**, 6, 3.
14. Fusco, S.; Borzacchiello, A.; Netti, P. A. *Journal of Bioactive and Compatible Polymers* **2006**, 21, 149.
15. Oh, J. K. *Soft Matter* **2011**, 7, 5096.
16. Gan, Z. H.; Jim, T. F.; Li, M.; Yuer, Z.; Wang, S. G.; Wu, C. *Macromolecules* **1999**, 32, 590.
17. Cui, H. G.; Webber, M. J.; Stupp, S. I. *Biopolymers* **2010**, 94, 1.
18. Zhao, X.; Pan, F.; Xu, H.; Yaseen, M.; Shan, H.; Hauser, C. A. E.; Zhang, S.; Lu, J. R. *Chem. Soc. Rev.* **2010**, 39, 3480.
19. Park, S. C.; Park, Y.; Hahm, K. S. *International Journal of Molecular Sciences* **2011**, 12, 5971.
20. Lavery, G.; Gorman, S. P.; Gilmore, B. F. *International Journal of Molecular Sciences* **2011**, 12, 6566.
21. Tew, G. N.; Scott, R. W.; Klein, M. L.; Degrado, W. F. *Accounts of chemical research* **2010**, 43, 30.
22. Rodrigues, L.; Banat, I. M.; Teixeira, J.; Oliveira, R. *Journal of Antimicrobial Chemotherapy* **2006**, 57, 609.
23. Seydlova, G.; Svobodova, J. *Central European Journal of Medicine* **2008**, 3, 123.
24. Faig, A.; Petersen, L. K.; Moghe, P. V.; Uhrich, K. E. *Biomacromolecules* **2014**, 15, 3328.
25. Faig, A.; Arthur, T. D.; Fitzgerald, P. O.; Chikindas, M.; Mintzer, E.; Uhrich, K. E. **2015**, *In Preparation*.

2. AMPHIPHILIC MACROMOLECULES FOR ATHEROSCLEROSIS

TREATMENT: IMPACT OF HYDROPHOBIC CHAIN COMPOSITION

[This work has been published in Biomacromolecules, year 2014, volume 15, pages 3328-3337, under the title “Impact of Hydrophobic Chain Composition on Amphiphilic Macromolecule Antiatherogenic Bioactivity.” Latrisha K. Petersen, Prabhas V. Moghe, and Kathryn E. Uhrich are co-authors for this work.]

2.1. Introduction

Atherosclerosis, a major cause of mortality worldwide, is an inflammatory disease characterized by arterial plaque development.¹⁻⁵ During the early stages of atherosclerosis, low-density lipoprotein (LDL) accumulates in the subendothelial space where various cells catalyze its oxidative modification.^{4,6-8} This oxidized LDL (oxLDL) initiates an inflammatory response, in which monocytes are recruited to sites of endothelial dysfunction, migrate into the subendothelial space, and subsequently differentiate into macrophages.^{1,3,4,6,7,9} Macrophages then internalize oxLDL primarily through scavenger receptors A (SRA) and B (CD36) resulting in unregulated modified lipid accumulation and foam cell formation.^{2,3,5-7,9} Foam cells promote the inflammatory process and lead to atherosclerotic plaque formation, narrowing the artery, and cardiovascular events, including hypertension, stroke, and myocardial infarction.^{2,3,6,9} In this

work, we seek to mitigate atherogenesis (Figure 2.1) via new designs of macromolecules that interfere with oxLDL uptake, and thus de-escalate the atherosclerotic development.

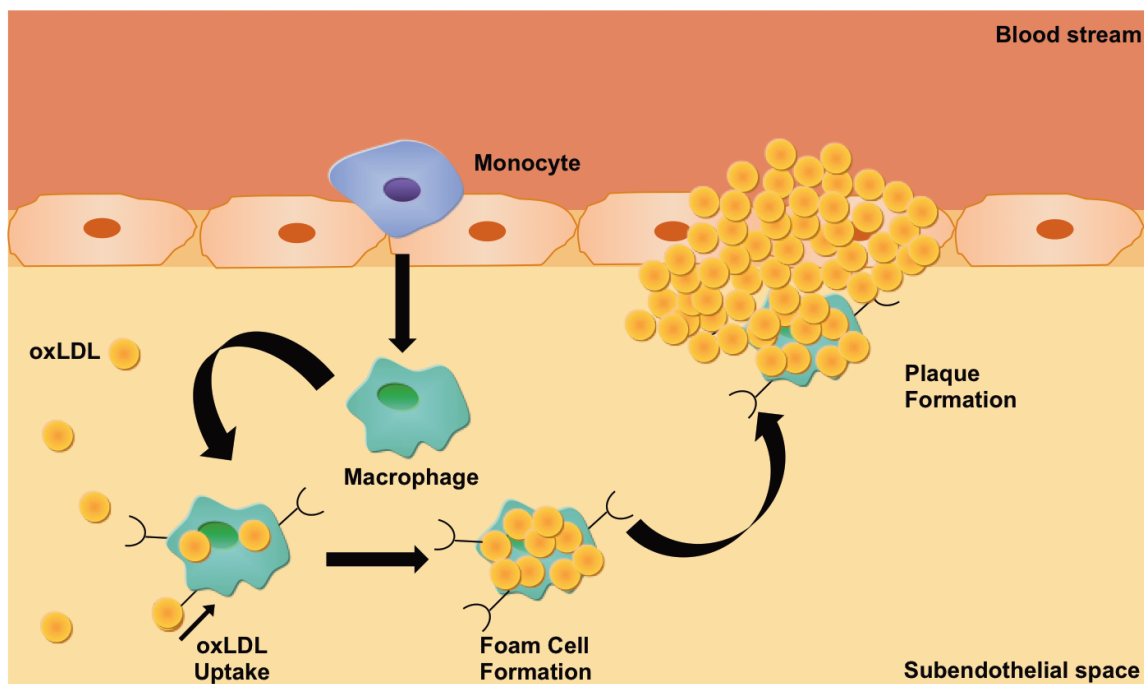


Figure 2.1. Schematic depicting the atherosclerotic cascade; this graphic was adapted from previous Rutgers theses^{10,11}

Statins are the most well known and widely prescribed therapeutic for treating coronary artery disease.^{12,13} They slow the atherosclerotic cascade through inhibiting hepatic cholesterol biosynthesis and subsequently increase the expression of hepatic LDL receptors to lower serum LDL levels. However, statins can have undesirable side effects, including muscle toxicity, cognitive problems, and metabolic issues (e.g., liver toxicity or thyroid conditions), and as a

result of their systemic administration and mechanism of action, statins do not directly treat atherogenic sites in the arteries.¹²⁻¹⁴ When statins are not tolerated by patients or when patients are genetically predisposed to increased LDL levels as in familial hypercholesterolemia, lipid apheresis therapies can be used to extracorporeally remove plasma lipoproteins (i.e., LDL) from the blood.¹⁵⁻¹⁹ Apheresis methods often utilize adsorbents, which contain ligands that interact with and retain LDL, including dextran sulfate, polyacrylate, heparin, and phosphates, and carriers such as poly(vinyl alcohol) microspheres, cellulose beads, nonwoven fabrics, and other polymer systems.^{15,16,18-21} While these therapies lower LDL levels and improve atherosclerosis outcomes, problems remain: long-term, expensive treatments (\$40,000-100,000 USD annually) are required to maintain efficacy, treatment access is limited, and many current adsorbents have low LDL selectivity and poor mechanical properties.^{16-19,21,22} Consequently, researchers are currently targeting various steps in the atherosclerotic cascade described above, including monocyte recruitment, macrophage-mediated cholesterol metabolism, and plaque regression to impede the inflammatory progression and improve treatment efficacy.⁶

As an alternative strategy to treat atherosclerosis, researchers are investigating means to abrogate the atherosclerotic cascade by preventing oxLDL trafficking and uptake within the blood vessel walls.^{23,24} *In vivo* studies have indicated that Apolipoprotein E-null mice deficient in certain scavenger receptors (e.g., SRA or CD36) result in significantly smaller atherosclerotic lesions and a decreased uptake of modified LDL (e.g., oxLDL).²³⁻²⁵ Given that

oxLDL uptake can lead to foam cell formation and atherosclerotic plaque development, inhibiting oxLDL uptake could impede atherogenesis. Previously, our lab demonstrated that amphiphilic macromolecules (AMs) inhibit scavenger receptor-mediated oxLDL uptake, particularly through competitive inhibition of SRA and CD36.²⁶ These sugar-based, PEGylated AMs are comprised of a sugar backbone that is acylated with aliphatic chains and conjugated to a poly(ethylene glycol) (PEG) tail.²⁷ Given their amphiphilicity, AMs self-assemble into nanoscale micelles in aqueous environments²⁷ with a PEG shell that may shield uptake by the reticuloendothelial system, potentially prolonging *in vivo* blood circulation times.²⁸ Upon discovering AMs' anti-atherosclerotic activity, various studies were conducted to elucidate their bioactive mechanism. Dynamic light scattering (DLS) studies indicated that AMs containing an anionic charge (e.g., carboxylate moiety) within their hydrophobic domain complex with unmodified LDL, but do not complex with oxLDL, likely due to charge repulsion resulting from oxLDL's increased net negative charge.²⁹ As these AMs did not interact with oxLDL yet prevented its accumulation in macrophages, further immunolocalization and antibody blocking assays were conducted and demonstrated that AMs interact with macrophage scavenger receptors and subsequently prevent oxLDL uptake through these receptors.^{26,30-32} A library of AMs was generated by systematically modifying AM structural elements, and quantitative structure-activity relationship models were developed to determine the most prominent athero-protective AM features.³³⁻³⁶ The hydrophobic domain plays a key role; the presentation of the aliphatic arms influences AM athero-protective bioactivity.³⁵⁻³⁷

Though structure-activity relationships provided significant insights regarding AM efficacy, a more rational approach for developing bioactive AMs with increased potency would be inspired by the physicochemical attributes of the scavenger receptor binding pockets. While certain scavenger receptors contain basic residues in their oxLDL binding domains,^{38,39} others contain hydrophobic residues near their oxLDL binding sites.⁴⁰ Increasing the AM hydrophobicity through extending alkyl chain lengths or decreasing PEG tail lengths could increase AM interactions with hydrophobic receptor pockets, whereas the addition of heteroatoms into the hydrophobic domain could enable hydrogen-bonding interactions with basic residues, ultimately reducing oxLDL uptake by mimicking scavenger receptor interactions with hydrophobic oxidized lipids.⁴¹⁻⁴³ To decipher which interactions more effectively influence athero-protective bioactivity through repressing oxLDL uptake, a series of novel ether-containing AMs (ether-AMs) capable of hydrogen-bonding was synthesized based on a linear tartaric acid (TA) backbone and compared to analogous AMs containing no ether moieties (alkyl-AMs) that would exhibit stronger hydrophobic interactions (Figure 2.2). The relative hydrophobicity of all AMs was varied by altering both the aliphatic chain and PEG tail lengths to determine whether more lipophilic AMs would mimic the interactions of hydrophobic, oxidized lipids with scavenger receptors and thereby exhibit increased athero-protective bioactivity.

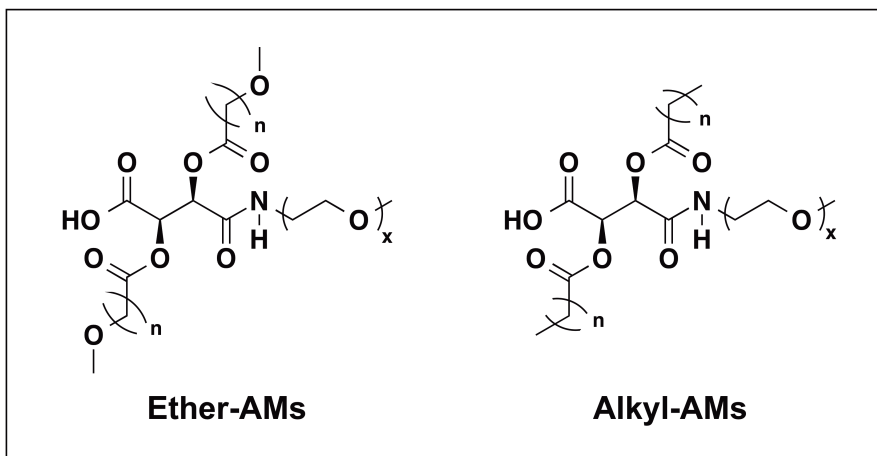


Figure 2.2. Chemical structure of ether- and alkyl-AMs

2.2. Results and Discussion

2.2.1. Synthesis

Ether-AMs were synthesized to assess whether incorporating heteroatoms, specifically ethers, into the terminal-end of hydrophobic alkyl chains would enhance AM bioactivity by promoting hydrogen-bonding interactions with scavenger receptor binding pockets, potentially reducing oxLDL uptake even further.

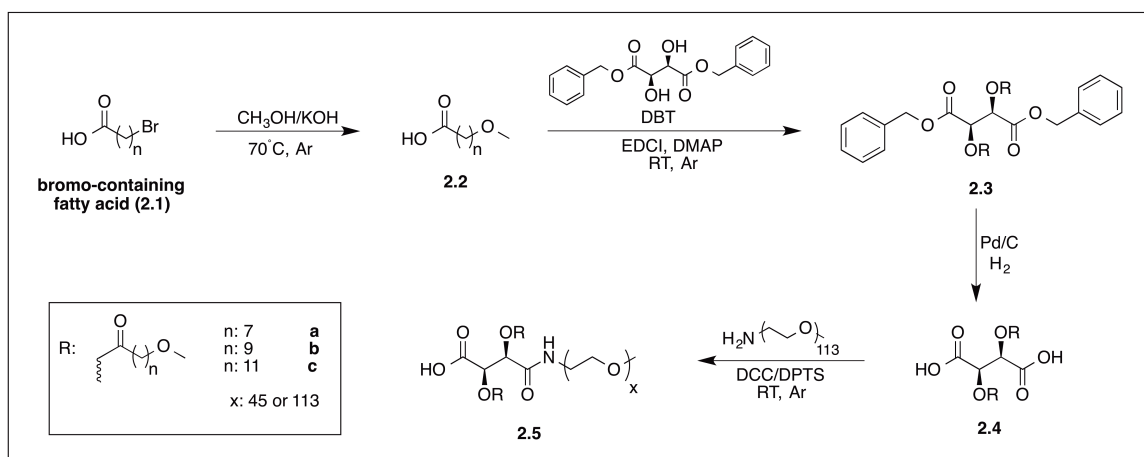


Figure 2.3. Synthetic scheme for ether-AMs; The different alkyl arm lengths investigated are denoted as a, b, and c in order of increasing length; The PEG M_w used is denoted numerically in kiloDaltons as a subscript with $x = 45$ yielding 2 kDa PEG and $x = 113$ yielding 5 kDa PEG (e.g., **2.5a₂** signifies an ether-AM containing the shortest alkyl chain length and a 2 kDa PEG tail)

To this end, a series of methoxy-terminated long-chain carboxylic acids was first synthesized to serve as the AMs' hydrophobic arms (Figure 2.3). Using the Williamson ether synthesis, potassium methoxide, generated from methanol (MeOH) and potassium hydroxide (KOH), was reacted with bromo-terminated alkanolic acids (**2.1**) to yield methoxy-terminated alkanolic acids (**2.2**) via an S_N2 reaction.⁴⁴ To acylate the TA backbone with **2.2**, typical AM synthetic methods were attempted in which methoxy-terminated alkanoyl chlorides were prepared from thionyl chloride and reacted with TA in the presence of a Lewis acid catalyst.²⁷ These conditions, however, required an excess of **2.2** and resulted in incomplete acylation. As an alternative, **2.2** was coupled to a dibenzyl tartrate

backbone (DBT) using 1-ethyl-3-(3-dimethylaminopropyl)carbodiimide (EDCI) coupling, resulting in complete acylation while using near stoichiometric amounts of **2.2**. The acylated DBT derivative (**2.3**) was subsequently deprotected via hydrogenolysis, using a 10 % w/w palladium on carbon (Pd/C) catalyst, to give the acylated TA product (**2.4**). To finally generate the ether-AMs (**2.5**), **2.4** was coupled to monomethoxy-poly(ethylene glycol)-amine (mPEG-NH₂) using dicyclohexylcarbodiimide (DCC) coupling with a 4-(dimethylamino)pyridinium 4-toluenesulfonate (DPTS) catalyst. A stoichiometric excess of **2.4** and DCC ensured that PEG coupled to only one of **2.4**'s two carboxylic acids. Ether-AM precursors' chemical structures were confirmed via proton (¹H) and carbon (¹³C) nuclear magnetic resonance (NMR) and Fourier transform infrared (FT-IR) spectroscopies and mass spectrometry (MS), while ether-AM structures and weight-averaged molecular weights (M_w) were verified by ¹H NMR spectroscopy and gel permeation chromatography (GPC), respectively.

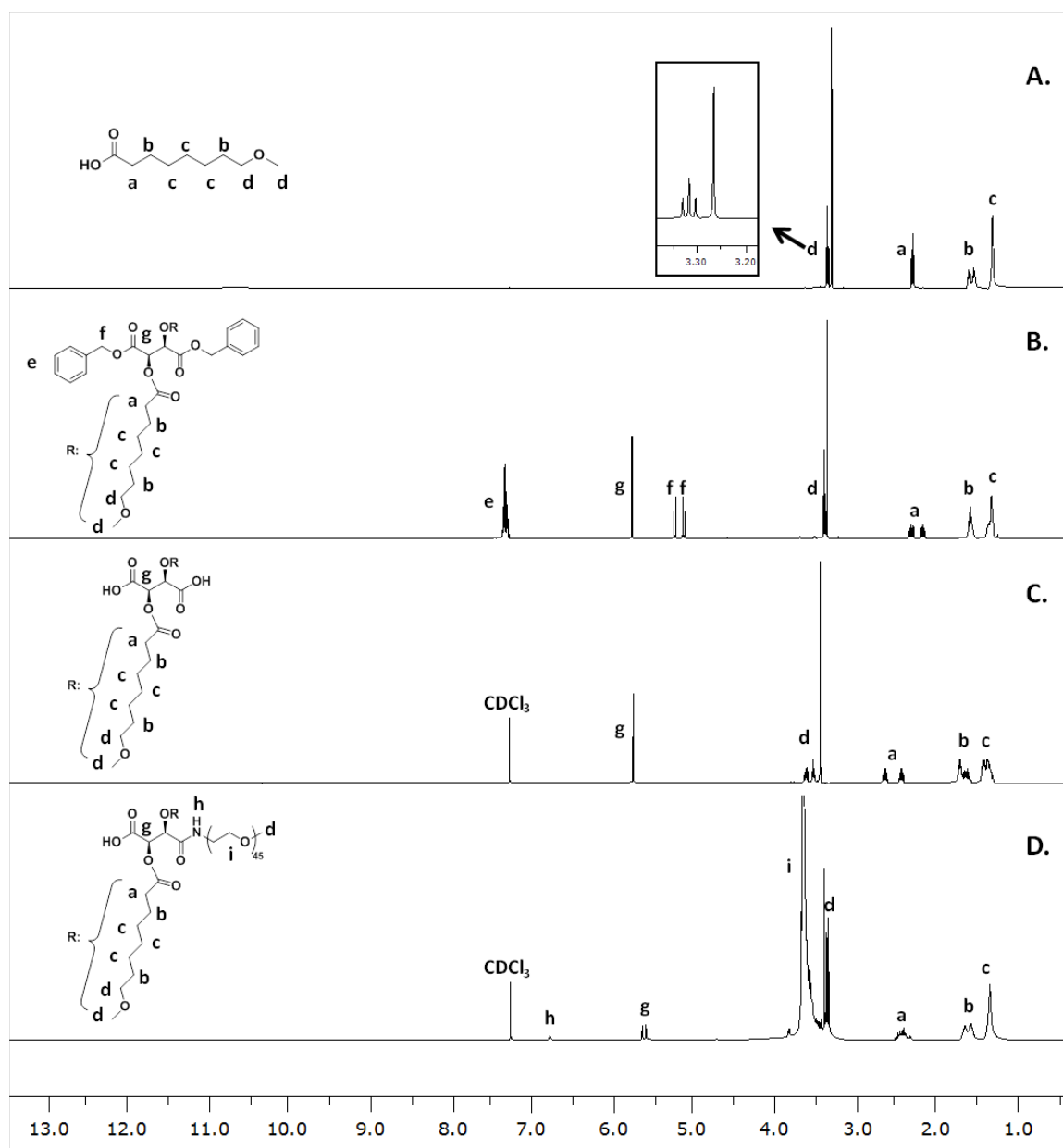


Figure 2.4. ^1H NMR spectra for $2.5a_2$ ether-AM synthesis as an example: 8-methoxyoctanoic acid **2.2a** (A), 2,3-bis(8-methoxyoctanoyl) DBT **2.3a** (B), 2,3-bis(8-methoxyoctanoyl) TA **2.4a** (C), and ether-AM **2.5a₂** (D)

^1H NMR spectroscopy was critical in affirming successful synthesis of ether-AMs and their precursors. Figure 2.4 presents the NMR spectra obtained

during the synthesis of **2.5a₂**, as an example. Successful 8-methoxyoctanoic acid (**2.2a**) synthesis was confirmed by the appearance of a triplet and singlet at 3.32 and 3.27 ppm (d in Figure 2.4A), corresponding to the methylene and methyl protons adjacent to the methoxy oxygen atom. The relative integration of DBT's methine singlet (g in Figure 2.4B) to signals associated with the 8-methoxyoctanoyl arms demonstrated complete acylation to form **2.3a**, with two aliphatic arms present per DBT backbone. Disappearance of the aromatic and benzyl proton signals (e and f in Figure 2.4B) illustrated the complete deprotection of **2.3a** to produce **2.4a** (Figure 2.4C). Finally, successful PEGylation to yield **2.5a₂** was confirmed by the appearance of a large ~200 proton PEG multiplet (i in Figure 2.4D). The 1:2 ratio of the amide proton signal (h in Figure 2.4D) to the methine proton signal of the TA backbone further indicated that PEG was only conjugated to one side of the TA derivative.

In addition to synthesizing ether-AMs, a series of analogous alkyl-AMs (Figure 2.5) was prepared to compare the influence of hydrogen-bonding and hydrophobic interactions on AM physicochemical and biological properties. These alkyl-AMs (**2.7**) only differed from ether-AMs in that the methoxy oxygen atom was replaced with a methylene group, yielding AMs with saturated aliphatic arms of analogous lengths to the ether-AMs. To synthesize these analogs, previously reported methods were used in which TA was reacted with an acyl chloride to generate a modified TA hydrophobe (**2.6**) that was subsequently coupled to mPEG-amine using DCC. AM and AM precursor chemical structures were confirmed via the aforementioned methods.

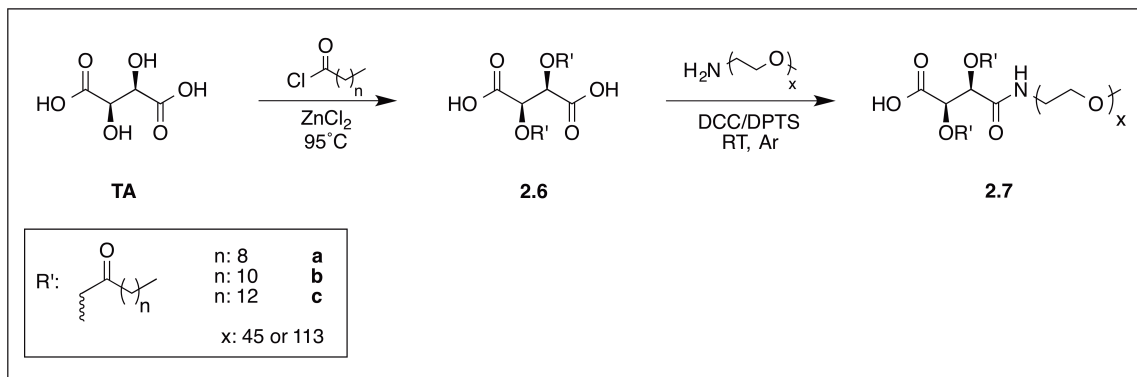


Figure 2.5. Synthetic scheme for alkyl AMs; The different alkyl arm lengths investigated are denoted as a, b, and c in order of increasing length; The PEG M_w used is denoted numerically in kiloDaltons as a subscript with $x = 45$ yielding 2 kDa PEG and $x = 113$ yielding 5 kDa PEG (e.g., **2.7a₂** signifies an alkyl-AM containing the shortest alkyl chain length and a 2 kDa PEG tail)

2.2.2. Physicochemical Characterization

Once the synthesis of all ether- and alkyl-AMs was confirmed, their physicochemical properties were evaluated. When AM concentrations in aqueous environments exceed a critical micelle concentration (CMC), they self-assemble into micelles; this transition was measured using an established fluorimetry assay.²⁷ In evaluating ether-AMs alone, it was observed that while keeping the PEG M_w constant, **2.5c** AMs exhibited slightly lower CMC values than **2.5a** and **2.5b**, which were comparable (Table 2.1). As **2.5c** AMs contained the most methylenes within the hydrophobic domain, these AMs were likely less

soluble in water as compared to **2.5a** and **2.5b**, resulting in lower CMC values. Furthermore, as micellization is entropically driven by the displacement of water molecules from the hydrophobic domain, these results likely stem from **2.5c** AMs having more water molecules associated with their hydrophobic domains prior to micellization, resulting in a larger entropic increase and thus a greater free energy decrease upon micellization.⁴⁵ Although **2.5c** AMs' CMC values were lower than those of other ether-AMs, all ether-AMs exhibited CMCs near 10^{-4} M.

Table 2.1. Physicochemical properties of ether- (**2.5**) and alkyl-AMs (**2.7**), with 2000 M_w compounds on the left and 5000 M_w compounds on the right

AM	CMC (M)	Size (nm)	AM	CMC (M)	Size (nm)
2.5a₂	1.97E-04	102.3 ± 0.3	2.5a₅	2.19E-04	111.4 ± 0.8
2.7a₂	9.79E-05	8.0 ± 0.1	2.7a₅	5.79E-05	15.3 ± 0.1
2.5b₂	1.99E-04	93.5 ± 1.4	2.5b₅	2.02E-04	119.8 ± 2.0
2.7b₂	3.43E-05	7.3 ± 0.1	2.7b₅	3.20E-05	11.2 ± 0.1
2.5c₂	1.24E-04	12.5 ± 0.0	2.5c₅	9.01E-05	28.7 ± 0.5
2.7c₂	6.94E-06	8.1 ± 0.1	2.7c₅	7.49E-06	10.6 ± 0.2

In comparing ether-AMs to their respective alkyl-AM analogs (e.g., **2.5a₂** vs. **2.7a₂**), all alkyl-AMs exhibited CMC values lower than the analogous ether-AMs (Figure 2.6), ranging approximately from 10^{-6} M to 10^{-4} M. Similar to the trends amongst the ether-AMs (**2.5**), the analogs' (**2.7**) lower CMC values likely

result from the increased hydrophobicity of **2.7** as compared to **2.5**. Given that lower CMCs can provide greater stability against dilution, the alkyl-AMs would be more likely to remain in micellar assemblies when diluted under physiological conditions.⁴⁶

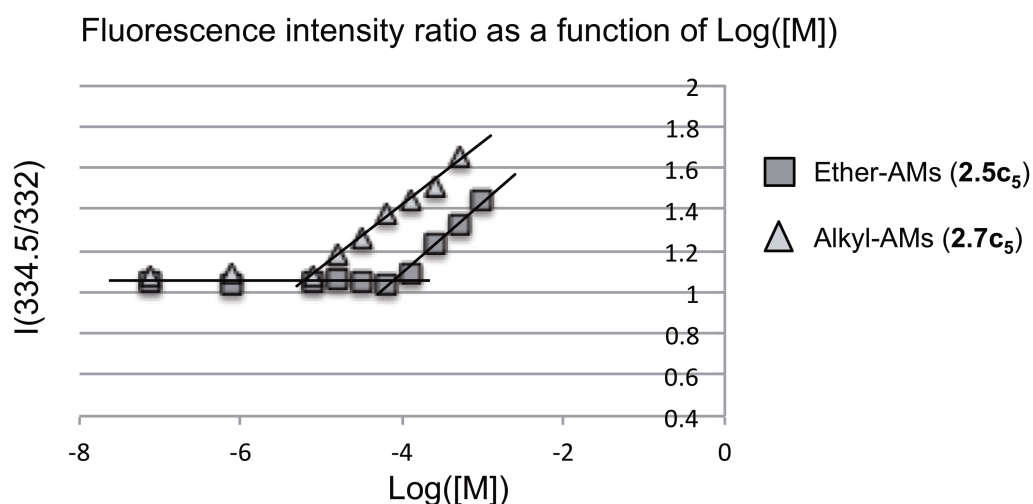


Figure 2.6. CMC curves of representative ether- (**2.5c₅**) and alkyl- (**2.7c₅**) AMs, in which the inflection point of the curves corresponds to AM CMC values; Alkyl-AMs continuously exhibited lower CMC values than analogous ether-AMs

To determine whether AM micelles exhibited nanoscale sizes suitable for biomedical applications, the micelles were next measured using DLS. Prior to DLS measurements, AMs were incubated in water for 24 h at 37 °C to mimic physiological conditions. In comparing the ether-AMs, **2.5a** and **2.5b** exhibited sizes near 100 nm while **2.5c** exhibited smaller sizes - regardless of PEG M_w (Table 2.1). The smaller sizes of **2.5c** AMs may result from enhanced

hydrophobic interactions upon micellization due to their larger hydrophobic domains,⁴⁷ which could overcome potential repulsion caused by the methoxy moieties. Furthermore, other investigators have reported that different micelle morphologies (e.g., spindle-like, rod-like, or bowl-like) result when increasing the length of block copolymers' hydrophobic domains.⁴⁸⁻⁵¹ Although the DLS method employed assumes Brownian motion of sphere-shape particles, it's plausible that alternate micelle morphologies are present, giving rise to the smaller particle sizes. Despite the range in sizes (12 – 119 nm), all ether-AMs remained within a size range (10 – 200 nm) considered optimal for enhanced stability *in vivo*.⁴⁶ In contrast to ether-AMs, all alkyl-AMs exhibited smaller sizes, ranging from 8 to 15 nm. As these analogs are more hydrophobic than the ether-AMs, these results correlate well with the ether-AM size trends, suggesting larger hydrophobic domains yield stronger hydrophobic interactions and smaller micelle sizes. Finally, all 2000 M_w AMs exhibited smaller sizes than their 5000 M_w counterparts (e.g., **2.5a₂** vs. **2.5a₅**). This phenomenon likely resulted from 2000 M_w AMs' smaller PEG size, as seen in previous literature.^{52,53} Despite variations in sizes, all ether-AMs exhibited suitable sizes for drug delivery applications, while some alkyl-AMs displayed sizes slightly smaller than the desirable size range.

2.2.3. Biological Activity

Prior to assessing ether- and alkyl-AMs' anti-atherogenic potential, cytotoxicity was screened in human monocyte-derived macrophages (HMDMs) at

concentrations ranging from 10^{-5} - 10^{-3} M (Figure 2.7). Treatments that resulted in 70 % or more viable cells were considered non-toxic. 70 % viability was arbitrarily chosen as the cut-off for toxicity, as this cut-off has been recommended for peripheral blood mononuclear cells (PBMCs),⁵⁴ which differentiate into HMDMs. While the most hydrophobic ether-AM, **2.5c₂**, was cytotoxic only at the highest concentration administered (10^{-3} M, Figure 2.7B), all other ether-AMs were non-toxic at all concentrations tested. Of the alkyl-AMs, **2.7b₂** and **2.7c₅** were cytotoxic at 10^{-3} M, and **2.7c₂** exhibited cytotoxicity at both 10^{-3} and 10^{-4} M. In agreement with previously published results on nanoscale systems,⁵⁵⁻⁵⁷ these results suggest that as AM hydrophobicity is increased, the macromolecules become more cytotoxic. Conversely, AMs with larger PEG tails showed improved cell viability over AMs with smaller molecular weight PEG tails (i.e., 5000 vs. 2000 Da, respectively). Furthermore, ether-AMs – containing two additional, ethereal oxygen atoms within their hydrophobic domain – are better tolerated by HMDMs than alkyl-AMs when administered at higher concentrations.

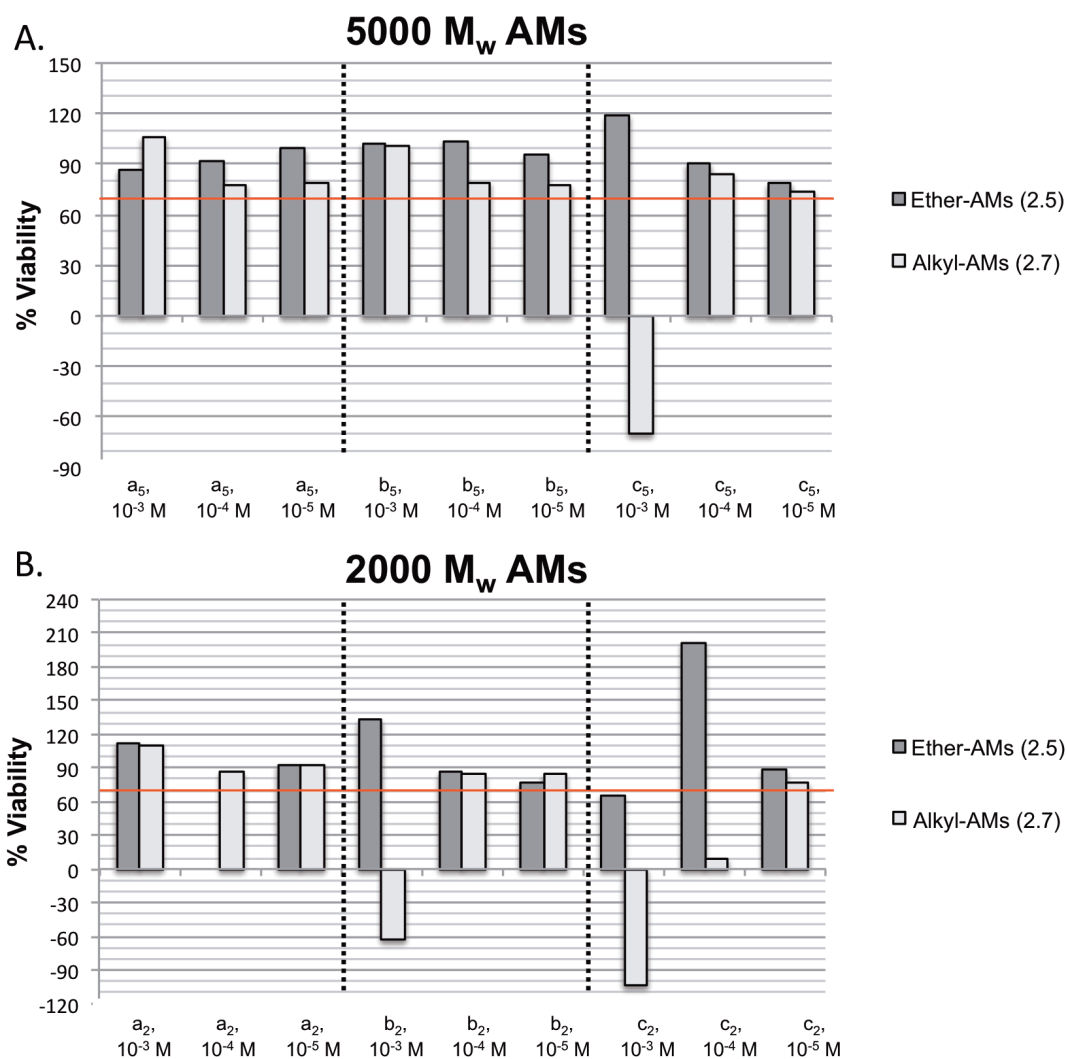


Figure 2.7. Cell viability screening results for varying concentrations of 5000 M_w (A) and 2000 M_w (B) AMs; AMs with different alkyl arm lengths are grouped between the dashed lines; The cell viability cut-off of 70 % is denoted as a red line on the graph; Compound **2.5a₂** at 10⁻⁴ M was included in oxLDL uptake studies although its viability was not assessed, as it was non-toxic at 10⁻³ M

To assess the impact of the hydrophobic chain architecture on AM anti-atherogenic bioactivity, HMDMs were co-incubated with AMs at concentrations

ranging from 10^{-5} - 10^{-3} M and fluorescently-labeled oxLDL. This broad range of concentrations (e.g., above and below CMC values) was investigated to determine the influence of concentration and the presence of micelles (or unimers) on AM bioactivity. Furthermore, all *in vitro* studies were conducted in the presence of serum proteins to mimic physiological conditions; however, serum proteins are capable of disrupting micelle integrity^{32,58-60} and may impact AM bioactivity. Previous studies have indicated that in comparison to serum-free conditions AMs' efficacy decreases in the presence of serum proteins, which may result from serum protein interactions with AMs.³⁴ The presence of serum proteins, therefore, allows for a more realistic understanding of ether- and alkyl-AM bioactivity.

As shown in Figure 2.8A, the hydrophobic chain composition and AM concentration play an integral role in 5000 M_w PEG tail AM anti-atherogenic bioactivity. As the ether-AMs' aliphatic chain length increases, their ability to inhibit oxLDL uptake increases, such that **2.5c₅** > **2.5b₅** > **2.5a₅**, with **2.5a₅** exhibiting no bioactivity. This phenomenon is concentration-dependent, with higher ether-AM concentrations resulting in more oxLDL uptake inhibition, except for **2.5a₅**. For example, while HMDMs treated with 10^{-4} M **2.5c₅** exhibit 73 % oxLDL uptake, those cells incubated with 10^{-3} M **2.5c₅** significantly repress oxLDL uptake to less than 2 % (Figure 2.8A). Furthermore, 10^{-3} M **2.5c₅** reduced the amount of oxLDL internalized by cells by such a significant magnitude that only 5.3 % of the cells had any oxLDL in them at all (Figure 2.9A). Given that **2.5b₅** administered at 10^{-3} M significantly inhibited oxLDL uptake (Figure 2.8A)

despite its larger-sized micelles, it appears that micelle size alone does not dictate AMs' anti-atherogenic potential. Further, as **2.5a₅** exhibited no bioactivity at 10^{-3} M despite its micellar assembly, it is likely that the chemical composition of the AM more strongly influences bioactivity than the corresponding micellar configuration. Although AM micellar structure does not demonstrate a pronounced effect on AM bioactivity, the increased size and PEG shielding provided by the micellar assembly would likely increase the AMs biological stability when administered in a clinical setting.^{28,46}

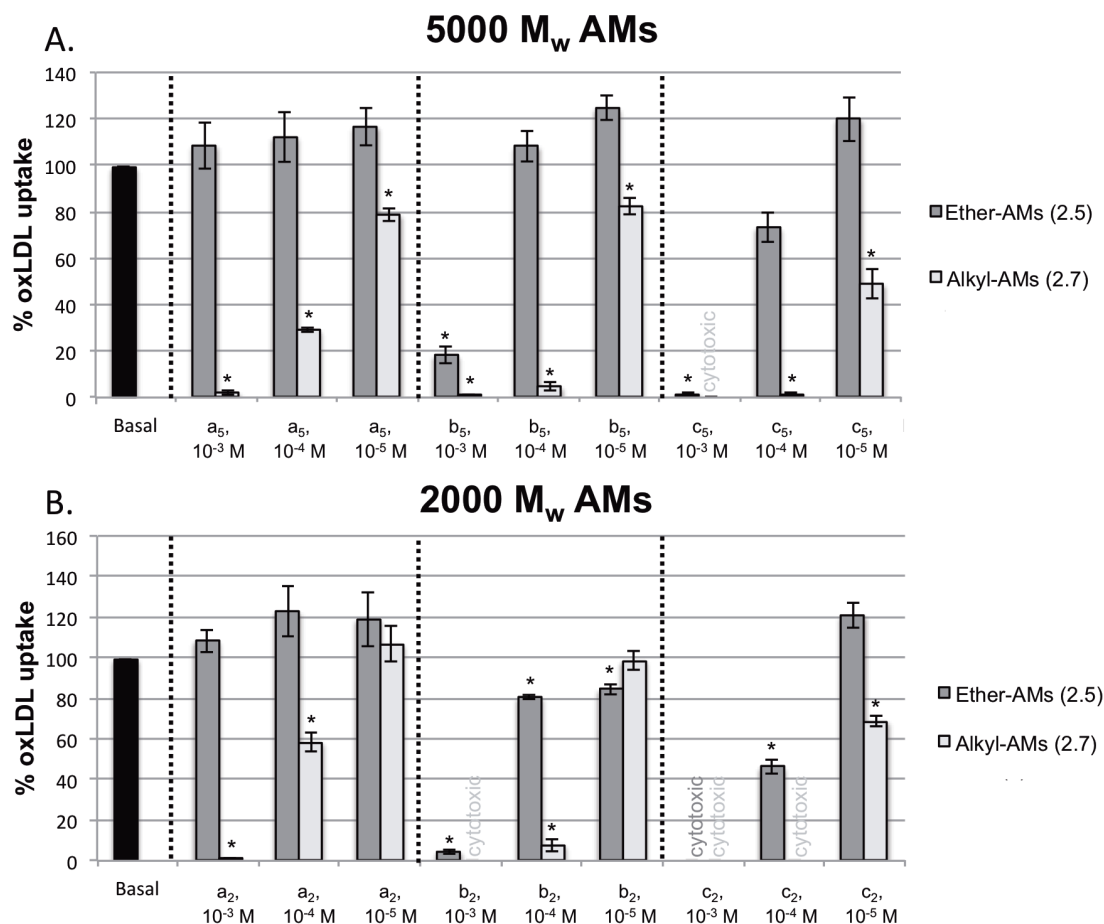


Figure 2.8. Effect of administering varying concentrations of 5000 M_w (A) and 2000 M_w (B) ether-AMs (dark grey) and alkyl-AM analogs (light grey) on % oxLDL uptake in HMDMs; AMs of specific alkyl lengths are grouped between the dash lines, and the AM treatments not investigated due to cytotoxicity are indicated as text on the graph; Significant deviations from the oxLDL positive control (black) are denoted by asterisks on the graph

Alkyl-AMs with 5000 M_w PEG tails (Figure 2.8A, light grey) show similar trends to the aforementioned ether-AMs (Figure 2.8A, dark grey), exhibiting reduced oxLDL uptake as AM concentration and/or alkyl chain length are

increased, however, they were much more efficacious in preventing oxLDL uptake than the ether-AMs. When administered at 10^{-4} M, for example, **2.7a₅** (29 %), **2.7b₅** (4.7 %), and **2.7c₅** (1.5 %) showed significantly lower oxLDL uptake than their corresponding ether-AMs **2.5a₅** (112 %), **2.5b₅** (108 %), and **2.5c₅** (73 %). In fact, the 10^{-3} M concentrations of the 5000 M_w alkyl-AMs were so potent that less than 7 % of HMDMs were positive for any oxLDL at all (Figure 2.9A). As alkyl-AMs repressed more oxLDL uptake than analogous ether-AMs and AM potency increased with increasing aliphatic arm length, these results indicate that hydrophobicity and the length of AMs' aliphatic arms play a more significant role than hydrogen-bonding in modulating athero-protective bioactivity. Given that macrophage scavenger receptors (e.g., CD36) contain hydrophobic residues near their oxLDL binding pockets,⁴⁰ it is plausible that AMs primarily interact with scavenger receptors through hydrophobic interactions, resulting in reduced oxLDL uptake. Furthermore, previous literature suggests that the scavenger receptor ligands of different lengths exhibit varying activity, likely resulting from how the ligands arrange within the receptor pocket.⁶¹ As previous research demonstrated that increasing AM hydrophobicity does not always improve bioactivity,³⁶ it is plausible that the longer aliphatic chains arrange more favorably within scavenger receptor binding pockets through the aforementioned hydrophobic interactions.

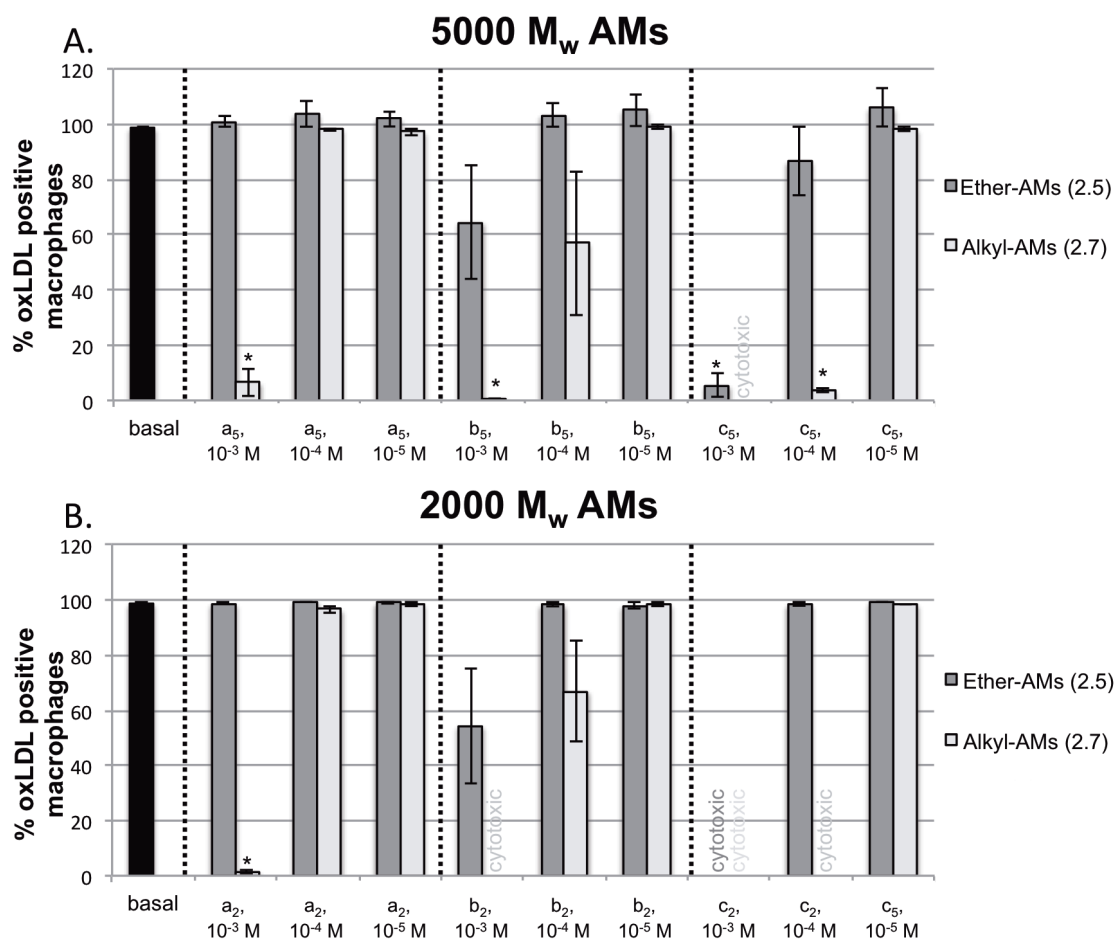


Figure 2.9. Percent of HMDMs positive for oxLDL after incubation with varying concentrations of 5000 M_w (A) and 2000 M_w (B) ether-AMs (dark grey) and alkyl-AM analogs (light grey); AMs of specific alkyl lengths are grouped between the dash lines, and the AM treatments not investigated due to cytotoxicity are indicated as text on the graph; Significant deviations from the oxLDL positive control (black) are denoted by asterisks on the graph

In comparing the 2000 M_w ether-AMs to the corresponding alkyl-AMs (Figure 2.8B), similar trends were apparent with AMs showing reduced oxLDL uptake as their concentration, hydrophobicity, and aliphatic chain length increase. Only **2.7a₂** significantly reduced the number of oxLDL positive HMDMs (1.4 %, Figure 2.9B) when administered at 10^{-3} M; fewer AM concentrations were investigated for these studies, however, due to toxicity. This data suggests that the amphiphilic balance provided by the higher molecular weight PEG chains is critical for minimizing cellular toxicity and highly hydrophobic domains are detrimental to cellular viability. Although AMs containing 2000 M_w PEG are relatively more hydrophobic than their 5000 M_w counterparts, PEG M_w did not have a pronounced effect on AM bioactivity. These results agree with previously published results, suggesting that while PEG size can modulate cytotoxicity, the AM hydrophobic domain dominates anti-atherogenic bioactivity.³⁴ While relatively high micromolar concentrations are required to achieve significant oxLDL uptake inhibition (i.e., 10^{-3} - 10^{-4} M) and may pose biocompatibility concerns, previous *in vivo* studies demonstrated that a previously synthesized AM containing a larger hydrophobic domain with a 5000 M_w PEG tail exhibits no significant toxicity in mice when administered via intraperitoneal injection at approximately 4500 μ M (2000 mg/kg).⁶² As the tested *in vivo* concentration is higher than *in vitro* concentrations used in this work, the most potent ether- and alkyl-AMs could serve as viable atherosclerosis treatments.

Collectively, these studies demonstrate that increasing hydrophobicity through longer aliphatic chains and minimal heteroatoms improves bioactivity. Although certain AM treatments, such as 10^{-4} M **2.7a₅**, exhibited a significant reduction in oxLDL uptake (29 %, Figure 2.8A), the majority of HMDMs (98 %, Figure 2.9A) were still positive for oxLDL. While this treatment reduced oxLDL uptake, oxLDL was still able to accumulate in macrophages that could, over time, elicit the atherosclerotic cascade. In comparing the dose response of the most efficacious AMs tested (Figure 2.10), **2.7c₅** is the most promising candidate for anti-atherosclerotic therapies: it has the lowest CMC value, effectively inhibits both oxLDL uptake and accumulation in macrophages at a lower concentration (10^{-4} M) than the other AMs tested, and was not cytotoxic at this concentration.

Studies assessing this candidate's *in vivo* bioactivity and biocompatibility are the focus of future work, aiming to identify an appropriate administration route that maximizes anti-atherosclerotic efficacy with minimal adverse effects.

2.3. Conclusion

Ether- and alkyl-AMs were synthesized to assess the relative contributions of hydrogen-bonding and hydrophobic interactions in oxLDL uptake inhibition in primary human macrophages. Ether-AMs displayed higher CMCs and larger hydrodynamic diameters than corresponding alkyl-AM analogs, likely due to their decreased hydrophobicity and the presence of hydrophilic moieties in the hydrophobic domain, respectively. Hydrophobicity and aliphatic chain length also played a critical role in the anti-atherogenic potential of the AMs to inhibit oxLDL accumulation, with more hydrophobic AMs (i.e., alkyl-AMs and/or AMs with longer aliphatic arms) showing a greater reduction in oxLDL uptake. However, the amphiphilic balance provided by the higher M_w PEG tails and ether moieties were beneficial for minimizing cellular toxicity. Therefore, AMs with larger PEG components (i.e., 5000 M_w PEG tails) and larger hydrophobic domains (i.e., longer alkyl chains and/or no ether moieties) were the lead candidates due to their combined biocompatibility and high oxLDL inhibition potential. These findings reinforce the significance of hydrophobicity and aliphatic chain length in modulating bioactivity, critical for the design of next-generation anti-atherogenic AMs.

2.4. Experimental

2.4.1. Materials

All reagents and solvents were purchased from Sigma-Aldrich (Milwaukee, WI) and used as received unless otherwise noted. 1 M hydrochloric acid (HCl), DBT, and polytetrafluoroethylene (PTFE) syringe filters were purchased from Fisher Scientific (Fair Lawn, NJ). Silica gel was purchased from VWR (Radnor, PA). mPEG-amine was purchased from Laysan Bio (Arab, AL) and azeotropically distilled with toluene prior to use. Reagents for cell culture, toxicity studies, and oxLDL uptake studies include human buffy coats purchased from The Blood Center of NJ (East Orange, NJ), Ficoll-Paque premium 1.077 g/mL purchased from GE Healthcare (Fairfield, CT), RPMI-1640 purchased from ATCC (Manassas, VA), macrophage colony stimulating factor (M-CSF) purchased from PeproTech (Rocky Hill, NJ), penicillin/streptomycin purchased from Lonza (Basel, Switzerland), alamarBlue® assay, fetal bovine serum (FBS) and Hoechst 33342 purchased from Life Technologies (Carlsbad, CA), unlabeled oxLDL purchased from Biomedical Technologies Inc. (Ward Hill, MA), and 3,3'-dioctadecyloxacarbocyanine- (DiO-) labeled oxLDL purchased from Kalen Biomedical (Montgomery Village, MD).

2.4.2. Characterization

NMR spectra were obtained using a Varian 400 or 500 MHz spectrophotometer. Samples were dissolved in deuterated chloroform (CDCl_3) and a few drops of dimethyl sulfoxide ($\text{DMSO}-d_6$) added, if necessary; trimethylsilane was used as an internal reference. FT-IR spectra were recorded on a Thermo Scientific Nicolet iS10 spectrophotometer using OMNIC software with an average of 32 scans. FT-IR samples were either pressed into potassium bromide (KBr) discs (1 wt % sample) or solvent-cast onto sodium chloride plates.

AM precursor molecular weights were determined using a ThermoQuest Finnigan LCQ-DUO system equipped with a syringe pump, an optional divert/inject valve, an atmospheric pressure ionization source, a mass spectrometer detector, and the Xcalibur data system. Samples were prepared at a concentration of 10 $\mu\text{g/mL}$ in MeOH or dichloromethane (DCM) using 1 % acetic acid or 1 % ammonia for positive or negative ion modes, respectively. AM M_w and polydispersity index (PDI) data were determined by GPC using a Waters LC system (Milford, MA), equipped with a 2414 refractive index detector, 1515 isocratic HPLC pump, 717plus autosampler, and a Jordi divinylbenzene mixed-bed GPC column (7.8 x 300 mm, Alltech Associates, Deerfield, IL). Samples were prepared at 10 mg/mL in DCM and filtered with 0.45 μm PTFE syringe filters prior to autoinjection. DCM was used as the eluent at a flow rate of 1 mL/min. An IBM ThinkCentre computer with WaterBreeze Version 3.20 software

was used for data collection and processing, with M_w calibrated against broad PEG standards (Waters, Milford, MA).

2.4.3. Synthesis of Ether-AMs

2.4.3.1. Synthesis of n-methoxyalkanoic acid chains (2.2)

The preparation of 8-methoxyoctanoic acid (**2.2a**) is presented as an example. According to modified literature procedures,⁶³ anhydrous MeOH (8 mL) was cooled to 0 °C, KOH (13.80 mmol) added, and the solution stirred for 30 min. A solution of 8-bromooctanoic acid (**2.1a**, 4.60 mmol) in anhydrous MeOH (7 mL) was then added via syringe. The reaction mixture was heated to reflux temperatures and stirred overnight. After cooling to room temperature, MeOH was removed *in vacuo* and the resulting crude mixture reconstituted in 1 M HCl (25 mL) and diethyl ether (5 mL). The crude product was extracted using diethyl ether (4 x 30 mL) and the combined organic layers were washed with 50:50 brine:H₂O (30 mL), dried over magnesium sulfate (MgSO₄), and the solvent removed *in vacuo*. **2.2a** was then purified on silica gel via column chromatography using a hexanes:acetic acid:ethyl acetate gradient (99.8:0.2:0 to 98:1:1).

8-methoxyoctanoic acid (2.2a). Yield: 0.70 g, 87 % (pale yellow oil). ¹H-NMR (500 MHz, CDCl₃): δ 3.32 (t, 2H, OCH₂), 3.27 (s, 3H, OCH₃), 2.26 (t, 2H, CH₂CO), 1.53 (m, 4H, CH₂), 1.27 (br, 6H, CH₂). ¹³C-NMR (500 MHz, CDCl₃): δ

179.57, 72.95, 58.51, 34.16, 29.53, 29.21, 29.14, 26.03, 24.80. FT-IR (cm^{-1} , thin film from diethyl ether): 3600-3100 (OH, COOH), 1709 (C=O, COOH). ESI-MS m/z : 173.3 [M-1].

10-methoxydecanoic acid (2.2b). Yield: 1.93 g, 84 % (light orange solid). ^1H -NMR (400 MHz, CDCl_3): δ 3.35 (t, 2H, OCH_2), 3.32 (s, 3H, OCH_3), 2.32 (t, 2H, CH_2CO), 1.57 (m, 4H, CH_2), 1.28 (br, 10H, CH_2). ^{13}C -NMR (500 MHz, CDCl_3): δ 179.53, 73.11, 58.53, 34.19, 29.64, 29.55, 29.52, 29.34, 29.21, 26.24, 24.94. FT-IR (cm^{-1} , thin film from DCM): 3600-3100 (OH, COOH), 1709 (C=O, COOH). ESI-MS m/z : 201.3 [M-1].

12-methoxydodecanoic acid (2.2c). Yield: 0.70 g, 80 % (white solid). ^1H -NMR (400 MHz, CDCl_3): δ 3.38 (t, 2H, OCH_2), 3.34 (s, 3H, OCH_3), 2.34 (t, 2H, CH_2CO), 1.60 (m, 4H, CH_2), 1.27 (br, 14H, CH_2). ^{13}C -NMR (500 MHz, CDCl_3): δ 180.08, 73.12, 58.61, 34.32, 29.77, 29.73, 29.68, 29.66, 29.59, 29.42, 29.25, 26.30, 24.90. FT-IR (cm^{-1} , KBr): 3600-3100 (OH, COOH), 1731 (C=O, COOH). ESI-MS m/z : 229.3 [M-1].

2.4.3.2. Synthesis of 2,3-bis(n-methoxyalkanoyl) DBT (2.3)

The synthesis of 2,3-bis(8-methoxyoctanoyl) DBT (**2.3a**) is presented as an example. DBT (0.67 mmol), **2.2a** (1.40 mmol), and catalytic 4-dimethylaminopyridine (DMAP, 0.13 mmol) were dissolved in anhydrous DCM (10 mL) under argon. Upon complete dissolution, EDCI (2.80 mmol) was added as a coupling reagent and the reaction was stirred overnight under argon. The

reaction mixture was diluted with DCM (25 mL) and washed with aqueous solutions of 10 % potassium bisulfite (3 x 40 mL) and saturated sodium bicarbonate (3 x 40 mL) to remove the EDCI urea byproduct and unreacted **2.2a**, respectively. The organic layer was then washed with brine (40 mL), dried over MgSO₄ and the product (**2.3a**) isolated *in vacuo*. As the product appeared as a viscous liquid for the shorter aliphatic chain lengths, yield was not calculated. Instead a two-step yield was calculated following the next synthetic step.

2,3-bis(8-methoxyoctanoyl) DBT (2.3a). Pale yellow viscous liquid. ¹H-NMR (500 MHz, CDCl₃): δ 7.32 (m, 10H, Ar-H), 5.74 (s, 2H, CH), 5.16 (dd, 4H, ArCH₂), 3.35 (t, 4H, OCH₂), 3.32 (s, 6H, OCH₃), 2.27 (quin, 2H, CH₂CO), 2.13 (quin, 2H, CH₂CO), 1.54 (m, 8H, CH₂), 1.28 (br, 12H, CH₂). ¹³C-NMR (500 MHz, CDCl₃): δ 171.25, 164.68, 133.81, 127.60, 127.59, 127.46, 71.78, 69.54, 66.62, 57.49, 32.33, 28.54, 28.01, 27.83, 24.92, 23.47. FT-IR (cm⁻¹, thin film from DCM): 1754 (C=O, ester). ESI-MS *m/z*: 665.2 [M+23].

2,3-bis(10-methoxydecanoyl) DBT (2.3b). Pale yellow viscous liquid. ¹H-NMR (500 MHz, CDCl₃): δ 7.31 (m, 10H, Ar-H), 5.75 (s, 2H, CH), 5.15 (dd, 4H, ArCH₂), 3.35 (t, 4H, OCH₂), 3.32 (s, 6H, OCH₃), 2.27 (quin, 2H, CH₂CO), 2.13 (quin, 2H, CH₂CO), 1.54 (m, 8H, CH₂), 1.25 (br, 20H, CH₂). ¹³C-NMR (500 MHz, CDCl₃): δ 172.53, 165.93, 135.04, 128.83, 128.82, 128.69, 73.11, 70.77, 67.85, 58.72, 33.61, 29.86, 29.64, 29.57, 29.35, 29.12, 26.33, 24.77. FT-IR (cm⁻¹, thin film from DCM): 1754 (C=O, ester). ESI-MS *m/z*: 721.4 [M+23].

2,3-bis(12-methoxydodecanoyl) DBT (2.3c). White solid. ¹H-NMR (500 MHz, CDCl₃): δ 7.23 (m, 10H, Ar-H), 5.68 (s, 2H, CH), 5.07 (dd, 4H, ArCH₂), 3.27

(t, 4H, OCH₂), 3.24 (s, 6H, OCH₃), 2.19 (quin, 2H, CH₂CO), 2.05 (quin, 2H, CH₂CO), 1.47 (m, 8H, CH₂), 1.17 (br, 28H, CH₂). ¹³C-NMR (500 MHz, CDCl₃): δ 172.42, 165.90, 135.07, 128.80, 128.67, 73.29, 70.84, 67.75, 58.61, 34.59, 29.87, 29.78, 29.73, 29.70, 29.62, 29.41, 29.13, 26.37, 24.77. FT-IR (cm⁻¹, KBr): 1770 (C=O, ester), 1743 (C=O, ester). ESI-MS *m/z*: 777.4 [M+23].

2.4.3.3. Synthesis of 2,3-bis(n-methoxyalkanoyl) TA (2.4)

The synthesis of 2,3-bis(8-methoxyoctanoyl) TA (**2.4a**) is presented as an example. **2.3a** (0.67 mmol, theoretical) was deprotected following modified literature procedures,^{36,64} using H₂ and a 10 % w/w Pd/C catalyst in a 1:1 DCM:MeOH solvent system (HPLC grade, 6 mL total). The reaction mixture was passed through a Celite filter using 1:1 DCM:MeOH (HPLC grade, 300 mL total) to remove the catalyst and the filtrate concentrated *in vacuo*. Pure product was precipitated from (**2.4a**) or triturated in (**2.4b** and **2.4c**) hexanes and isolated via vacuum filtration.

2,3-bis(8-methoxyoctanoyl) TA (2.4a). Two-step yield: 0.24 g, 77 % (off-white solid). ¹H-NMR (400 MHz, CDCl₃): δ 5.72 (s, 2H, CH), 3.57 (m, 2H, OCH₂), 3.49 (m, 2H, OCH₂), 3.40 (s, 6H, OCH₃), 2.59 (quin, 2H, CH₂CO), 2.39 (quin, 2H, CH₂CO), 1.66 (m, 8H, CH₂), 1.33 (m, 12H, CH₂). ¹³C-NMR (500 MHz, CDCl₃): δ 172.86, 168.10, 73.07, 70.90, 58.34, 34.06, 28.39, 28.20, 28.18, 25.55, 24.85. FT-IR (cm⁻¹, KBr): 3650 - 3300 (OH, COOH), 1762 (C=O, ester), 1736 (C=O, COOH). ESI-MS *m/z*: 461.1 [M-1].

2,3-bis(10-methoxydecanoyl) TA (2.4b). Two-step yield: 0.53 g, 85 % (white powder). $^1\text{H-NMR}$ (500 MHz, CDCl_3): δ 5.76 (s, 2H, CH), 3.46 (t, 4H, OCH_2), 3.37 (s, 6H, OCH_3), 2.45 (t, 4H, CH_2CO), 1.62 (m, 8H, CH_2), 1.31 (br, 20H, CH_2). $^{13}\text{C-NMR}$ (500 MHz, CDCl_3): δ 172.90, 168.51, 73.26, 70.74, 58.35, 33.79, 29.12, 28.87, 28.74, 28.59, 28.39, 25.76, 24.72. FT-IR (cm^{-1} , KBr): 3650 - 3300 (OH, COOH), 1760 (C=O, ester), 1736 (C=O, COOH). ESI-MS m/z : 517.3 [M-1].

2,3-bis(12-methoxydodecanoyl) TA (2.4c). Two-step yield: 0.17 g, 99 % (white powder). $^1\text{H-NMR}$ (500 MHz, CDCl_3 with $\text{DMSO-}d_6$): δ 5.69 (s, 2H, CH), 3.36 (t, 4H, OCH_2), 3.33 (s, 6H, OCH_3), 2.42 (m, 4H, CH_2CO), 1.59 (m, 8H, CH_2), 1.26 (br, 28H, CH_2). $^{13}\text{C-NMR}$ (500 MHz, CDCl_3 with $\text{DMSO-}d_6$): δ 171.89, 167.42, 72.23, 70.22, 57.85, 33.15, 29.00, 28.93, 28.89, 28.84, 28.79, 28.62, 28.36, 25.50, 24.11. FT-IR (cm^{-1} , KBr): 3650 - 3300 (OH, COOH), 1761 (C=O, ester), 1737 (C=O, COOH). ESI-MS: m/z : 573.9 [M-1].

2.4.3.4. Synthesis of ether-AMs (2.5)

The synthesis of ether-AMs is presented as an example (**2.5a₂**). Following a modified literature procedure,²⁷ **2.4a** (0.45 mmol) and catalytic DPTS (0.15 mmol) were dissolved in a mixture of anhydrous DCM (10 mL) and anhydrous dimethylformamide (DMF, 3 mL). This solution was added to 2 kDa mPEG-amine (0.15 mmol). Upon complete dissolution of PEG, DCC (1 M in DCM, 0.48 mmol) was added dropwise via syringe and the reaction stirred for 48 h at room

temperature under argon. The reaction mixture was cooled to -20 °C and the white solid precipitate (dicyclohexylurea) removed via vacuum filtration. The filtrate was then diluted with DCM (25 mL) and washed with 0.1 M HCl (1 x 40 mL) and brine (2 x 40 mL). The organic layer was dried over MgSO₄ and concentrated *in vacuo*. Ether-AM (**2.5a₂**) was then precipitated from diethyl ether (50 mL) and isolated via centrifugation (Hettich EBA 12, Beverly, MA; 1370 x g, 5 min) and the diethyl ether decanted. The product was washed with diethyl ether (50 mL x 4) and isolated with centrifugation and decanting, as above. The PEG M_w used to synthesize the ether-AMs will be denoted numerically in kiloDaltons as a subscript (e.g., **2.5a₂**).

2.5a₂. Yield: 0.28 g, 78 % (beige waxy solid). ¹H-NMR (400 MHz, CDCl₃): δ 6.79 (br, 1H, CONH), 5.62 (dd, 2H, CH), 3.63 (m, ~200H, CH₂CH₂O), 3.35 (m, ~13H, 2OCH₃, OCH₂), 2.41 (m, 4H, CH₂CO), 1.59 (m, 8H, CH₂), 1.32 (br, 12H, CH₂). M_w: 2.5 kDa; PDI 1.1.

2.5a₅. Yield: 1.34 g, 85 % (off-white powder). ¹H-NMR (400 MHz, CDCl₃): δ 6.66 (br, 1H, CONH), 5.62 (dd, 2H, CH), 3.64 (m, ~500H, CH₂CH₂O), 3.35 (m, ~13H, 2OCH₃, OCH₂), 2.42 (m, 4H, CH₂CO), 1.60 (m, 8H, CH₂), 1.33 (br, 12H, CH₂). M_w: 6.2 kDa, PDI 1.1.

2.5b₂. Yield: 0.22 g, 63 % (beige waxy solid). ¹H-NMR (500 MHz, CDCl₃): δ 6.62 (br, 1H, CONH), 5.58 (dd, 2H, CH), 3.65 (m, ~200H, CH₂CH₂O), 3.34 (m, ~13H, 2OCH₃, OCH₂), 2.44 (m, 4H, CH₂CO), 1.60 (m, 8H, CH₂), 1.30 (br, 20H, CH₂). M_w: 2.3 kDa, PDI 1.1.

2.5b₅. Yield: 0.34 g, 98 % (off-white solid). ¹H-NMR (400 MHz, CDCl₃): δ 6.70 (br, 1H, CONH), 5.58 (dd, 2H, CH), 3.64 (m, ~500H, CH₂CH₂O), 3.34 (m, ~13H, 2OCH₃, OCH₂), 2.41 (m, 4H, CH₂CO), 1.59 (m, 8H, CH₂), 1.29 (br, 20H, CH₂). M_w: 6.3 kDa, PDI 1.1.

2.5c₂. Yield: 0.27 g, 55 % (beige waxy solid). ¹H-NMR (500 MHz, CDCl₃): δ 6.90 (br, 1H, CONH), 5.56 (dd, 2H, CH), 3.65 (m, ~200H, CH₂CH₂O), 3.38 (m, ~13H, 2OCH₃, OCH₂), 2.40 (m, 4H, CH₂CO), 1.58 (m, 8H, CH₂), 1.27 (br, 28H, CH₂). M_w: 2.6 kDa, PDI 1.1.

2.5c₅. Yield: 0.13 g, 78 % (off-white solid). ¹H-NMR (500 MHz, CDCl₃): δ 6.67 (br, 1H, NH), 5.54 (dd, 2H, CH), 3.65 (m, ~500H, CH₂CH₂O), 3.38 (m, ~13H, 2OCH₃, OCH₂), 2.41 (m, 4H, CH₂CO), 1.60 (m, 8H, CH₂), 1.27 (br, 28H, CH₂). M_w: 6.4 kDa, PDI 1.1.

2.4.4. Synthesis of Alkyl-AMs

2.4.4.1. Synthesis of aliphatic TA derivatives (2.6)

The synthesis of aliphatic TA derivatives is presented as an example (**2.6a**). Aliphatic TA derivatives were synthesized following a modified literature procedure.⁶⁵ In brief, TA (7.00 mmol) and zinc chloride (2.20 mmol) were suspended neat in decanoyl chloride (52.50 mmol) and heated to 95 °C. After stirring 24 h, the reaction mixture was cooled to room temperature and quenched with H₂O (30 mL) and diethyl ether (100 mL), then vigorously stirred for 30 min.

This solution was washed with H₂O (5 x 100 mL) and the organic layer concentrated *in vacuo* to yield a viscous brown liquid. Pure product (**2.6**) was precipitated from 1 L stirring hexanes and isolated via vacuum filtration. The length of the product's aliphatic chains will be indicated by the lettering **a-c**, with a given TA derivative (e.g., **2.6a**) having aliphatic chains of analogous length to the previously discussed n-methoxyalkanoyl derivatives (e.g., **2.4a**).

2.6a. Yield: 2.46 g, 77 % (off-white powder). ¹H-NMR (500 MHz, CDCl₃): δ 5.76 (s, 2H, CH), 2.44 (m, 4H, CH₂CO), 1.65 (m, 4H, CH₂), 1.27 (br, 24H, CH₂), 0.88 (t, 6H, CH₃). ¹³C-NMR (500 MHz, CDCl₃): δ 172.74, 172.00, 70.19, 33.80, 32.09, 29.63, 29.49, 29.41, 29.17, 24.85, 22.89, 14.31. ESI-MS *m/z*: 457.0 [M-1].

2.6b. Yield: 2.22 g, 74 % (off-white powder). ¹H-NMR (500 MHz, CDCl₃): δ 5.76 (s, 2H, CH), 2.43 (m, 4H, CH₂CO), 1.64 (m, 4H, CH₂), 1.26 (br, 32H, CH₂), 0.87 (t, 6H, CH₃). ¹³C-NMR (500 MHz, CDCl₃): δ 172.68, 172.12, 70.20, 33.78, 32.14, 29.85, 29.68, 29.58, 29.43, 29.18, 24.86, 22.91, 14.32. ESI-MS *m/z*: 513.1 [M-1].

2.6c. Yield: 3.51 g, 89 % (off-white powder). ¹H-NMR (500 MHz, CDCl₃ with DMSO-*d*₆): δ 5.66 (s, 2H, CH), 2.40 (m, 4H, CH₂CO), 1.63 (m, 4H, CH₂), 1.26 (br, 40H, CH₂), 0.88 (t, 6H, CH₃). ¹³C-NMR (500 MHz, CDCl₃ with DMSO-*d*₆): δ 172.61, 168.15, 70.91, 33.85, 31.96, 29.74, 29.71, 29.70, 29.69, 29.53, 29.40, 29.33, 29.08, 24.80, 22.73, 14.22. ESI-MS *m/z*: 569.1 [M-1].

2.4.4.2. Synthesis of alkyl-AMs (2.7)

The synthesis of alkyl-AMs is presented as an example (**2.7a₂**). Alkyl-AMs were prepared in the same manner as were the previously discussed ether-AMs, using **2.6a** (0.50 mmol), DPTS (0.17 mmol), mPEG-amine (0.17 mmol), and DCC (0.53 mmol). Additional anhydrous DMF was used if necessary to fully solubilize **2.6** prior to adding it to mPEG-amine. The PEG M_w used to synthesize the alkyl-AM will also be denoted numerically in kiloDaltons as a subscript (e.g., **2.7a₂**).

2.7a₂. Yield: 0.25 g, 60 % (off-white waxy solid). $^1\text{H-NMR}$ (400 MHz, CDCl_3): δ 6.97 (br, 1H, CONH), 5.55 (dd, 2H, CH), 3.65 (m, ~200H, OCH_2), 3.39 (s, 3H, OCH_3), 2.40 (m, 4H, CH_2CO), 1.62 (m, 4H, CH_2), 1.26 (br, 24H, CH_2), 0.88 (t, 6H, CH_3). M_w : 1.9 kDa, PDI 1.1.

2.7a₅. Yield: 0.40 g, quantitative (off-white solid). $^1\text{H-NMR}$ (400 MHz, CDCl_3): δ 6.90 (br, 1H, CONH), 5.53 (dd, 2H, CH), 3.66 (m, ~500H, OCH_2), 3.38 (s, 3H, OCH_3), 2.39 (m, 4H, CH_2CO), 1.63 (m, 4H, CH_2), 1.26 (br, 24H, CH_2), 0.88 (t, 6H, CH_3). M_w : 5.3 kDa, PDI 1.1.

2.7b₂. Yield: 0.30 g, 60 % (off-white waxy solid). $^1\text{H-NMR}$ (400 MHz, CDCl_3): δ 6.84 (br, 1H, CONH), 5.54 (dd, 2H, CH), 3.66 (m, ~200H, OCH_2), 3.38 (s, 3H, OCH_3), 2.40 (m, 4H, CH_2CO), 1.62 (m, 4H, CH_2), 1.25 (br, 32H, CH_2), 0.88 (t, 6H, CH_3). M_w : 2.1 kDa, PDI 1.1.

2.7b₅. Yield: 0.36 g, quantitative (off-white solid). $^1\text{H-NMR}$ (400 MHz, CDCl_3): δ 6.85 (br, 1H, CONH), 5.56 (dd, 2H, CH), 3.65 (m, ~500H, OCH_2), 3.38 (s, 3H, OCH_3), 2.41 (m, 4H, CH_2CO), 1.61 (m, 4H, CH_2), 1.25 (br, 32H, CH_2), 0.89 (t, 6H, CH_3). M_w : 5.4 kDa, PDI 1.1.

2.7c₂. Yield: 0.28 g, 55 % (off-white waxy solid). ¹H-NMR (500 MHz, CDCl₃): δ 6.91 (br, 1H, CONH), 5.55 (dd, 2H, CH), 3.66 (m, ~200H, OCH₂), 3.38 (s, 3H, OCH₃), 2.41 (m, 4H, CH₂CO), 1.62 (m, 4H, CH₂), 1.26 (br, 40H, CH₂), 0.88 (t, 6H, CH₃). M_w: 2.1 kDa, PDI 1.1.

2.7c₅. Yield: 0.50 g, quantitative (off-white solid). ¹H-NMR (400 MHz, CDCl₃): δ 6.92 (br, 1H, CONH), 5.53 (dd, 2H, CH), 3.64 (m, ~500H, OCH₂), 3.38 (s, 3H, OCH₃), 2.40 (m, 4H, CH₂CO), 1.62 (m, 4H, CH₂), 1.25 (br, 40H, CH₂), 0.88 (t, 6H, CH₃). M_w: 5.8 kDa, PDI 1.1.

2.4.5. Critical Micelle Concentration Measurements

AMs were dissolved in HPLC grade H₂O and diluted to a series of concentrations ranging from 1×10^{-3} to 1×10^{-10} M. Separately, a stock solution of pyrene was prepared in HPLC grade acetone (5×10^{-6} M) and 0.5 mL of this solution was added to a series of vials. Acetone was removed *in vacuo* and AM solutions (5 mL) were added. AM-pyrene solutions were incubated for 48 h at 37 °C with gentle agitation (60 rpm) to allow pyrene to partition into the AM micelles. Fluorescence studies were then conducted on a RF-5301PC spectrofluorometer (Shimadzu Scientific Instruments, Columbia, Maryland), using pyrene as the fluorescent probe. Emission was measured from 300 – 360 nm with a 390 nm excitation wavelength. Upon micelle formation, pyrene partitions into the micelle hydrophobic core and the maximum wavelength emission shifts from 332 nm to 334.5 nm. The ratio of absorption of pyrene in micelles (334.5 nm) to pyrene

alone (332 nm) was thus plotted against the logarithm of AM concentration, and the inflection point of this curve was taken as the CMC.²⁷

2.4.6. Dynamic Light Scattering Measurements

DLS analysis was performed on Zetasizer Nano ZS90 instrument (Malvern Instruments, Southboro, MA) in triplicate with a 90° scattering angle. AM samples were dissolved in HPLC grade H₂O (10 mg/mL) and equilibrated for 24 h at 37 °C with gentle agitation (60 rpm). Solutions were passed through 0.45 µm PTFE syringe filters prior to size measurements and Z-average sizes were collected and analyzed.

2.4.7. Cell Culture

[Cell culture was performed by Dr. Latrisha Petersen, Department of Biomedical Engineering, Rutgers University, Piscataway, NJ]

PBMCs were isolated from human buffy coats (Blood Center of New Jersey; East Orange, NJ) by centrifugation through a Ficoll-Paque density gradient (GE Healthcare). PBMCs were plated into T-175 flasks, and monocytes selected via adherence after 24 h. Monocytes were cultured for 7 d in RPMI 1640 (ATCC) supplemented with 10 % FBS, 1 % penicillin/streptomycin, and 50 ng/mL M-CSF for differentiation into HMDMs.^{32,37}

2.4.8. Cell Viability Studies

[Cell viability studies were performed by Dr. Latrisha Petersen, Department of Biomedical Engineering, Rutgers University, Piscataway, NJ]

To screen cellular toxicity of the AMs, the alamarBlue assay was carried out according to manufacturer's protocol. In brief, HMDMs were plated in a 96-well plate at 150,000 cells/mL in basal media (RPMI 1640 supplemented with 10 % FBS and 1 % penicillin/streptomycin) and allowed to rest for 24 h. Cells were then treated with the desired concentration of AM (10^{-5} - 10^{-3} M) diluted in basal media for 24 h. Following incubation, the treatment (media containing specific AM concentrations) was removed and alamarBlue (diluted 1 to 10 in basal media) was added to each well and cells incubated for 24 h. The supernatant was then transferred to a new plate and absorbance read on a spectrophotometer (Infinite 200 Pro, Tecan, Männedorf, Switzerland) at 570 and 600 nm.

2.4.9. OxLDL Uptake by Macrophages

[OxLDL uptake studies were performed under the guidance of Dr. Latrisha Petersen, Department of Biomedical Engineering, Rutgers University, Piscataway, NJ]

HMDMs were co-cultured with DiO-labeled oxLDL (1 $\mu\text{g/mL}$) and unlabeled oxLDL (4 $\mu\text{g/mL}$) with or without different AM concentrations, ranging from 10^{-5} - 10^{-3} M, in basal media (RPMI 1640 supplemented with 10 % FBS and 1 % penicillin/streptomycin) for 24 h. Treatments were then removed and replaced with cold phosphate buffered saline (PBS) and placed on ice packs. HMDMs were removed from wells by vigorous pipetting and transferred to 5 mL tubes, centrifuged at 1000 rpm for 10 min, and fixed in 1 % paraformaldehyde (150 μL). The oxLDL fluorescence associated with HMDMs was quantified on a FACScalibur (Becton Dickinson, Franklin Lakes, NJ) flow cytometer, collecting 10,000 events/sample, and analyzed with Flow Jo software (Treestar, Ashland, OR). This study included a minimum of 3 experimental replicates. Data is presented as % oxLDL uptake as determined by the following equation:

$$\% \text{ oxLDL Uptake} = 100 * \frac{\text{DiO oxLDL MFI of treatment sample}}{\text{DiO oxLDL MFI of oxLDL only control sample}}$$

2.4.10. Statistical Analysis

OxLDL uptake studies were conducted in experimental triplicate. The results were then evaluated using a Student's t-Test, with significance criteria assuming a 95 % confidence level ($P < 0.05$). Standard error of the mean is reported in the form of error bars on the graphs of the final data.

2.5. References

1. Orford, J. L.; Selwyn, A. P.; Ganz, P.; Popma, J. J.; Rogers, C. *American Journal of Cardiology* **2000**, 86, 6H.
2. Ross, R. *N. Engl. J. Med.* **1999**, 340, 115.
3. Li, A. C.; Glass, C. K. *Nature Medicine* **2002**, 8, 1235.
4. Pirillo, A.; Norata, G. D.; Catapano, A. L. *Mediators of inflammation* **2013**, 12.
5. Yu, X.-H.; Fu, Y.-C.; Zhang, D.-W.; Yin, K.; Tang, C.-K. *Clinica Chimica Acta* **2013**, 424, 245.
6. Saha, P.; Modarai, B.; Humphries, J.; Mattock, K.; Waltham, M.; Burnand, K. G.; Smith, A. *Current Opinion in Pharmacology* **2009**, 9, 109.
7. Choudhury, R. P.; Lee, J. M.; Greaves, D. R. *Nature Clinical Practice Cardiovascular Medicine* **2005**, 2, 309.
8. Steinberg, D. *Journal of Biological Chemistry* **1997**, 272, 20963.
9. Tiwari, R. L.; Singh, V.; Barthwal, M. K. *Medicinal Research Reviews* **2008**, 28, 483.
10. Iverson, N. M. *Multifunctional polymers for inhibition of oxidized lipoprotein accumulation and inflammation in macrophage cells*, 2010.
11. Plourde, N. M. *Structure-binding activity relations of amphiphilic polymers and macrophage scavenger receptors*, 2010.
12. Ahmad, S.; Madsen, C. S.; Stein, P. D.; Janovitz, E.; Huang, C.; Ngu, K.; Bisaha, S. R.; Kennedy, L. J.; Chen, B. C.; Zhao, R. L.; Sitkoff, D.; Monshizadegan, H.; Yin, X.; Ryan, C. S.; Zhang, R. G.; Giancarli, M.; Bird, E.; Chang, M.; Chen, X.; Setters, R.; Search, D.; Zhuang, S. B.; Nguyen-Tran, V.; Cuff, C. A.; Harrity, T.; Darienzo, C. J.; Li, T.; Reeves, R. A.; Blonar, M. A.; Barrish, J. C.; Zahler, R.; Robl, J. A. *J. Med. Chem.* **2008**, 51, 2722.
13. Maron, D. J.; Fazio, S.; Linton, M. F. *Circulation* **2000**, 101, 207.
14. Golomb, B. A.; Evans, M. A. *Am. J. Cardiovasc. Drugs* **2008**, 8, 373.
15. Wang, W.; Xie, H.; Sun, L.; Ou, L.; Wang, L.; Yu, Y.; Kong, D. *Biomedical Materials* **2009**, 4.

16. Ma, K.-w.; Dai, X.-z.; Feng, S.-y.; Jing, A.-h.; Yang, J.-y. *Transfusion and Apheresis Science* **2011**, *44*, 3.
17. Robinson, J. G. *Journal of managed care pharmacy : JMCP* **2013**, *19*, 139.
18. Page, M. M.; Bell, D. A.; Hooper, A. J.; Watts, G. F.; Burnett, J. R. *Best practice & research. Clinical endocrinology & metabolism* **2014**, *28*, 387.
19. Li, J.; Hou, Y.; Chen, X.; Ding, X.; Liu, Y.; Shen, X.; Cai, K. *Journal of Materials Science-Materials in Medicine* **2014**, *25*, 1055.
20. Heuck, C.-C. *German medical science : GMS e-journal* **2011**, *9*, Doc02.
21. Cao, Y.; Wang, H.; Yang, C.; Zhong, R.; Lei, Y.; Sun, K.; Liu, J. *Applied Surface Science* **2011**, *257*, 7521.
22. Taseva, K.; Fischer, S.; Passauer, J.; Weiss, N.; Bornstein, S. R.; Julius, U. *Atherosclerosis Supplements* **2013**, *14*, 45.
23. Goyal, T.; Mitra, S.; Khaidakov, M.; Wang, X. W.; Singla, S.; Ding, Z. F.; Liu, S. J.; Mehta, J. L. *Curr. Atherosclerol. Rep.* **2012**, *14*, 150.
24. Febbraio, M.; Podrez, E. A.; Smith, J. D.; Hajjar, D. P.; Hazen, S. L.; Hoff, H. F.; Sharma, K.; Silverstein, R. L. *J. Clin. Invest.* **2000**, *105*, 1049.
25. Suzuki, H.; Kurihara, Y.; Takeya, M.; Kamada, N.; Kataoka, M.; Jishage, K.; Ueda, O.; Sakaguchi, H.; Higashi, T.; Suzuki, T.; Takashima, Y.; Kawabe, Y.; Cynshi, O.; Wada, Y.; Honda, M.; Kurihara, H.; Aburatani, H.; Doi, T.; Matsumoto, A.; Azuma, S.; Noda, T.; Toyoda, Y.; Itakura, H.; Yazaki, Y.; Horiuchi, S.; Takahashi, K.; Kruijt, J. K.; vanBerkel, T. J. C.; Steinbrecher, U. P.; Ishibashi, S.; Maeda, N.; Gordon, S.; Kodama, T. *Nature* **1997**, *386*, 292.
26. Chnari, E.; Nikitzuk, J. S.; Wang, J.; Uhrich, K. E.; Moghe, P. V. *Biomacromolecules* **2006**, *7*, 1796.
27. Tian, L.; Yam, L.; Zhou, N.; Tat, H.; Uhrich, K. E. *Macromolecules* **2004**, *37*, 538.
28. Yamamoto, Y.; Nagasaki, Y.; Kato, Y.; Sugiyama, Y.; Kataoka, K. *Journal of Controlled Release* **2001**, *77*, 27.
29. Chnari, E.; Lari, H. B.; Tian, L.; Uhrich, K. E.; Moghe, P. V. *Biomaterials* **2005**, *26*, 3749.

30. Iverson, N. M.; Plourde, N. M.; Sparks, S. M.; Wang, J. Z.; Patel, E. N.; Shah, P. S.; Lewis, D. R.; Zablocki, K. R.; Nackman, G. B.; Uhrich, K. E.; Moghe, P. V. *Biomaterials* **2011**, 32, 8319.
31. Plourde, N. M.; Kortagere, S.; Welsh, W.; Moghe, P. V. *Biomacromolecules* **2009**, 10, 1381.
32. York, A. W.; Zablocki, K. R.; Lewis, D. R.; Gu, L.; Uhrich, K. E.; Prud'homme, R. K.; Moghe, P. V. *Adv. Mater.* **2012**, 24, 733.
33. Wang, J.; Plourde, N. M.; Iverson, N.; Moghe, P.; Uhrich, K. E. *Int. J. Nanomed.* **2007**, 2, 697.
34. Iverson, N. M.; Sparks, S. M.; Demirdirek, B.; Uhrich, K. E.; Moghe, P. V. *Acta Biomaterialia* **2010**, 6, 3081.
35. Hehir, S.; Plourde, N. M.; Gu, L.; Poree, D. E.; Welsh, W. J.; Moghe, P. V.; Uhrich, K. E. *Acta Biomaterialia* **2012**, 8, 3956.
36. Poree, D. E.; Zablocki, K.; Faig, A.; Moghe, P. V.; Uhrich, K. E. *Biomacromolecules* **2013**, 14, 2463.
37. Lewis, D. R.; Kholodovych, V.; Tomasini, M. D.; Abdelhamid, D.; Petersen, L. K.; Welsh, W. J.; Uhrich, K. E.; Moghe, P. V. *Biomaterials* **2013**, 34, 7950.
38. Platt, N.; Gordon, S. *J. Clin. Invest.* **2001**, 108, 649.
39. Ohki, I.; Ishigaki, T.; Oyama, T.; Matsunaga, S.; Xie, Q. H.; Ohnishi-Kameyama, M.; Murata, T.; Tsuchiya, D.; Machida, S.; Morikawa, K.; Tate, S. *Structure* **2005**, 13, 905.
40. Collot-Teixeira, S.; Martin, J.; McDennott-Roe, C.; Poston, R.; McGregor, J. L. *Cardiovascular research* **2007**, 75, 468.
41. Boullier, A.; Bird, D. A.; Chang, M. K.; Dennis, E. A.; Friedman, P.; Gillotte-Taylor, K.; Horkko, S.; Palinski, W.; Quehenberger, O.; Shaw, P.; Steinberg, D.; Terpstra, V.; Witztum, J. L. In *Atherosclerosis VI*; Numano, F., Gimbrone, M. A., Eds.; New York Acad Sciences: New York, 2001; Vol. 947, p 214.
42. Chisolm, G. M.; Steinberg, D. *Free Radical Biology and Medicine* **2000**, 28, 1815.
43. Podrez, E. A.; Poliakov, E.; Shen, Z. Z.; Zhang, R. L.; Deng, Y. J.; Sun, M. J.; Finton, P. J.; Shan, L.; Gugiu, B.; Fox, P. L.; Hoff, H. F.; Salomon, R. G.; Hazen, S. L. *Journal of Biological Chemistry* **2002**, 277, 38503.

44. Li, J. J. In *Name Reactions*; Springer: 2014, p 628.
45. Rosen, M. J.; Kunjappu, J. T. *Surfactants and interfacial phenomena*; John Wiley & Sons, 2012.
46. Kim, S.; Shi, Y.; Kim, J. Y.; Park, K.; Cheng, J.-X. *Expert opinion on drug delivery* **2010**, 7, 49.
47. Yang, J. S.; Zhou, Q. Q.; He, W. *Carbohydr. Polym.* **2013**, 92, 223.
48. Hamley, I. W. *Block copolymers in solution: fundamentals and applications*; Wiley, 2005.
49. Cai, C.; Zhu, W.; Chen, T.; Lin, J.; Tian, X. *Journal of Polymer Science Part a-Polymer Chemistry* **2009**, 47, 5967.
50. Owen, S. C.; Chan, D. P. Y.; Shoichet, M. S. *Nano Today* **2012**, 7, 53.
51. Xiao, M. Y.; Xia, G. J.; Wang, R.; Xie, D. Q. *Soft Matter* **2012**, 8, 7865.
52. Gao, H. J.; Liu, J. J.; Yang, C. H.; Cheng, T. J.; Chu, L. P.; Xu, H. Y.; Meng, A. M.; Fan, S. J.; Shi, L. Q.; Liu, J. F. *Int. J. Nanomed.* **2013**, 8, 4229.
53. Gao, Z. G.; Lukyanov, A. N.; Singhal, A.; Torchilin, V. P. *Nano Lett.* **2002**, 2, 979.
54. Cox, J. H.; Ferrari, G.; Bailer, R. T.; Koup, R. A. *Journal of the Association for Laboratory Automation* **2004**, 9, 16.
55. Nogueira, D. R.; Moran, M. C.; Mitjans, M.; Martinez, V.; Perez, L.; Vinardell, M. P. *Eur. J. Pharm. Biopharm.* **2013**, 83, 33.
56. Halets, I.; Shcharbin, D.; Klajnert, B.; Bryszewska, M. *Int. J. Pharm.* **2013**, 454, 1.
57. Richards, D.; Ivanisevic, A. *Chem. Soc. Rev.* **2012**, 41, 2052.
58. Gaucher, G.; Dufresne, M. H.; Sant, V. P.; Kang, N.; Maysinger, D.; Leroux, J. C. *Journal of controlled release : official journal of the Controlled Release Society* **2005**, 109, 169.
59. Savic, R.; Azzam, T.; Eisenberg, A.; Maysinger, D. *Langmuir* **2006**, 22, 3570.
60. Chen, H.; Kim, S.; He, W.; Wang, H.; Low, P. S.; Park, K.; Cheng, J. X. *Langmuir* **2008**, 24, 5213.

61. Guaderrama-Diaz, M.; Solis, C. F.; Velasco-Loyden, G.; Laclette, J.; Mas-Oliva, J. *Mol. Cell. Biochem.* **2005**, 271, 123.
62. Lewis, D. R. PhD Thesis, Rutgers University, 2014.
63. Goodman, M. M.; Callahan, A. P.; Knapp, F. F. *J. Med. Chem.* **1985**, 28, 807.
64. Ihre, H.; De Jesus, O. L. P.; Frechet, J. M. J. *Journal of the American Chemical Society* **2001**, 123, 5908.
65. Tian, L. PhD Thesis, Rutgers University, 2004.

3. BISCATIONIC TARTARIC ACID-BASED AMPHIPHILES: CHARGE LOCATION IMPACTS ANTIMICROBIAL ACTIVITY

[This work is in preparation for publication, under the title “Biscationic Tartaric Acid-Based Amphiphiles: Charge Location Impacts Antimicrobial Activity.” Timothy D. Arthur, Patrick O. Fitzgerald, Michael L. Chikindas, Evan Mintzer, and Kathryn E. Uhrich are co-authors for this work.]

3.1. Introduction

The development of antibiotic-resistant bacteria is a prevalent concern that has prompted the development of new antimicrobial agents.¹⁻⁴ As an alternative to conventional antibiotics, antimicrobial peptides (AMPs) have received widespread attention. Many of the naturally occurring AMPs elicit antibacterial activity by targeting the cellular membrane.¹⁻³ Although these peptides have diverse primary structures, many exhibit a net cationic charge and facially amphiphilic secondary structure in which hydrophobic and hydrophilic domains exist on opposite ‘faces’ of the molecule;⁵ it is the cationic, amphiphilic character that appears to give rise to AMPs’ unique mechanism of action.¹⁻³ These AMPs first interact with negatively charged bacterial membranes via electrostatic interactions.^{2,6} After the initial interaction, AMPs’ hydrophobic domains interact with the hydrophobic membrane interior, ultimately disrupting

the membrane and resulting in cell death.^{2,6} Owing to their membrane-targeting activity, AMPs exhibit reduced instances of bacterial resistance and are promising antibiotic alternatives.^{2,7,8} High production costs and instability in the presence of proteases, however, has limited their clinical application.^{3,9,10}

In an effort to overcome AMPs' current drawbacks, many researchers have synthesized peptidomimetic compounds containing AMPs' key physicochemical properties, namely a net cationic charge and amphiphilic structure. LaDow et al. developed a series of aryl-based bicephalic amphiphiles (two cationic heads, one hydrophobic tail, Figure 3.1) of varying hydrocarbon tail length and determined that bicephalic compounds were more likely to be effective against both gram-positive and gram-negative bacteria than conventional monocationic amphiphiles.¹¹ Building upon this work, Grenier et al. designed a series of bipyridinium-based gemini amphiphiles (two cationic heads, two hydrophobic tails, Figure 3.1) that demonstrated improved antimicrobial activity over bicephalic amphiphiles, with optimum activity occurring at intermediate hydrocarbon tail lengths.⁷ Further, Mondal et al. conjugated cationic lysine residues onto glucose to generate bicephalic amphiphiles that may mimic peptide post-translational modifications of AMPs.¹² In addition to investigating small molecule amphiphiles as antimicrobial agents, researchers have also studied oligomers¹³ and polymers^{9,14-16} in an attempt to develop potent bioactives. Paslay et al., for instance, developed a series of poly(methacrylamide) (co)polymers which demonstrated increasing antimicrobial activity with increasing primary amine content.¹⁴



Figure 3.1. Representation of different amphiphile architectures investigated for antimicrobial applications; Cationic groups are depicted in blue while hydrophobic regions are depicted in red

In evaluating the diverse array of antimicrobial peptides and amphiphiles that have been developed, one trend becomes apparent: antimicrobial activity is largely influenced by a molecule's hydrophobic-to-charge ratio.^{2,7,11,15,16} Very few studies, however, have compared amphiphiles possessing identical hydrophobic-to-charge ratios with varying charge locations. Studies by LaDow et al. revealed that the spacing between cationic charges on structurally similar bicephalic amphiphiles, containing the same hydrophobic-to-charge ratio, does influence antimicrobial activity.¹¹ Within this work, the approach was expanded by not only exploring the specific impact of charge location on cationic amphiphiles' antimicrobial activity, but also delving into amphiphiles' specific membrane activity.

To investigate this correlation, two series of sugar-based biscationic amphiphiles were synthesized with varying charge locations and varying, yet equivalent, hydrophobic-to-charge ratios. Each series had differing amphiphile architectures as a result of their charge location. Whereas one series more

closely resembled gemini amphiphiles (two heads, two tails, Figure 3.2), which have been widely investigated for antimicrobial applications,^{7,17,18} the other was more bolaamphiphilic (two heads connected via one tail, Figure 3.2). We hypothesized that the gemini-like amphiphiles would exhibit improved antimicrobial activity compared to the bola-like amphiphiles due to their more facially amphiphilic structure and that each series' antimicrobial activity would increase with increasing hydrophobic-to-charge ratio due to enhanced hydrophobic interactions, leading to membrane permeabilization. Upon successful synthesis of all amphiphiles, their antimicrobial activity was assessed against gram-negative and gram-positive bacteria. The lead compounds were further evaluated, specifically, their interactions with model membranes via Langmuir monolayer techniques and isothermal titration calorimetry (ITC) were measured.

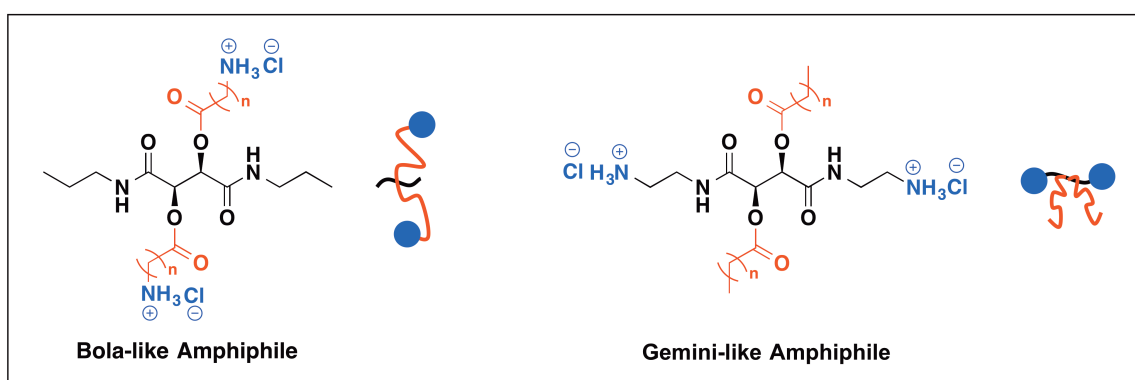


Figure 3.2. Chemical structures and representations of bola-like (left) and gemini-like (right) cationic amphiphiles

3.2. Results and Discussion

3.2.1. Synthesis and Characterization

To explore the impact of charge location on antimicrobial activity, two series of cationic amphiphiles (gemini- and bola-like) were synthesized with equivalent hydrophobic-to-charge ratios (Figure 3.2). Both series employed tartaric acid, an inexpensive naturally occurring compound produced in fruits,¹⁹ as a backbone that could provide two distinct chemical moieties for further modification. By altering the charge location on these tartaric acid-based molecules, two structurally diverse amphiphile series were developed.

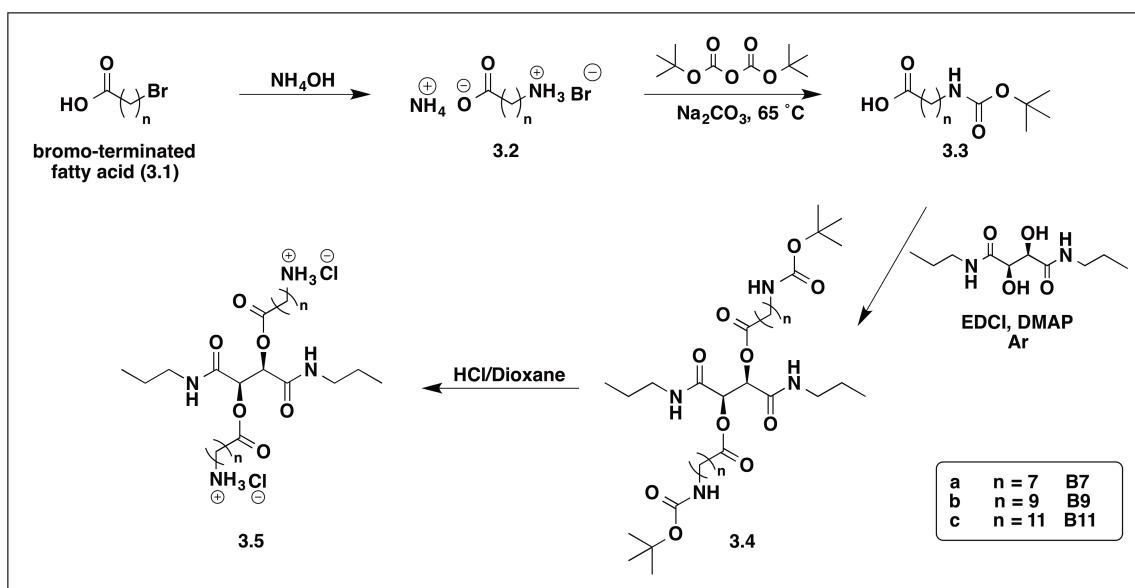


Figure 3.3. Synthetic scheme for bola-like amphiphiles; Final amphiphile structures are denoted as **B7**, **B9**, or **B11** depending on the number of methylenes within their hydrophobic domain

Bola-like amphiphiles resulted when cationic charges were incorporated at the terminal ends of hydrophobic acyl arms (Figure 3.3). This series was synthesized by first reacting bromo-containing alkanolic acids (**3.1**) with concentrated ammonium hydroxide to generate amine-terminated alkanolic acid intermediates (**3.2**). The amine-terminated alkanolic acids were then tert-butyloxycarbonyl- (Boc-) protected (**3.3**) using di-tert-butyl dicarbonate. Initial attempts to generate **3.4** involved coupling **3.3** to a dibenzyl tartrate (DBT) backbone, deprotecting the benzyl groups to yield a diacid, and subsequently coupling the diacid to propylamine (2 eq). While DBT coupling and deprotection were successful, a suitable condition for propyl amine coupling was not identified. As an alternative, an N,N-dipropyl tartramide (PT) backbone was synthesized according to literature procedures.²⁰ **3.3** was then coupled to this PT backbone using carbodiimide coupling to generate **3.4**. Following successful acylation, **3.4** was deprotected using hydrochloric acid (HCl) in dioxane to generate the final bola-like amphiphiles (**3.5**, Figure 3.3) as chloride salts.

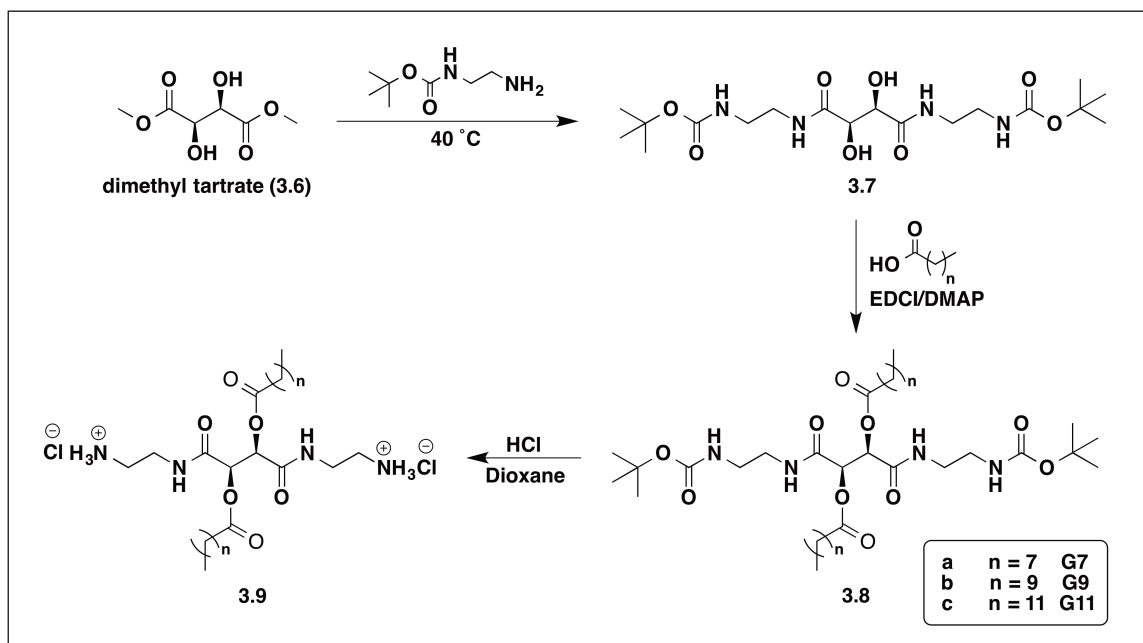


Figure 3.4. Synthetic scheme for gemini-like amphiphiles; Final amphiphile structures are denoted as **G7**, **G9**, or **G11** depending on the number of methylenes within their hydrophobic domain

A series of gemini-like amphiphiles was synthesized by incorporating cationic charges at the tartaric acid backbone. These amphiphiles possessed analogous molecular weights, chemical moieties (e.g., number of amine moieties or methylene units), and hydrophobic-to-charge ratios as the bola-like amphiphiles, differing only in their charge location. To synthesize these molecules, dimethyl tartrate was first reacted with N-Boc-ethylenediamine via an aminolysis reaction to generate **3.7** (Figure 3.4). **3.7** was then acylated with alkanolic acids of varying hydrophobic chain lengths using carbodiimide coupling and the Boc protecting groups removed using HCl in dioxane to generate the final amphiphile structures (**3.9**, Figure 3.4).

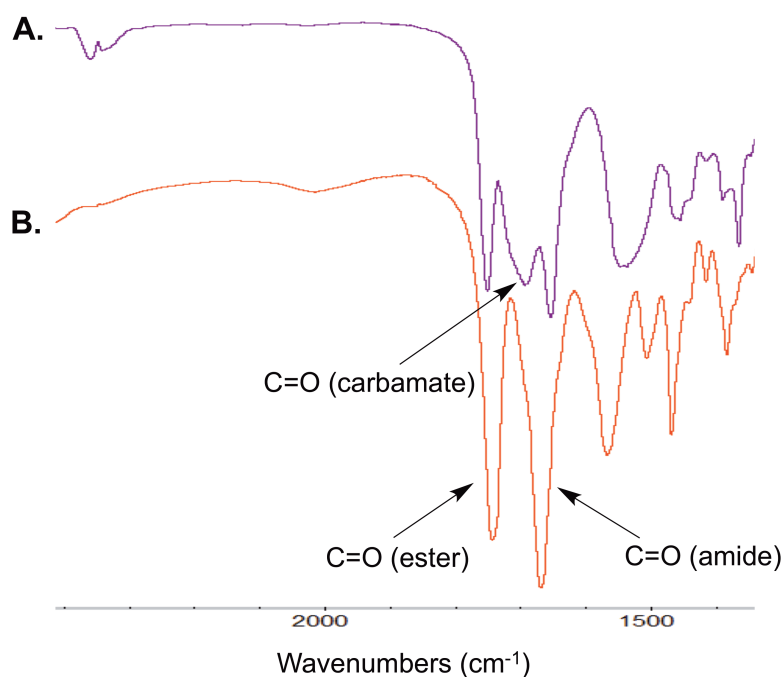


Figure 3.5. FT-IR spectra showing the carbonyl region for **B11** synthesis as an example: **3.4c** (A) and **B11 (3.5c)**, B)

All amphiphiles' and intermediates' chemical structures were confirmed via nuclear magnetic resonance (NMR) and Fourier-transform infrared (FT-IR) spectroscopies and mass spectrometry (MS). Both NMR and FT-IR spectroscopy were especially useful in confirming the synthesis of the final amphiphile structures (**3.5** and **3.9**). Figure 3.5 and Figure 3.6 present FT-IR and NMR data for **B11 (3.5c)** and **G11 (3.9c)**, respectively, as examples. The FT-IR spectra indicate that the bola-like amphiphile precursor **3.4c**, contains three distinct carbonyl moieties: ester, carbamate, and amide (Figure 3.5A). After deprotection, no carbamate group is present yet the ester and amide carbonyls

remain intact (Figure 3.5B), indicating that the Boc groups have been removed without influencing the amphiphile backbone structure, ultimately yielding the final bola-like amphiphile **B11**. Similarly, a representative proton (^1H) NMR spectrum for the gemini-like amphiphile synthesis shows a large singlet at 1.44 ppm (a in Figure 3.6A) indicative of the methyl protons in **3.8c**'s Boc protecting group. Upon deprotection (Figure 3.6B), this singlet disappears, suggesting successful **G11** synthesis. Furthermore, the backbone methylenes (c and c' in Figure 3.6) split after deprotection, depicting the change in the methylenes' chemical environment upon removal of Boc groups. MS served to reinforce FT-IR and NMR results and further confirm successful amphiphile synthesis.

Once the synthesis of all amphiphiles was confirmed, antimicrobial activity was screened using the disk diffusion method. Within this method, bacteria are grown on agar plates in the presence of paper disks that have been impregnated

with varying concentrations of test compound.²¹ If the compounds have antibacterial activity they prevent bacterial growth as they diffuse away from the paper disks, exhibiting zones of inhibition.

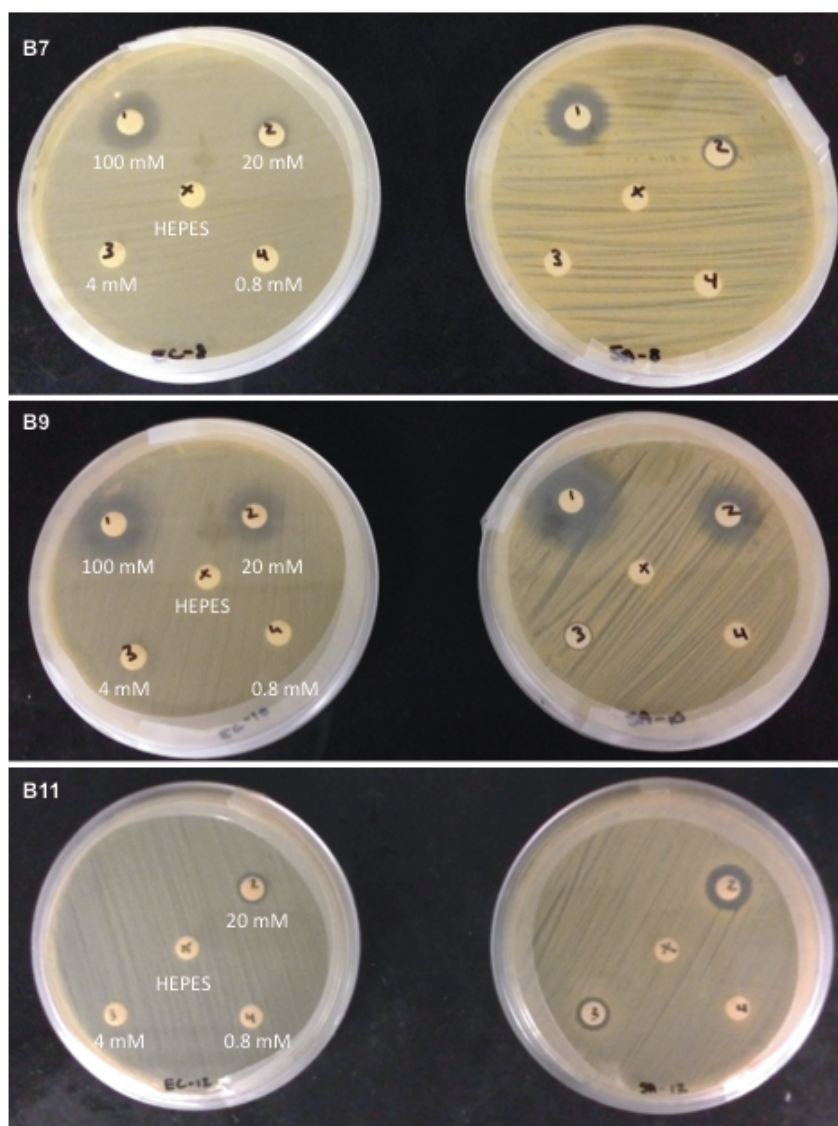


Figure 3.7. Antimicrobial screening of bola-like amphiphiles **B7** (top), **B9** (middle), and **B11** (bottom) against *E. coli* (left) and *S. aureus* (right) as determined by a disk diffusion assay; Zones of inhibition (i.e., no bacterial growth) correspond to antimicrobial activity

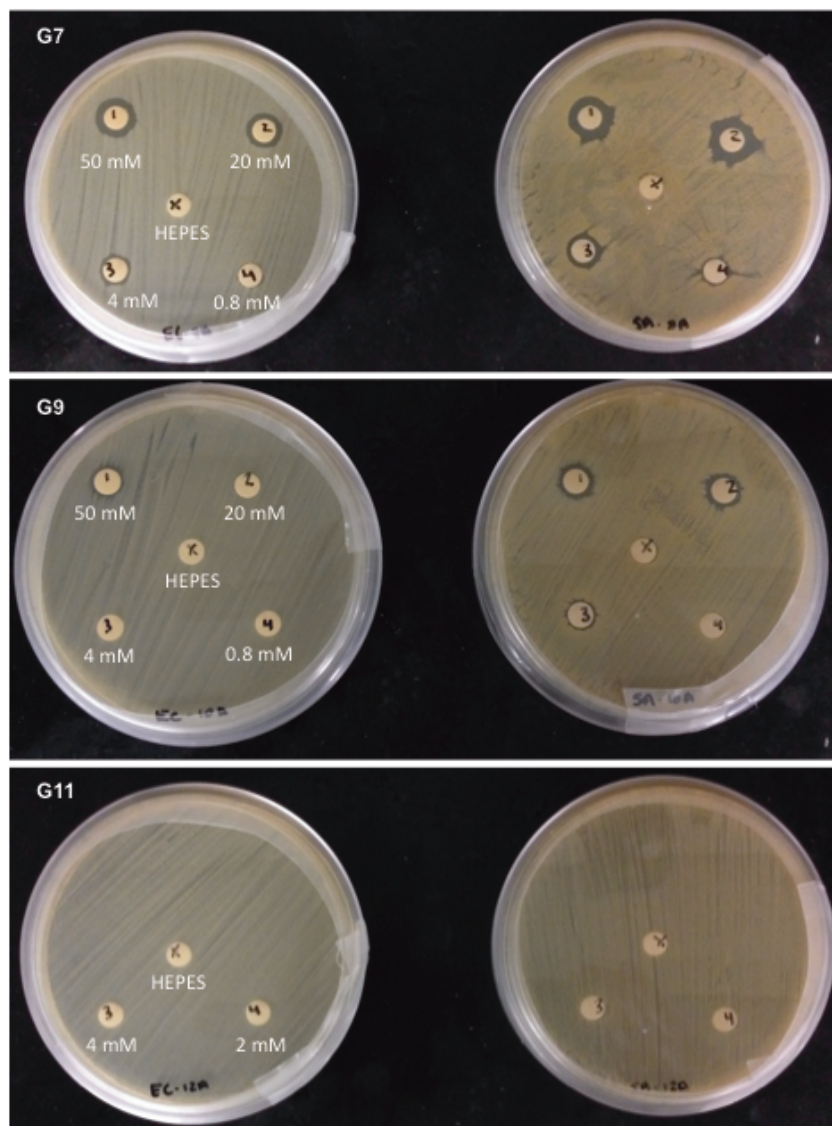


Figure 3.8. Antimicrobial screening of gemini-like amphiphiles **G7** (top), **G9** (middle), and **G11** (bottom) against *E. coli* (left) and *S. aureus* (right) as determined by a disk diffusion assay; Zones of inhibition (i.e., no bacterial growth) correspond to antimicrobial activity

Staphylococcus aureus and *Escherichia coli* were chosen during this screening as representative strains of gram-positive and gram-negative bacteria, respectively. This qualitative assay indicated that all amphiphiles except **G11** – the most hydrophobic gemini-like amphiphile – exhibited activity against *S. aureus* and *E. coli* in the millimolar range (4 – 100 mM, Figure 3.7-Figure 3.8). While this method is excellent for screening, it is not always suitable for the assessment of hydrophobic compounds as they diffuse more slowly through the agar and may not accurately depict bioactivity.²² Consequently, a broth microdilution assay was carried out to quantitatively assess amphiphile activity. Amphiphiles were incubated with either *S. aureus* or *E. coli* in Tryptic Soy Broth (TSB); the lowest amphiphile concentrations that yielded no visible bacterial growth were taken as the minimum inhibitory concentration (MIC) values. Aliquots from MIC experiments were subsequently transferred to Tryptic Soy Agar (TSA) plates and incubated overnight to ascertain amphiphiles' minimum bactericidal concentration (MBC) values – the lowest amphiphile concentrations that prevent colony formation. With the exception of **G11**, whose antibacterial assessment was hampered by poor aqueous solubility, all amphiphiles exhibited MICs within the low micromolar to low millimolar range with MBCs either identical to or double the MIC value (Table 3.1). These results suggest that upon reaching a critical concentration all amphiphiles not only inhibit bacterial growth but also kill the bacteria (Table 3.1).

Table 3.1. MICs and MBCs (μM) of amphiphiles^a

Amphiphile	<i>S. aureus</i> (G+)	<i>E. coli</i> (G-)
B7	500 (1000)	1000 (2000)
B9	125 (250)	500 (500)
B11	25 (50)	100 (100)
G7	63 (125)	63 (125)
G9	500 (1000)	125 (250)
G11	>200 (>200)	>200 (>200)
Streptomycin Sulfate ^b	<172 (<172)	<172 (<172)

^aData represented in MIC (MBC) format

^bStreptomycin sulfate was used as a positive control at 172 μM (100 $\mu\text{g/mL}$)

In comparing amphiphiles' antibacterial activity, it became apparent that the hydrophobic-to-charge ratio, which was investigated by varying the number of methylene units present in amphiphiles' hydrophobic domains, significantly influenced amphiphile bioactivity (Table 3.1). Within the bola-like series (**B7**, **B9**, **B11**), amphiphiles exhibited increasing antibacterial activity as the number of methylene units increased, with **B11** demonstrating the highest potency against gram-positive (MIC: 25 μM) and gram-negative (MIC: 100 μM) bacteria. These results align with previous findings, which indicate increasing acyl chain lengths can result in enhanced bioactivity so long as solubility is not drastically diminished.¹¹ Furthermore, a recent study by Palermo et al. indicated that antimicrobial activity increases as the spacer length between ammonium ions and a methacrylate polymer backbone increases.¹⁶ Given that the methylenes of

the bola-like amphiphiles' acyl arms are analogous to such spacer units, these compounds may behave similarly, with longer acyl arms allowing for enhanced membrane penetration and increased bioactivity. In contrast to the trends noted for the bola-like amphiphiles, gemini-like amphiphiles (**G7**, **G9**, **G11**) exhibited decreased antimicrobial activity with increasing acyl chain length. Previous studies have indicated that amphiphiles' with poor solubility exhibit decreased antibacterial activity, as they are incapable of reaching the bacterial membrane.^{3,7,11} Upon increasing gemini-like amphiphiles' acyl chain length to **G11**, the amphiphile could not dissolve above 200 μM in TSB. It is plausible that gemini-like amphiphiles' decreased solubility in TSB compromised their antibacterial activity. Although solubility effects may have influenced the gemini-like amphiphile series, **G7** exhibited high efficacy against both *S. aureus* and *E. coli* (MICs: 63 μM). As compounds that exhibit MIC values ≤ 50 $\mu\text{g/mL}$ are commonly considered antimicrobial,⁹ broth microdilution studies enabled us to identify two lead compounds – **B11** and **G7** – whose micromolar MIC values correspond to 17.5 and 37.0 $\mu\text{g/mL}$, respectively.

When the two series' effects on gram-positive and gram-negative bacteria were compared, diverging trends emerged. Bola-like amphiphiles generally exhibited higher activity against *S. aureus*, which may result from bola amphiphiles' tendency to penetrate membranes without causing membrane disruption.²³ Given that gram-negative bacteria contain an additional outer membrane, this potential mechanism of action could have rendered bola-like amphiphiles less active against *E. coli*. In contrast, gemini-like amphiphiles

generally exhibited preferential activity against *E. coli*, which indicates that gemini-like amphiphiles may act through a different bactericidal mechanism. Despite these differences, all amphiphiles killed *E. coli* more rapidly than they did *S. aureus* (Table 3.2). These results suggest that the molecules more readily interact with the gram-negative outer membrane, than the gram-positive peptidoglycan layer. Both bacteria possess a net negative charge; however, the gram-negative outer membrane, lacking a thick outer peptidoglycan layer,²⁴ is directly accessible to the cationic heads of the amphiphiles.

Table 3.2. Time killing (h) of selected strains by amphiphiles^a

Amphiphile	<i>S. aureus</i> (G+)	<i>E. coli</i> (G-)
B7	8	4
B9	24	8
B11	24	8
G7	24	8
G9	8	4
Streptomycin Sulfate ^b	8	1

^aAs the amphiphiles have different solubilities, this assay was performed at the respective MBC concentrations

^bStreptomycin sulfate was used as a positive control at 172 μ M (100 μ g/mL)

3.2.3. Biophysical Assessment

Two amphiphiles – **B11** and **G7** – were identified as lead antimicrobial agents. As many AMPs interact with bacterial membranes,^{1,2} we hypothesized that these lead compounds may also interact with bacterial membranes as part of their bactericidal mechanisms. To this end, Langmuir monolayer assays and ITC experiments were conducted to ascertain how the lead compounds interact with model membrane systems. Given that bola-like and gemini-like amphiphiles exhibited different activities against gram-positive and gram-negative bacteria, biophysical studies aimed to further understand whether **B11** and **G7** would exhibit different interactions with model membranes.

3.2.3.1. Langmuir monolayer studies: B11 and G7 can preferentially penetrate anionic biomembranes

Langmuir monolayer techniques were employed to understand amphiphile/lipid interactions. Within these studies, neutral 1,2-dioleoyl-*sn*-glycero-3-phosphocholine (DOPC) monolayers served to mimic eukaryotic membranes, whereas anionic 1,2-dioleoyl-*sn*-glycero-3-phospho-(1'-*rac*-glycerol) (DOPG) or DOPC:DOPG (1:1 mole ratio) monolayers served to mimic bacterial membranes and elucidate the influence of charge on membrane interactions. Monolayers of varying initial surface pressures were spread at the air/buffer interface and the surface pressure increase monitored upon injection of either **B11** or **G7** into the aqueous subphase. By plotting the change in surface pressure as a function of initial surface pressure, the x-intercept – corresponding

to the amphiphiles' maximum insertion pressure (MIP) – was extrapolated.²⁵ MIP values denote the maximum pressure at which monolayer insertion is favorable and provide a quantitative means to compare amphiphile/lipid interactions. As MIP values higher than 30-35 mN/m are indicative of biomembrane penetration,²⁵ this methodology provides insight into **B11** and **G7** interactions with eukaryotic and/or bacterial membranes.

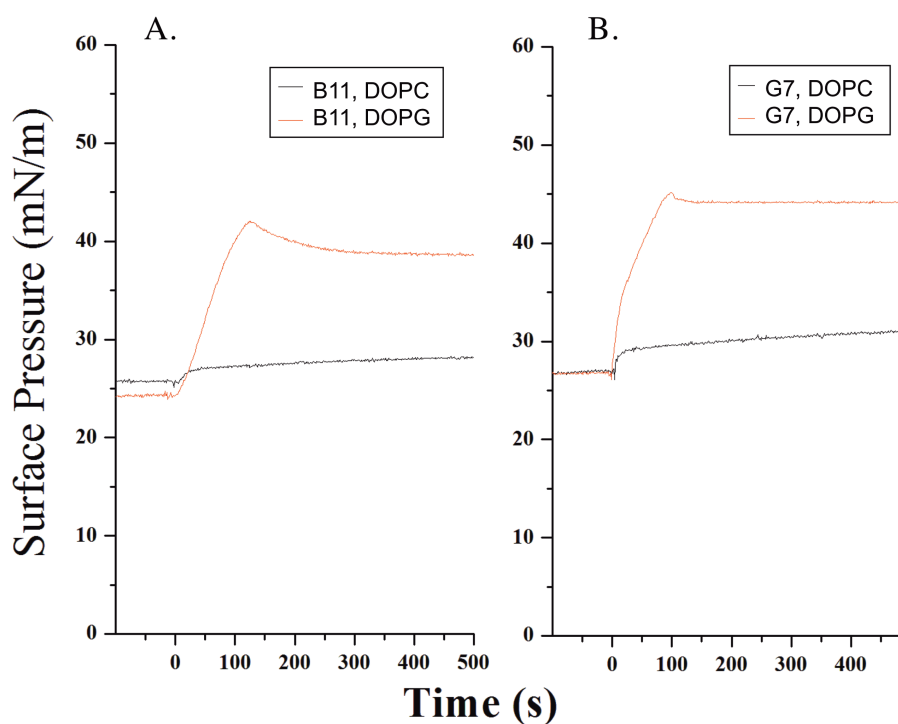


Figure 3.9. Raw Langmuir monolayer data depicting the surface pressure increase upon injection of **B11** (A) or **G7** (B) into the aqueous subphase of a trough containing DOPC (black) or DOPG (red) monolayers at initial surface pressures of approximately 25 mN/m

B11 and **G7** exhibited no significant incorporation into neutral DOPC monolayers (Figure 3.9), with negligible changes in surface pressure and no linear regression with increasing initial surface pressures. In contrast, both amphiphiles interacted with anionic monolayers, exhibiting a surface pressure increase (Figure 3.9), which decreased with higher initial surface pressures (Figure 3.10). This enhanced membrane activity in the presence of anionic lipids has been previously reported⁹ and may indicate that the amphiphiles behave similarly to cationic AMPs, which initially interact with bacterial membranes via electrostatic interactions.^{2,6} In DOPG and DOPC:DOPG monolayers, **B11** exhibited MIP values of 40 and 42 mN/m, respectively, whereas **G7** exhibited MIP values of 46 and 52 mN/m, respectively (Figure 3.10). In general, **G7**'s higher MIP values indicate enhanced interactions with anionic monolayers. As all MIP values were greater than the biomembrane lateral pressure and comparable to MIP values of known AMPs,²⁵ it is plausible that both **B11** and **G7** are capable of intercalating within anionic bacterial membranes. In comparing amphiphile interactions with the two different anionic lipid systems, both amphiphiles exhibited higher MIP values in the presence of DOPC:DOPG monolayer mixtures. This phenomenon could result from DOPC's smaller head group area²⁶ enabling a more favorable insertion of amphiphiles into the lipid monolayer.

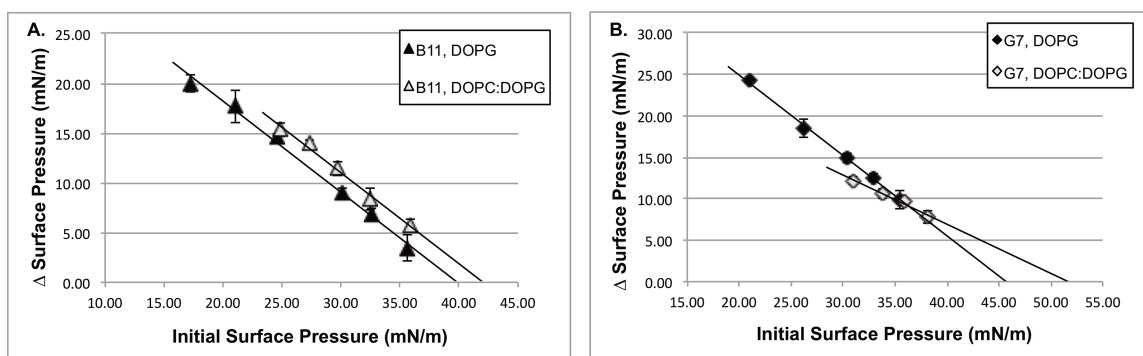


Figure 3.10. Interaction of **B11** (A, triangles) and **G7** (B, diamonds) with DOPG (black) or DOPC:DOPG (1:1 mole ratio, light grey) lipid monolayers indicated by change in surface pressure as a function of initial surface pressure

3.2.3.2. Langmuir monolayer studies: electrostatic contributions in membrane interaction differ for B11 and G7

In addition to extrapolating MIP values, a second parameter that provides useful information for analyzing membrane interaction is the maximum surface pressure increase measured during Langmuir monolayer studies.²⁵ **G7** exhibits a maximum surface pressure increase of 24 mN/m in the presence of pure DOPG, which decreases to 12 mN/m in the presence of DOPC:DOPG (Figure 3.10B). This dependence of maximum surface pressure increase on the mole fraction of anionic lipid has been previously reported²⁷ and indicates an electrostatic contribution in membrane binding. **B11** also exhibits a decrease in maximum surface pressure increase when changing the lipid system from DOPG to DOPC:DOPG, yet to a smaller extent (20 mN/m to 15 mN/m, Figure 3.10A) than

G7; this result reflects a lesser dependence on electrostatic interactions. The notable difference in electrostatic contribution suggests that **B11** relies on a combination of electrostatic and hydrophobic interactions to elicit bacterial death, whereas **G7**'s bactericidal mechanism may be largely driven by electrostatic interactions. A primarily electrostatic mechanism of action could be hampered by increasing hydrophobic content, potentially resulting in gemini-like amphiphiles' decreased activity with increasing hydrophobic-to-charge ratio.

3.2.3.3. ITC studies: B11 and G7 operate via different bactericidal mechanisms

While Langmuir monolayer studies provided valuable insight into amphiphile's interactions with biomembranes, ITC was used to investigate amphiphiles' interactions with bilayers, a more biologically accurate model membrane system. Large unilamellar vesicles (LUVs) comprised of pure DOPC or DOPC:DOPG (1:1 mole ratio) were prepared to mimic eukaryotic and bacterial membranes, respectively; these LUVs were titrated into a sample cell containing amphiphile solution (i.e., **B11** or **G7** dissolved in 4-(2-hydroxyethyl)-1-piperazineethanesulfonic acid, HEPES, buffer).

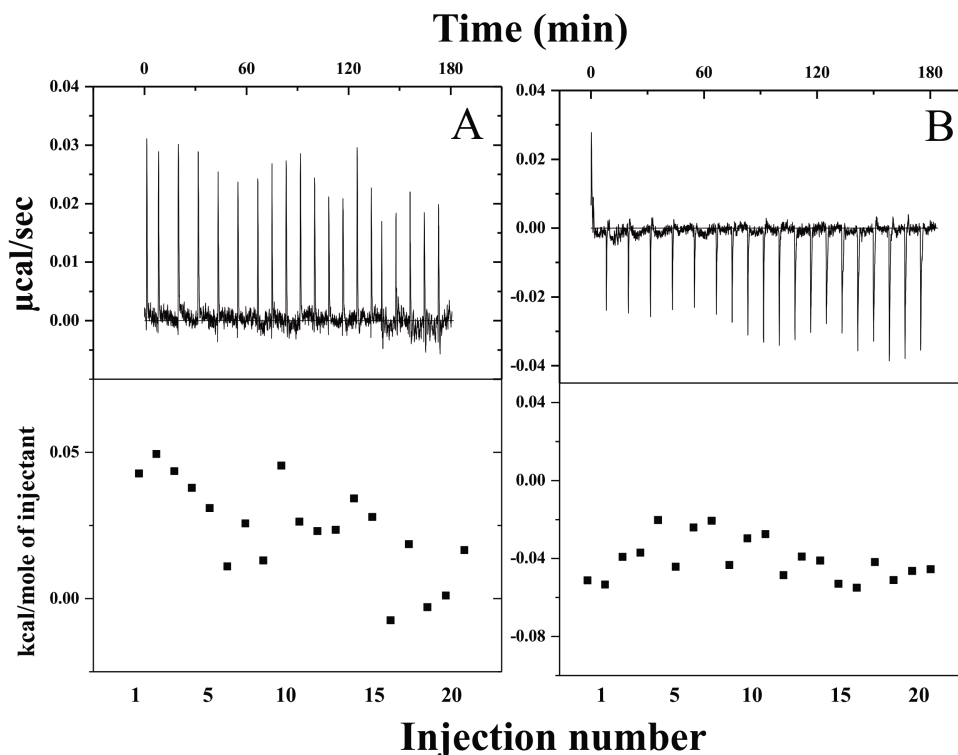


Figure 3.11. ITC traces obtained from titrating DOPC into **B11** (A) and **G7** (B); Upper curves depict heat flow as a function of time, whereas lower curves depict the corresponding integrated area of each peak as a function of injection number; Heat flow was negligible for both titrations

Both **B11** and **G7** exhibited no interaction with neutral DOPC LUVs, evidenced by negligible heat signals during the titration (Figure 3.11). As eukaryotic membranes also exhibit a net neutral charge, these results may indicate that both amphiphiles would interact minimally with eukaryotic cells, a correlation that has been previously depicted by Epand et al.²⁸ In investigating anionic LUVs (i.e., DOPC:DOPG), both lead amphiphiles exhibited binding interactions, and the heats associated with these interactions generally

decreased as the titrations progressed. As LUVs were added into the titration cell, amphiphiles would bind to LUVs, leaving less amphiphiles available for binding and resulting in smaller heat signals in subsequent LUV injections until all amphiphiles were removed from the bulk solution.²⁹⁻³² **B11** exhibited endothermic binding interactions, indicated by a positive enthalpy change (Figure 3.12A). Such binding interactions often result from the displacement of counterions or water molecules upon hydrophobic-hydrophobic interactions,^{29,33,34} suggesting **B11**'s hydrophobic domain may penetrate into the hydrophobic membrane interior of the anionic LUVs and that binding is largely influenced via hydrophobic-hydrophobic interactions. As **B11** did not interact with DOPC (i.e., neutral) LUVs yet did interact with DOPC:DOPG (i.e., anionic) LUVs, we hypothesized that an initial electrostatic interaction occurred. Although electrostatic interactions result in exothermic heat signals, it is plausible **B11**'s stronger dependence on hydrophobic-hydrophobic interactions resulted in the observed positive enthalpy change.³⁵

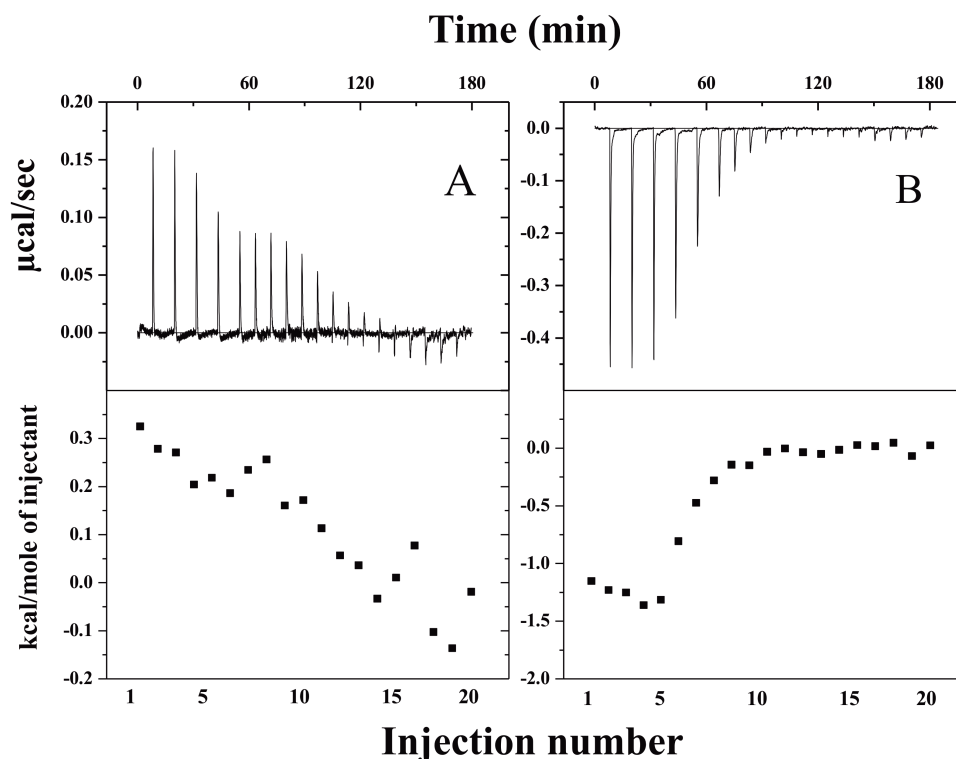


Figure 3.12. ITC traces obtained from titrating DOPC:DOPG (1:1 mole ratio) into **B11** (A) and **G7** (B); Upper curves depict heat flow as a function of time, whereas lower curves depict the corresponding integrated area of each peak as a function of injection number

In contrast to **B11**, **G7** exhibited a negative enthalpy change under identical conditions (Figure 3.12B), which suggests an exothermic, electrostatic interaction between **G7** and anionic LUVs.²⁸ This exothermic interaction supports Langmuir monolayer data, which indicated that **G7**'s membrane insertion activity involved a larger electrostatic contribution than that of **B11**.

The diverging energetics of binding indicate that **B11** and **G7** may act via different bactericidal mechanisms and could explain why the two classes of

molecules exhibit preferential bioactivity against different bacteria strains. For instance, gemini-like amphiphiles demonstrated preferential activity against gram-negative bacteria. As **G7** exhibits electrostatic interactions with anionic LUVs, these amphiphiles may interact favorably with the negatively charged lipopolysaccharides (LPSs) on the outer membrane of gram-negative bacteria, potentially neutralizing LPS or displacing divalent cations associated with LPS and ultimately distorting the outer membrane.^{1,2} Additionally, LPS has reduced permeability to hydrophobic molecules¹¹ which may explain why gemini-like amphiphiles with smaller hydrophobic components exhibited improved bioactivity. In contrast, bola-like amphiphiles exhibited preferential activity against gram-positive bacteria with **B11** demonstrating endothermic binding interactions, indicative of hydrophobic-hydrophobic interactions, with anionic LUVs. These molecules likely rely on an initial electrostatic interaction, with the negatively charged peptidoglycan matrix of gram-positive bacteria, followed by intercalation into the membrane's hydrophobic domain. Over time this intercalation may result in membrane destabilization through various potential mechanisms, such as membrane thinning or pore formation.^{1,2,6,12} Although the specific bactericidal mechanisms of **G7** and **B11** require further elucidation, antimicrobial studies in conjunction with biophysical experiments indicate the significant influence of charge location on amphiphile activity.

3.3. Conclusion

Bola-like and gemini-like amphiphiles were synthesized to understand the specific influence of charge location on antibacterial activity. Bola-like amphiphiles exhibited increased activity with increasing hydrophobic-to-charge ratios, likely resulting from a combination of both hydrophobic and electrostatic interactions with bacterial membranes. In contrast, gemini-like amphiphiles demonstrated a different trend, with antibacterial activity increasing as hydrophobic-to-charge ratios decreased. This phenomenon may have resulted from the decreased solubility of more hydrophobic gemini-like amphiphiles or from gemini-like amphiphiles relying primarily on electrostatic interactions in their bactericidal mechanism. Additionally, bola-like amphiphiles exhibited preferential bioactivity against gram-positive bacteria whereas gemini-like amphiphiles exhibited preferential activity against gram-negative bacteria, further suggesting that the two amphiphile series possess inherently different bactericidal mechanisms and ultimately interact with different components of bacteria membranes. These studies reveal that, in addition to the hydrophobic-to-charge ratio, charge location significantly modulates cationic amphiphiles' antibacterial activity and bactericidal mechanism. Through understanding this influence of charge location, antimicrobial agents could be designed to target different bacteria types and/or membrane structures.

3.4. Experimental

3.4.1. Materials

All reagents and solvents were purchased from Sigma-Aldrich (Milwaukee, WI) and used as received unless otherwise noted. 1 M HCl, concentrated ammonium hydroxide, deuterated methanol (CD_3OD), Petri dishes, and cotton swabs were purchased from Fisher Scientific (Fair Lawn, NJ). Muller-Hinton agar and blank paper disks were purchased from Becton Dickinson (Franklin Lakes, NJ). DOPC and DOPG were purchased from Avanti Polar Lipids, Inc. (Alabaster, AL) and used without further purification. PT was prepared according to published procedures.²⁰ HEPES buffer was prepared at 10 mM, pH 7.4 and filtered prior to use. For broth microdilution and kinetic kill assays, bacterial strains *Escherichia coli* ATCC[®] 43895[™] and *Staphylococcus aureus* Rosenbach ATCC[®] 29213[™] were received from the American Tissue Culture Collection (ATCC, Manassass, VA, USA). The *E. coli* and *S. aureus* strains were chosen because they are representative of gram-negative and gram-positive pathogens, respectively.

3.4.2. Characterization

¹H and carbon (¹³C) NMR spectra were obtained using a Varian 400 or 500 MHz spectrometer. Samples were dissolved in deuterated chloroform (CDCl_3), dimethyl sulfoxide ($\text{DMSO}-d_6$), or CD_3OD using trimethylsilane or deuterated solvent ($\text{DMSO}-d_6$ or CD_3OD) as an internal reference. FT-IR spectra

were obtained using a Thermo Scientific Nicolet iS10 spectrophotometer equipped with OMNIC software. FT-IR samples were either pressed into potassium bromide (KBr) discs (1 wt % sample) or solvent-cast onto sodium chloride plates; each spectrum was an average of 32 scans. Molecular weights were determined using a ThermoQuest Finnigan LCQ-DUO system equipped with an atmospheric pressure ionization source, a mass spectrometer detector, and the Xcalibur data system. Samples were prepared at a concentration of 10 $\mu\text{g/mL}$ in methanol (MeOH) or 50:50 MeOH:dichloromethane (DCM).

3.4.3. Synthesis of Bola-like Amphiphiles

3.4.3.1. Synthesis of Boc-protected alkanolic acids (3.3)

Following modified literature procedures,^{36,37} bromo-terminated alkanolic acid (**3.1**, 3.62 mmol) was either dissolved (**3.1a**) or suspended (**3.1b-c**) in concentrated ammonium hydroxide (10-100 mL) and stirred for 24-48 h. Upon complete consumption of starting material (monitored by thin layer chromatography, 75:25 hexanes/ethyl acetate with acetic acid), the reaction mixture was concentrated *in vacuo* to isolate an amine-terminated alkanolic acid intermediate (**3.2**). The intermediate was then suspended in a 1:1 mixture of dioxane and 10 % sodium carbonate (14 mL each) and gently warmed to 30 °C. If necessary, additional water (5 mL) was added to improve stirring. Di-tert-butyl dicarbonate (3.98 mmol) was added and the reaction stirred under reflux

temperatures (65 °C) overnight. The reaction mixture was concentrated *in vacuo* and the resulting crude mixture reconstituted in 1 M HCl and diethyl ether and subsequently extracted with diethyl ether (4 x 80 mL). The combined organic layers were washed with 1:1 brine/water (80 mL total), dried over magnesium sulfate (MgSO₄), and the product (**3.3**) isolated *in vacuo*.

8-Bocaminooctanoic acid (3.3a). Yield: 1.67 g, 78 % (off-white solid). ¹H-NMR (500 MHz, CDCl₃): δ 4.56 (br, 1H), 3.10 (m, 2H), 2.34 (t, 2H), 1.63 (m, 2H), 1.45 (m, 17H). ¹³C-NMR (500 MHz, CDCl₃): δ 179.54, 156.29, 79.34, 40.77, 34.25, 30.16, 29.17, 29.10, 28.64, 26.77, 24.83. FT-IR (cm⁻¹, thin film from chloroform, CHCl₃): 3367 (NH), 1698 (C=O, acid and carbamate). ESI-MS *m/z*: 258.1 [M-1].

10-Bocaminodecanoic acid (3.3b). Yield: 1.09 g, 97 % (off-white solid). ¹H-NMR (500 MHz, CDCl₃): δ 4.59 (br, 1H), 3.07 (m, 2H), 2.30 (t, 2H), 1.60 (m, 2H), 1.41 (m, 21H). ¹³C-NMR (500 MHz, CDCl₃): δ 179.61, 156.30, 79.31, 40.81, 34.33, 30.18, 29.49, 29.38, 29.32, 29.22, 28.62, 26.93, 24.91. FT-IR (cm⁻¹, thin film from CHCl₃): 3367 (NH), 1721 (C=O, acid), 1686 (C=O, carbamate). ESI-MS *m/z*: 286.1 [M-1].

12-Bocaminododecanoic acid (3.3c). Yield: 1.00 g, 97 % (off-white solid). ¹H-NMR (500 MHz, CDCl₃): δ 4.61 (br, 1H), 3.10 (m, 2H), 2.33 (t, 2H), 1.63 (m, 2H), 1.44 (m, 25H). ¹³C-NMR (500 MHz, CDCl₃): δ 179.56, 156.29, 79.31, 40.85, 34.33, 30.21, 29.66, 29.56, 29.46, 29.41, 29.26, 28.64, 28.45, 27.00, 24.94. FT-IR (cm⁻¹, thin film from CHCl₃): 3368 (NH), 1722 (C=O, acid), 1686 (C=O, carbamate). ESI-MS *m/z*: 314.2 [M-1].

3.4.3.2. Synthesis of 2,3-bis(Boc-protected alkanoyl) PT (3.4)

PT (1.36 mmol), **3.3** (2.99 mmol), and catalytic 4-dimethylaminopyridine (DMAP, 0.57 mmol) were dissolved in anhydrous DCM (27 mL) and dimethylformamide (DMF, 13 mL) under nitrogen. Upon complete dissolution, 1-ethyl-3-(3-dimethylaminopropyl)carbodiimide (EDCI, 5.71 mmol) was added and the reaction stirred overnight under nitrogen. The reaction mixture was concentrated *in vacuo*, reconstituted in DCM, and washed with aqueous solutions of 10 % potassium bisulfite (KHSO₄, 3 x 80 mL) and saturated sodium bicarbonate (NaHCO₃, 3 x 80 mL). The organic layer was then washed with brine (80 mL), dried over MgSO₄, and the product (**3.4**) isolated *in vacuo*.

8-Bocaminooctanoyl PT (3.4a). Yield: 1.25 g, 95 % (pale-yellow solid). ¹H-NMR (500 MHz, CDCl₃): δ 6.27 (br, 2H), 5.60 (s, 2H), 4.57 (br, 2H), 3.20 (m, 4H), 3.10 (m, 4H), 2.40 (t, 4H), 1.63 (m, 4H), 1.44 (m, 38H), 0.91 (t, 6H). ¹³C-NMR (500 MHz, CDCl₃): δ 172.30, 166.38, 156.20, 79.22, 72.45, 41.44, 40.72, 34.00, 30.18, 29.09, 29.03, 28.65, 26.76, 24.82, 22.86, 11.49. FT-IR (cm⁻¹, thin film from CHCl₃): 3290 (NH), 1752 (C=O, ester), 1694 (C=O, carbamate), 1655 (C=O, amide). ESI-MS *m/z*: 737.1 [M+23].

10-Bocaminodecanoyl PT (3.4b). Yield: 0.81 g, 95 % (pale-yellow solid). ¹H-NMR (500 MHz, CDCl₃): δ 6.24 (br, 2H), 5.61 (s, 2H), 4.54 (br, 2H), 3.21 (m, 4H), 3.10 (m, 4H), 2.40 (t, 4H), 1.62 (m, 4H), 1.51 (m, 46H), 0.91 (t, 6H). ¹³C-NMR (500 MHz, CDCl₃): δ 171.18, 165.18, 154.96, 78.05, 71.20, 40.17, 39.59,

32.86, 29.04, 28.28, 28.17, 28.12, 27.96, 27.43, 25.73, 23.71, 21.64, 10.25. FT-IR (cm^{-1} , thin film from CHCl_3): 3280 (NH), 1751 (C=O, ester), 1694 (C=O, carbamate), 1652 (C=O, amide). ESI-MS m/z : 793.2 [M+23].

12-Bocaminododecanoyl PT (3.4c). Yield: 0.79 g, quantitative (pale-yellow solid). ^1H -NMR (400 MHz, CDCl_3): δ 6.35 (br, 2H), 5.61 (s, 2H), 4.54 (br, 2H), 3.19 (m, 4H), 3.09 (m, 4H), 2.39 (t, 4H), 1.62 (m, 4H), 1.43 (m, 54H), 0.90 (t, 6H). ^{13}C -NMR (500 MHz, CDCl_3): δ 171.15, 165.20, 154.99, 77.93, 71.27, 40.20, 39.61, 32.86, 29.06, 28.69, 28.49, 28.38, 28.26, 28.22, 28.03, 27.43, 25.79, 23.74, 21.63, 10.27. FT-IR (cm^{-1} , thin film from CHCl_3): 3281 (NH), 1751 (C=O, ester), 1694 (C=O, carbamate), 1655 (C=O, amide). ESI-MS m/z : 849.3 [M+23].

3.4.3.3. Synthesis of bola-like amphiphiles (3.5)

Boc groups were deprotected following modified procedures.³⁸ In brief, HCl (4 M in dioxane, 50.78 mmol) was cooled to 0 °C under nitrogen, **3.4** added (1.27 mmol), and the reaction stirred at 0 °C for 30 min. The reaction mixture was then warmed to room temperature, stirred an additional 3 h, and concentrated *in vacuo*. Crude product was dissolved in minimal MeOH (10 mL) and aliquots (1 mL) were added to ten 50 mL centrifuge tubes containing diethyl ether (45 mL each), resulting in the precipitation of **3.5**. **3.5** was isolated via centrifugation (Hettich EBA 12, Beverly, MA; 1370 x g , 5 min) and decanting the ether. Bola-like amphiphiles will be referred to as Bx, where B denotes bola-like and x refers to the number of methylenes in the acyl arms.

B7 (3.5a). Yield: 0.55 g, 96 % (off-white solid). $^1\text{H-NMR}$ (400 MHz, CD_3OD): δ 8.25 (br, 2H), 5.57 (s, 2H), 3.15 (m, 4H), 2.92 (t, 4H), 2.48 (m, 4H), 1.64 (m, 8H), 1.51 (m, 4H), 1.39 (br, 12H), 0.90 (t, 6H). $^{13}\text{C-NMR}$ (500 MHz, CD_3OD): δ 172.65, 167.62, 72.58, 41.18, 39.56, 33.24, 28.62, 27.29, 26.06, 24.36, 22.42, 10.51. FT-IR (cm^{-1} , KBr): 3422 (NH), 1751 (C=O, ester), 1655 (C=O, amide). ESI-MS m/z : 258.0 [(M+2)/2].

B9 (3.5b). Yield: 0.72 g, 95 % (off-white solid). $^1\text{H-NMR}$ (500 MHz, CD_3OD): δ 8.24 (br, 2H), 5.56 (s, 2H), 3.14 (m, 4H), 2.91 (t, 4H), 2.46 (m, 4H), 1.63 (m, 8H), 1.50 (m, 4H), 1.34 (br, 20H), 0.89 (t, 6H). $^{13}\text{C-NMR}$ (500 MHz, CD_3OD): δ 172.68, 167.54, 72.54, 41.06, 39.60, 33.29, 29.09, 29.08, 28.94, 28.88, 27.39, 26.24, 24.49, 22.40, 10.50. FT-IR (cm^{-1} , KBr): 3288 (NH), 1749 (C=O, ester), 1670 (C=O, amide). ESI-MS m/z : 286.5 [(M+2)/2].

B11 (3.5c). Yield: 0.86 g, 97 % (off-white solid). $^1\text{H-NMR}$ (400 MHz, CD_3OD): δ 8.23 (br, 2H), 5.56 (s, 2H), 3.14 (m, 4H), 2.91 (t, 4H), 2.45 (m, 4H), 1.63 (m, 8H), 1.50 (m, 4H), 1.32 (br, 28H), 0.89 (t, 6H). $^{13}\text{C-NMR}$ (500 MHz, CD_3OD): δ 172.68, 167.55, 72.54, 41.07, 39.61, 33.33, 29.37, 29.34, 29.29, 29.22, 29.03, 28.94, 27.41, 26.27, 24.54, 22.41, 10.50. FT-IR (cm^{-1} , KBr): 3288 (NH), 1744 (C=O, ester), 1668 (C=O, amide). ESI-MS m/z : 627.4 [M+1].

3.4.4. Synthesis of Gemini-like Amphiphiles

3.4.4.1. Synthesis of 2-Bocaminoethyltartramide (2-Boc-AET) (3.7)

2-Boc-AET was prepared according to modified literature procedures.²⁰ In brief, dimethyl tartrate (**3.6**, 2.43 mmol) was dissolved in anhydrous tetrahydrofuran (7.5 mL) under nitrogen. N-Boc-ethylenediamine (6.79 mmol) was added and the reaction mixture stirred at 40 °C overnight. The crude reaction mixture was concentrated *in vacuo* and pure product (**3.7**) was triturated in diethyl ether (25 mL) and isolated via vacuum filtration. To improve yields, the filtrate was reconcentrated *in vacuo*, triturated, and vacuum filtered to isolate additional pure product. Yield: 1.93 g, 91% (white solid). ¹H-NMR (400 MHz, DMSO-*d*₆): δ 7.79 (br, 2H), 6.81 (br, 2H), 5.43 (d, 2H), 4.20 (d, 2H), 3.12 (m, 4H), 2.99 (m, 4H), 1.36 (s, 18H). ¹³C-NMR (500 MHz, DMSO-*d*₆): δ 172.84, 156.35, 78.39, 73.22, 40.43, 39.28, 28.92. FT-IR (cm⁻¹, KBr): 3356 (NH), 1687 (C=O, carbamide), 1629 (C=O, amide). ESI-MS *m/z*: 457.2 [M+23].

3.4.4.2. Synthesis of 2,3-bis(alkanoyl) Boc-AET (**3.8**)

Following methods similar to those described for the synthesis of **3.4**, alkanoyl acid (2.53 mmol), **3.7** (1.51 mmol), and DMAP (0.48 mmol) were dissolved in anhydrous DCM (50 mL) and anhydrous DMF (25 mL) under nitrogen. EDCI (4.83 mmol) was added, the reaction stirred overnight, and concentrated *in vacuo*. The crude mixture was reconstituted in DCM, washed with aqueous solutions of 10 % KHSO₄ (3 x 80 mL), saturated NaHCO₃ (3 x 80 mL), and brine (80 mL), dried over MgSO₄, and concentrated *in vacuo*. This

crude product was triturated in hexanes (160 mL) for 4 h and pure product (**3.8**) isolated via vacuum filtration.

Nonanoyl-Boc-AET (3.8a). Yield: 0.76 g, 93 % (white solid). $^1\text{H-NMR}$ (500 MHz, CDCl_3): δ 7.05 (br, 2H), 5.58 (s, 2H), 5.18 (br, 2H), 3.30 (m, 8H), 2.45 (m, 4H), 1.63 (m, 4H), 1.44 (s, 18 H), 1.27 (br, 20H), 0.88 (t, 6H). $^{13}\text{C-NMR}$ (500 MHz, CDCl_3): δ 172.37, 167.04, 157.11, 79.94, 72.45, 41.21, 39.99, 34.06, 32.03, 29.46, 29.36, 29.31, 28.62, 24.90, 22.85, 14.31. FT-IR (cm^{-1} , thin film from CHCl_3): 3369 (NH), 1748 (C=O, ester), 1690 (C=O, carbamide), 1660 (C=O, amide). ESI-MS m/z : 737.4 [M+23].

Undecanoyl-Boc-AET (3.8b). Yield: 0.60 g, 84 % (white solid). $^1\text{H-NMR}$ (500 MHz, CDCl_3): δ 7.13 (br, 2H), 5.59 (s, 2H), 5.22 (br, 2H), 3.28 (m, 8H), 2.45 (m, 4H), 1.63 (m, 4H), 1.44 (s, 18H), 1.26 (br, 28H), 0.88 (t, 6H). $^{13}\text{C-NMR}$ (500 MHz, CDCl_3): δ 172.39, 167.08, 157.11, 79.90, 72.45, 41.16, 39.98, 34.04, 32.11, 29.80, 29.72, 29.53, 29.51, 29.32, 28.61, 24.90, 22.89, 14.32. FT-IR (cm^{-1} , thin film from CHCl_3): 3368 (NH), 1742 (C=O, ester), 1690 (C=O, carbamide), 1660 (C=O, amide). ESI-MS m/z : 793.4 [M+23].

Tridecanoyl-Boc-AET (3.8c). Yield: 0.89 g, 94 % (white solid). $^1\text{H-NMR}$ (500 MHz, CDCl_3): δ 7.07 (br, 2H), 5.58 (s, 2H), 5.18 (br, 2H), 3.28 (m, 8H), 2.44 (m, 4H), 1.63 (m, 4H), 1.44 (s, 18H), 1.26 (br, 36H), 0.88 (t, 6H). $^{13}\text{C-NMR}$ (500 MHz, CDCl_3): δ 172.36, 167.06, 157.11, 79.93, 72.45, 41.22, 39.97, 34.05, 32.14, 29.89, 29.87, 29.86, 29.73, 29.57, 29.53, 29.33, 28.62, 24.91, 22.91, 14.33. FT-IR (cm^{-1} , thin film from CHCl_3): 3367 (NH), 1740 (C=O, ester), 1689 (C=O, carbamide), 1659 (C=O, amide). ESI-MS m/z : 849.4 [M+23].

3.4.4.3. Synthesis of gemini-like amphiphiles (3.9)

Boc groups were deprotected following the methods outlined for the synthesis of **3.5**. Briefly, HCl (4 M in dioxane, 24.18 mmol) was cooled to 0 °C under nitrogen, **3.8** added (0.60 mmol), and the reaction stirred at 0 °C for 30 min. If necessary, additional anhydrous dioxane (3 mL) was added to improve stirring. The reaction mixture was warmed to room temperature, stirred an additional 3 h, and concentrated *in vacuo*. Crude product was dissolved in minimal MeOH (6 mL) and aliquots (1 mL) were added to six 50 mL centrifuge tubes containing diethyl ether (45 mL each), resulting in the precipitation of **3.9**. **3.9** was isolated via centrifugation (Hettich EBA 12, Beverly, MA; 1370 x *g*, 5 min) and decanting the ether. Gemini-like amphiphiles will be referred to as G_x, where G denotes gemini-like and x refers to the number of methylenes in the acyl arms.

G7 (3.9a). Yield: 0.39 g, 95 % (clear, off-white solid). ¹H-NMR (500 MHz, CD₃OD): δ 8.64 (br, 2H), 5.58 (s, 2H), 3.52 (m, 4H), 3.09 (m, 4H), 2.49 (m, 4H), 1.62 (m, 4H), 1.31 (br, 20H), 0.90 (t, 6H). ¹³C-NMR (500 MHz, CD₃OD): δ 172.92, 168.94, 72.47, 39.46, 36.90, 33.42, 31.84, 29.25, 29.14, 29.00, 24.61, 22.54, 13.28. FT-IR (cm⁻¹, KBr): 3455 (NH), 1744 (C=O, ester), 1644 (C=O, amide). ESI-MS *m/z*: 515.3 [M+1].

G9 (3.9b). Yield: 0.42 g, quantitative (off-white solid). ¹H-NMR (500 MHz, CD₃OD): δ 8.62 (br, 2H), 5.57 (s, 2H), 3.50 (m, 4H), 3.08 (m, 4H), 2.47 (m, 4H),

1.61 (m, 4H), 1.29 (br, 28H), 0.90 (t, 6H). ^{13}C -NMR (500 MHz, CD_3OD): δ 172.91, 168.95, 72.47, 39.46, 36.92, 33.43, 31.90, 29.57, 29.48, 29.30, 29.01, 24.62, 22.56, 13.27. FT-IR (cm^{-1} , KBr): 3435 (NH), 1739 (C=O, ester), 1652 (C=O, amide). ESI-MS m/z : 571.3 $[\text{M}+1]$.

G11 (3.9c). Yield: 0.40 g, 94 % (white solid). ^1H -NMR (500 MHz, CD_3OD): δ 8.62 (br, 2H), 5.57 (s, 2H), 3.52 (m, 4H), 3.09 (m, 4H), 2.49 (m, 4H), 1.62 (m, 4H), 1.29 (br, 36H), 0.89 (t, 6H). ^{13}C -NMR (500 MHz, CD_3OD): δ 172.90, 168.95, 72.48, 39.47, 36.92, 33.43, 31.91, 29.64, 29.62, 29.61, 29.49, 29.32, 29.02, 24.63, 22.56, 13.27. FT-IR (cm^{-1} , KBr): 3448 (NH), 1744 (C=O, ester), 1641 (C=O, amide). ESI-MS m/z : 314.4 $[(\text{M}+2)/2]$.

3.4.5. Antimicrobial Screening

[Bacteria inocula and agar plates were prepared by Dr. Susan Skelly, Division of Life Sciences, Rutgers University, Piscataway, NJ]

Amphiphiles' antimicrobial activity against gram-negative (*E. coli*) and gram-positive (*S. aureus*) bacteria was first screened using the disk diffusion method.²¹ Bacteria inocula were grown overnight in nutrient broth (EMD Chemicals, Gibbstown, NJ) at 37 °C under shaking conditions to give a bacterial count of approximately 10^8 CFU/mL. Muller-Hinton agar was poured into sterile Petri dishes to a thickness of 4 mm. The agar plate was then inoculated with the bacteria broth culture using a sterile cotton swab. Separately, amphiphiles were

dissolved in HEPES buffer at concentrations ranging from 0.8 mM to 100 mM. Sterile paper disks (6 mm diameter) were impregnated with 20 μ L of test solution and the disks placed onto the inoculated agar plates. Plates were incubated at 37 °C for 20 h, after which zones of inhibition were measured with a ruler. HEPES buffer served as a negative control.

3.4.6. Broth Microdilution Assay

[Broth microdilution studies were performed by Timothy Arthur, Department of Microbiology and Biochemistry, Rutgers University, New Brunswick, NJ]

The broth microdilution method was modified from previous studies.¹¹ Briefly, amphiphiles were serially diluted 2-fold in TSB and 100 μ L aliquots of each dilution were transferred to a 96-well microtiter plate in triplicate. *S. aureus* and *E. coli* were grown on TSA at 37 °C for 24 h, and sterile double-distilled water was inoculated with isolated colonies from these overnight plates. Inoculum concentration was adjusted to 5×10^6 CFU/mL with ultraviolet-visible (UV-Vis) spectroscopy at 600 nm. Aliquots (100 μ L) were transferred to the 96-well microtiter plate to achieve a final concentration of 5×10^5 CFU/well. Plates were incubated at 37 °C for 24 h. The lowest amphiphile concentration that yielded no visible growth was recorded as the MIC. Aliquots (100 μ L) were withdrawn from each well that exhibited bacterial inhibition and transferred to

TSA. Plates were incubated at 37 °C for 24 h. The lowest concentration that yielded no colonies was recorded as the MBC. Each experiment was performed a minimum of three times.

3.4.7. Kinetic Kill Assays

[Kinetic kill studies were performed by Timothy Arthur, Department of Microbiology and Biochemistry, Rutgers University, New Brunswick, NJ]

To determine the kinetic killing effects of the amphiphiles, the *S. aureus* and *E. coli* were tested against their respective MBCs in a modified time kill assay.¹¹ Briefly, the compounds were diluted to their respective MBCs in sterile TSB. Aliquots (100 µL) were transferred to a 96-well microtiter plate. Sterile double-distilled water was inoculated with isolated colonies from the overnight plates. Inoculum concentration was adjusted to 5×10^6 CFU/mL with UV-Vis spectroscopy at 600 nm. Aliquots (100 µL) were transferred to the 96-well microtiter plate to achieve a final concentration of 5×10^5 CFU/well. At 1, 2, 4, 8 and 24 h, 100 µL aliquots were transferred to TSA. Plates were incubated at 37 °C for 24 h. The time at which there were no colonies was recorded. Each experiment was performed a minimum of three times.

3.4.8. Langmuir Monolayer Studies

The ability of amphiphiles to penetrate lipid monolayers was analyzed using a Langmuir surface balance equipped with a custom-built microtrough from KSV-Nima (Biolin Scientific, Espoo, Finland). Lipid solutions were prepared by dissolving DOPC, DOPG, or DOPC/DOPG (1:1 mole ratio) in HPLC grade CHCl_3 (~1.2 mg/mL total lipid). After rinsing with an ethanol/MeOH mixture, the trough was filled with HEPES buffer and the surface aspirated to remove surface-active particles. Using a Hamilton syringe (Reno, NV), small aliquots of lipid solution were applied to the air/buffer interface to obtain varying initial surface pressures ranging from approximately 17 mN/m to 38 mN/m. After solvent evaporation and monolayer equilibration (at least 500 s), 5 μL of **B11** or **G7** dissolved in HEPES buffer (5 mM initial amphiphile) was injected into the aqueous subphase via a side port to avoid puncturing the monolayer and the surface pressure increase monitored over time. Data were collected and processed using KSV Nima and Origin software.

3.4.9. Isothermal Titration Calorimetry

High sensitivity isothermal titration calorimetry (MicroCal VP-ITC, Malvern Instruments, Westborough, MA) was used to assess the energetics of amphiphile interactions with lipid vesicles. LUVs comprised of DOPC or DOPC:DOPG (1:1 mole ratio) were prepared following a published extrusion method.³⁹ In brief, dried lipid films (pure DOPC or DOPC:DOPG 1:1 mole ratio) were hydrated with HEPES buffer, subject to 5 freeze-thaw cycles, and extruded through 100 nm

polycarbonate filters 10 times using a nitrogen-driven device (Lipex Biomembranes, Vancouver, BC, Canada).

The ITC sample cell (~1.4 mL) was filled with solutions of 25 μ M **B11** or **G7** dissolved in HEPES buffer, and the reference cell was filled with the same buffer. The syringe (250 μ L) was filled with LUV dispersions containing 5 mM total lipid. All solutions were degassed for 10 min prior to each experiment. Upon system equilibration and a 1 μ L pre-injection, 5 μ L aliquots were injected into the sample cell every 11 min for the first 4 injections, after which time aliquots were injected in 8-min intervals. Data were collected and processed using proprietary software from MicroCal. All experiments were performed at least in triplicate. Titrations of LUVs into buffer were conducted as negative controls and subtracted from experimental data.

3.5. References

1. Park, S. C.; Park, Y.; Hahm, K. S. *International Journal of Molecular Sciences* **2011**, *12*, 5971.
2. Lavery, G.; Gorman, S. P.; Gilmore, B. F. *International Journal of Molecular Sciences* **2011**, *12*, 6566.
3. Tew, G. N.; Scott, R. W.; Klein, M. L.; Degrado, W. F. *Accounts of chemical research* **2010**, *43*, 30.
4. Boucher, H. W.; Talbot, G. H.; Bradley, J. S.; Edwards, J. E., Jr.; Gilbert, D.; Rice, L. B.; Scheld, M.; Spellberg, B.; Bartlett, J. *Clinical Infectious Diseases* **2009**, *48*, 1.
5. Zhao, Y. *Current Opinion in Colloid & Interface Science* **2007**, *12*, 92.
6. Brogden, K. A. *Nature Reviews Microbiology* **2005**, *3*, 238.

7. Grenier, M. C.; Davis, R. W.; Wilson-Henjum, K. L.; LaDow, J. E.; Black, J. W.; Caran, K. L.; Seifert, K.; Minbiole, K. P. C. *Bioorganic & Medicinal Chemistry Letters* **2012**, 22, 4055.
8. Ling, L. L.; Schneider, T.; Peoples, A. J.; Spoering, A. L.; Engels, I.; Conlon, B. P.; Mueller, A.; Schaberle, T. F.; Hughes, D. E.; Epstein, S.; Jones, M.; Lazarides, L.; Steadman, V. A.; Cohen, D. R.; Felix, C. R.; Fetterman, K. A.; Millett, W. P.; Nitti, A. G.; Zullo, A. M.; Chen, C.; Lewis, K. *Nature* **2015**, advance online publication.
9. Scorciapino, M. A.; Pirri, G.; Vargiu, A. V.; Ruggerone, P.; Giuliani, A.; Casu, M.; Buerck, J.; Wadhwani, P.; Ulrich, A. S.; Rinaldi, A. C. *Biophys. J.* **2012**, 102, 1039.
10. Hancock, R. E. W.; Sahl, H.-G. *Nature Biotechnology* **2006**, 24, 1551.
11. LaDow, J. E.; Warnock, D. C.; Hamill, K. M.; Simmons, K. L.; Davis, R. W.; Schwantes, C. R.; Flaherty, D. C.; Willcox, J. A. L.; Wilson-Henjum, K.; Caran, K. L.; Minbiole, K. P. C.; Seifert, K. *European Journal of Medicinal Chemistry* **2011**, 46, 4219.
12. Mondal, D.; Zhanel, G. G.; Schweizer, F. *Carbohydrate Research* **2011**, 346, 588.
13. Liu, D. H.; Choi, S.; Chen, B.; Doerksen, R. J.; Clements, D. J.; Winkler, J. D.; Klein, M. L.; DeGrado, W. F. *Angewandte Chemie-International Edition* **2004**, 43, 1158.
14. Paslay, L. C.; Abel, B. A.; Brown, T. D.; Koul, V.; Choudhary, V.; McCormick, C. L.; Morgan, S. E. *Biomacromolecules* **2012**, 13, 2472.
15. Gabriel, G. J.; Madkour, A. E.; Dabkowski, J. M.; Nelson, C. F.; Nusslein, K.; Tew, G. N. *Biomacromolecules* **2008**, 9, 2980.
16. Palermo, E. F.; Vemparala, S.; Kuroda, K. *Biomacromolecules* **2012**, 13, 1632.
17. Zhang, Y.; Ding, M. M.; Zhou, L. J.; Tan, H.; Li, J. H.; Xiao, H. N.; Li, J. S.; Snow, J. *Polymer Chemistry* **2012**, 3, 907.
18. Isabel Martin, V.; de la Haba, R. R.; Ventosa, A.; Congiu, E.; Julio Ortega-Calvo, J.; Luisa Moya, M. *Colloids and Surfaces B-Biointerfaces* **2014**, 114, 247.
19. Wu, R.; Al-Azemi, T. F.; Bisht, K. S. *Biomacromolecules* **2008**, 9, 2921.

20. Tounsi, N.; Dupont, L.; Mohamadou, A.; Aplincourt, M.; Plantier-Royon, R.; Massicot, F.; Harakat, D.; Portella, C. *Journal of Inorganic Biochemistry* **2005**, *99*, 2423.
21. Murray, P. R.; Baron, E. J.; Pfaller, M. A.; Tenover, F. C.; Tenover, R. H. *Manual of Clinical Microbiology*; 7th ed.; ASM Press: Washington, DC, 1999.
22. Klancnik, A.; Piskernik, S.; Jeršek, B.; Mozina, S. S. *J. Microbiol. Methods* **2010**, *81*, 121.
23. O'Toole, G. A.; Wathier, M.; Zegans, M. E.; Shanks, R. M. Q.; Kowalski, R.; Grinstaff, M. W. *Cornea* **2012**, *31*, 810.
24. Salton, M.; Kim, K. *Medical Microbiology*; 4th ed.; University of Texas Medical Branch at Galveston: Galveston (TX), 1996.
25. Calvez, P.; Bussières, S.; Demers, E.; Salesse, C. *Biochimie* **2009**, *91*, 718.
26. Kleinschmidt, J. H.; Tamm, L. K. *Biophys. J.* **2002**, *83*, 994.
27. Kennedy, M. T.; Brockman, H.; Rusnak, F. *Biochemistry* **1997**, *36*, 13579.
28. Epand, R. F.; Mowery, B. P.; Lee, S. E.; Stahl, S. S.; Lehrer, R. I.; Gellman, S. H.; Epand, R. M. *J. Mol. Biol.* **2008**, *379*, 38.
29. Seelig, J. *Biochim. Biophys. Acta-Rev. Biomembr.* **1997**, *1331*, 103.
30. Breukink, E.; Ganz, P.; de Kruijff, B.; Seelig, J. *Biochemistry* **2000**, *39*, 10247.
31. Domingues, T. M.; Mattei, B.; Seelig, J.; Perez, K. R.; Miranda, A.; Riske, K. A. *Langmuir* **2013**, *29*, 8609.
32. Binder, H.; Lindblom, G. *Biophys. J.* **2003**, *85*, 982.
33. Gabriel, G. J.; Pool, J. G.; Som, A.; Dabkowski, J. M.; Coughlin, E. B.; Muthukumar, M.; Tew, G. N. *Langmuir* **2008**, *24*, 12489.
34. Seelig, J. *Biochim. Biophys. Acta-Biomembr.* **2004**, *1666*, 40.
35. Livne, L.; Kovachi, T.; Sarig, H.; Epand, R. F.; Zaknoon, F.; Epand, R. M.; Mor, A. *Chemistry & Biology* **2009**, *16*, 1250.
36. Orwig, K. S.; Lassetter, M. R.; Hadden, M. K.; Dix, T. A. *J. Med. Chem.* **2009**, *52*, 1803.

37. Amara, N.; Mashiach, R.; Amar, D.; Krief, P.; Spieser, S. A. H.; Bottomley, M. J.; Aharoni, A.; Meijler, M. M. *Journal of the American Chemical Society* **2009**, *131*, 10610.
38. Han, G.; Tamaki, M.; Hruby, V. *Journal of Peptide Research* **2001**, *58*, 338.
39. Zhang, T.; Muraih, J. K.; Tishbi, N.; Herskowitz, J.; Victor, R. L.; Silverman, J.; Uwumarenogie, S.; Taylor, S. D.; Palmer, M.; Mintzer, E. *Journal of Biological Chemistry* **2014**, *289*, 11584.

4. APPENDIX: MISCELLANEOUS PROJECTS

This appendix summarizes a series of smaller projects, related to the overall goal of developing bioactive amphiphiles for therapeutic applications. The projects include preliminary work that can serve as a foundation for future experiments, work done by collaborators, and exploration into the optimization of commonly used synthetic methods.

4.1. Quaternary-Ammonium Containing Amphiphiles for Intracranial Applications

Atherosclerosis, a leading cause of cardiovascular disease, is characterized by the accumulation of oxidized low-density lipoprotein (oxLDL) in the vascular intima, its scavenger receptor-mediated uptake by macrophages, and the resulting formation of lipid-rich inflammatory cells and arterial plaque.¹⁻⁹ As discussed in Chapter 2, amphiphilic macromolecules (AMs), comprised of an acylated sugar backbone conjugated to a poly(ethylene glycol) (PEG) tail, are promising cardiovascular disease treatments owing to their ability to reduce macrophage-mediated oxLDL uptake. These macromolecules self-assemble into nanoscale micelles and competitively inhibit oxLDL uptake through interacting with macrophage scavenger receptors.^{10,11} Although AM micelles have

demonstrated promising bioactivity *in vitro*, micelle integrity is often compromised *in vivo* due to large dilutions^{12,13} and serum protein binding.¹³⁻¹⁶

To overcome potential issues with AM micelle stability, York *et al.* formulated AMs into kinetically stabilized nanoparticles (NPs), composed of an AM shell and hydrophobic core solute.¹⁷ These NPs exhibited increased stability while maintaining anti-atherogenic biological efficacy.¹⁷ Furthermore, when administered to atherosclerotic mice, AM NPs accumulated in lesion sites of the aortic arch.¹⁸ While these studies suggest that AM NPs could be useful treatments for coronary artery disease, peripheral artery diseases may benefit from this treatment as well. For instance, intracranial artery disease (ICAD) is characterized by plaque accumulation in arteries of the brain (e.g., middle cerebral artery) and can result in stroke and transient ischemic attack (i.e., mini stroke).¹⁹ To treat ICAD, AMs would need to cross the blood brain barrier (BBB). Literature has indicated that NPs functionalized with quaternary ammonium (QA) moieties are capable of crossing the BBB.²⁰ Therefore, this work sought to functionalize bioactive AMs with QA moieties. These modified AMs could then be formulated into NPs and evaluated for intracranial applications (Figure 4.1). The different synthetic methodologies investigated for QA modification are presented.

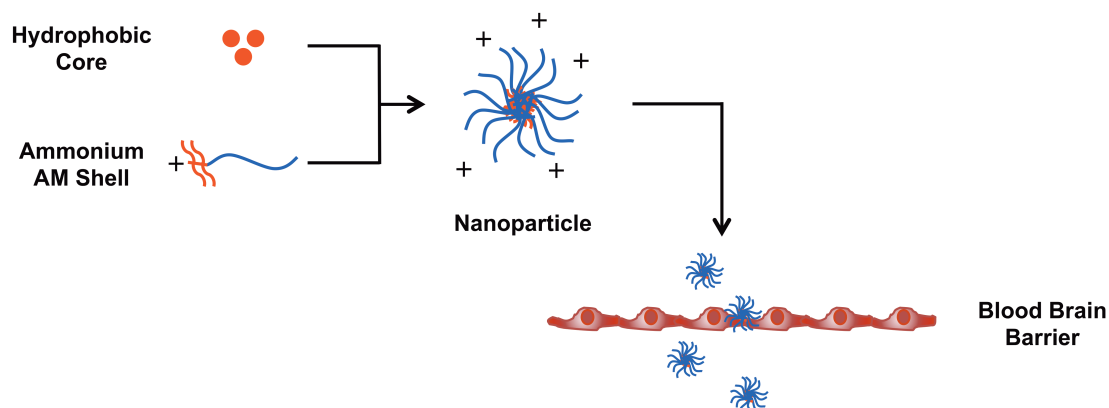


Figure 4.1. Depiction of QA-containing AM NP formulation for intracranial applications

4.1.1. Results and Discussion

To generate QA-containing AMs, synthetic methods concentrated on modifying a highly efficacious AM, **M12P5**, which is composed of a mucic acid backbone modified with dodecyl acyl chains and a 5 kDa PEG tail. Initial attempts investigated coupling choline chloride, a hydroxy-terminated quaternary ammonium salt, to this AM. Two reaction conditions were investigated: carbodiimide coupling using 4-dimethylaminopyridine (DMAP) as catalyst and acyl chloride activation followed by esterification (Figure 4.2). The limited solubility of choline chloride in organic solvents, however, may have hampered reaction efficacy. While proton (^1H) nuclear magnetic resonance (NMR) spectroscopy suggested a change in methine protons' chemical environment, the success of these reactions was inconclusive as analytical data (NMR spectra,

Fourier transform infrared spectra, and thermal properties) were masked by the AMs' large PEG component.

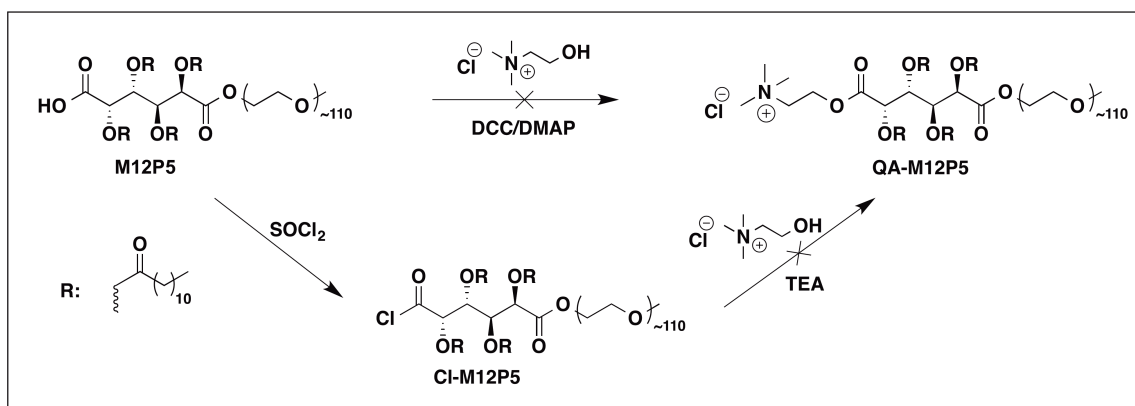


Figure 4.2. Synthetic methods investigated to conjugate choline chloride to **M12P5**

To overcome these issues, a new synthetic approach was proposed in which the AM's hydrophobic domain, **M12**, would be modified with a QA moiety prior to PEG functionalization (Figure 4.3), thereby simplifying structural characterizations. This approach employed a protected diamine starting material, instead of an ethanolamine salt (i.e., choline chloride), which exhibited improved organic solubility and would yield a more physiologically stable amide bond in the final AM structure. Within this synthesis, the AM hydrophobic domain, **M12**, was first reacted with N-Boc-ethylenediamine using carbodiimide coupling. Using dilute reaction conditions and stoichiometric equivalents of all reagents, the mono-coupled **M12** derivative, **Boc-M12**, was successfully isolated

in high yields (85 %). **Boc-M12** was subsequently deprotected using trifluoroacetic acid (TFA), to generate **Amine-M12** as a TFA salt.

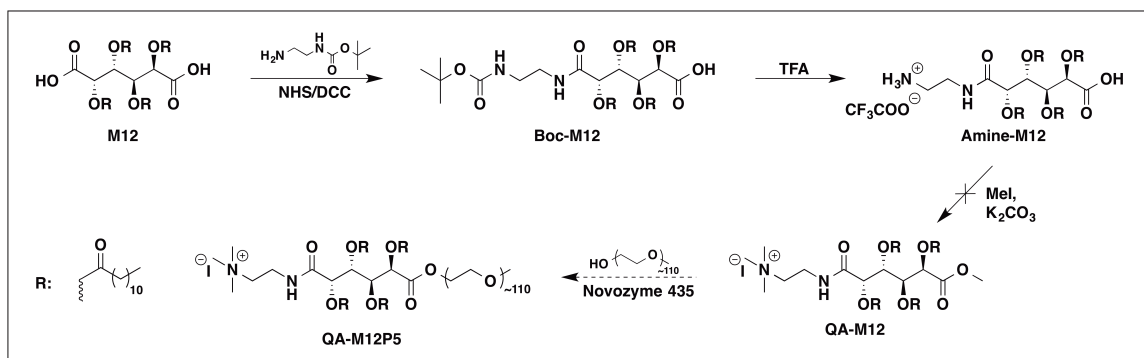


Figure 4.3. Proposed synthesis of **QA-M12P5** via a **QA-M12** intermediate

The synthesis of both **Boc-M12** and **Amine-M12** could be confirmed using ^1H NMR spectroscopy. The appearance of a large singlet at 1.45 ppm and a multiplet at 3.28 ppm (g and j in Figure 4.4B) were indicative of successful N-Boc-ethylenediamine conjugation. Furthermore, the relative integration of Boc methyl protons to protons of **M12** confirmed that the N-Boc-ethylenediamine was only conjugated to one of **M12**'s carboxylic acids. The synthesis of **Amine-M12** could subsequently be confirmed by the disappearance of Boc methyl and carbamate protons (absence of g and i in Figure 4.4C). Mass spectrometry (MS) further confirmed ^1H NMR spectral data.

Upon successful **Amine-M12** synthesis, amine alkylation conditions were investigated using methyl iodide (MeI) and potassium carbonate (K_2CO_3), with dimethyl formamide (DMF) as solvent. Numerous reaction conditions were explored, varying the equivalents of MeI and K_2CO_3 , temperature, and time. Reaction progress, monitored using 1H NMR spectroscopy and MS, suggested the initial formation of a methyl ester. While product formation was observed in MS after 24 h, NMR indicated the reaction was incomplete. Furthermore, MS

indicated that the reaction conditions investigated resulted in degradation over time (Figure 4.5), likely through the base-catalyzed cleavage of acyl arms.

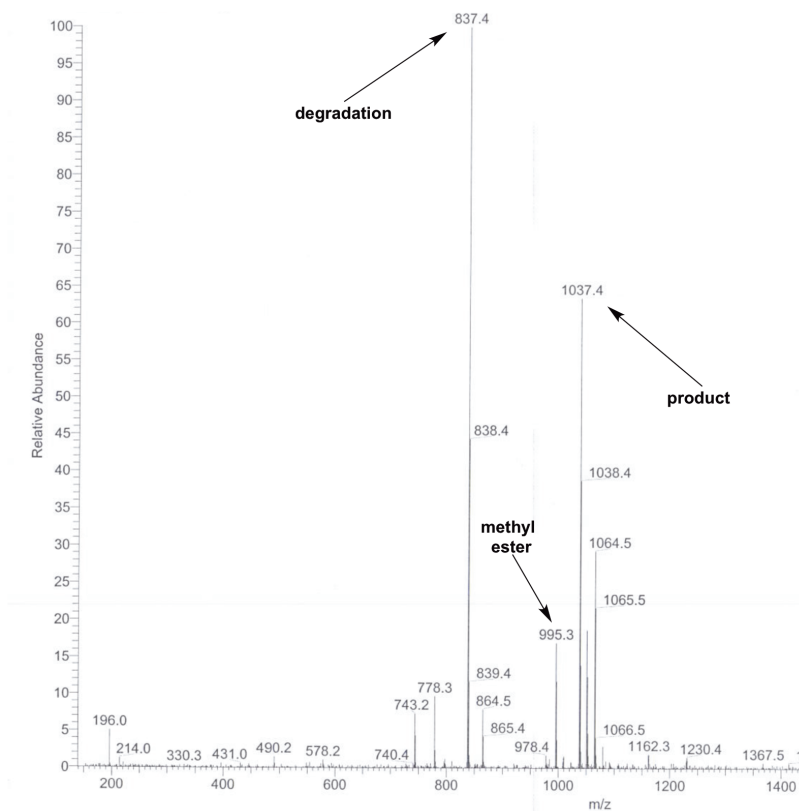


Figure 4.5. MS of reaction after 48 h, indicating the presence of **Boc-M12** methyl ester, **QA-M12** product, and degradation product

Although the synthetic methods investigated did not produce **QA-M12** as intended, they provided guidance as to what synthetic methodologies could be explored. Given that both DMF and K_2CO_3 are hygroscopic substances, it is plausible that hydroxide ions were generated in solution, promoting hydrolysis of the hydrophobic acyl arms. To circumvent these issues, future alkylation attempts can investigate drying reagents prior to or during the reaction (e.g.,

using 4Å sieves) and/or investigating less hygroscopic compounds. Furthermore, K_2CO_3 's poor solubility in organic solvents may have hindered reaction efficiency. Therefore, other bases with improved organic solubility, including tributylamine and 1,2,2,6,6-pentamethylpiperidine, which have shown promise in similar reactions,²¹ can be investigated for this application.

In addition to adjusting alkylation conditions, alternate synthetic pathways can be investigated. Through coupling N-Boc-ethylenediamine to **M12P5**, using reaction conditions similar to those employed for **Boc-M12** synthesis, **Boc-M12P5** can be synthesized. Given that the 1H NMR chemical shifts for **Boc-M12** have been elucidated in this work, the characterization of **Boc-M12P5** should be feasible despite the abundance of PEG protons. This compound can then be deprotected using TFA and alkylated using the methodologies outlined above to generate **QA-M12P5**.

4.1.2. Experimental

4.1.2.1. Synthesis of Boc-M12

M12 (1.12 mmol), and N-hydroxysuccinimide (NHS, 1.12 mmol) were dissolved in anhydrous dichloromethane (DCM, 80 mL) and DMF (10 mL) under N_2 . Dicyclohexylcarbodiimide (DCC, 1 M in DCM, 1.18 mmol) was added dropwise over 1 h. Upon complete DCC addition, the reaction mixture was stirred 1 h, followed by addition of N-Boc-ethylenediamine (1.18 mmol). After

stirring 2 d, the mixture was cooled to -20 °C and vacuum filtered to remove the solid urea byproduct. Filtrate was diluted with DCM, washed with aqueous solutions of 0.1 M hydrochloric acid (HCl, 2x) and brine (2x), dried over magnesium sulfate (MgSO₄), and concentrated *in vacuo*. The resulting solid was triturated in diethyl ether, filtered, and the filtrate concentrated *in vacuo* to an off-white solid which was further triturated in acetonitrile. White solid was subsequently isolated via vacuum filtration and dried *in vacuo*. Yield: 1.04 g, 85 % (white powder). ¹H-NMR (500 MHz, CDCl₃): δ 7.02 (br, 1H, NHCO), 5.75-5.11 (m, 4H, CH), 4.95 (br, 1H, NHCO), 3.28 (m, 4H, CH₂N), 2.36 (m, 8H, CH₂), 1.59 (m, 8H, CH₂), 1.45 (s, 9H, CH₃CO), 1.26 (br, 64H, CH₂), 0.88 (t, 12H, CH₃). ESI-MS *m/z*: 1079.5 [M-1].

4.1.2.2. Synthesis of Amine-M12

Boc-M12 (0.46 mmol) was dissolved in anhydrous DCM (25 mL) under N₂ and cooled to 0 °C. TFA (18.48 mmol) was added dropwise and the reaction mixture warmed gradually to ambient temperatures. Upon complete consumption of **Boc-M12** starting material (monitored by thin layer chromatography, TLC, 75:25 hexanes:ethyl acetate with 5 drops acetic acid), the reaction mixture was concentrated *in vacuo* to yield **Amine-M12** as a TFA salt. Yield: quantitative (sticky amber solid). ¹H-NMR (500 MHz, CDCl₃): δ 9.06 (br, COOH), 7.73 (br, 2H, NH), 7.44 (br, 1H, NHCO), 5.63-5.24 (m, 4H, CH), 3.41 (m,

4H, CH₂N), 2.38 (m, 8H, CH₂), 1.57 (m, 8H, CH₂), 1.25 (br, 64H, CH₂), 0.88 (t, 12H, CH₃). ESI-MS *m/z*: 981.5 [M+1].

4.1.3. References

1. Orford, J. L.; Selwyn, A. P.; Ganz, P.; Popma, J. J.; Rogers, C. *American Journal of Cardiology* **2000**, 86, 6H.
2. Ross, R. *N. Engl. J. Med.* **1999**, 340, 115.
3. Li, A. C.; Glass, C. K. *Nature Medicine* **2002**, 8, 1235.
4. Pirillo, A.; Norata, G. D.; Catapano, A. L. *Mediators of inflammation* **2013**, 12.
5. Yu, X.-H.; Fu, Y.-C.; Zhang, D.-W.; Yin, K.; Tang, C.-K. *Clinica Chimica Acta* **2013**, 424, 245.
6. Saha, P.; Modarai, B.; Humphries, J.; Mattock, K.; Waltham, M.; Burnand, K. G.; Smith, A. *Current Opinion in Pharmacology* **2009**, 9, 109.
7. Choudhury, R. P.; Lee, J. M.; Greaves, D. R. *Nature Clinical Practice Cardiovascular Medicine* **2005**, 2, 309.
8. Steinberg, D. *Journal of Biological Chemistry* **1997**, 272, 20963.
9. Tiwari, R. L.; Singh, V.; Barthwal, M. K. *Medicinal Research Reviews* **2008**, 28, 483.
10. Tian, L.; Yam, L.; Zhou, N.; Tat, H.; Uhrich, K. E. *Macromolecules* **2004**, 37, 538.
11. Chnari, E.; Nikitczuk, J. S.; Wang, J.; Uhrich, K. E.; Moghe, P. V. *Biomacromolecules* **2006**, 7, 1796.
12. Kim, S.; Shi, Y.; Kim, J. Y.; Park, K.; Cheng, J.-X. *Expert opinion on drug delivery* **2010**, 7, 49.
13. Savic, R.; Azzam, T.; Eisenberg, A.; Maysinger, D. *Langmuir* **2006**, 22, 3570.

14. Gaucher, G.; Dufresne, M. H.; Sant, V. P.; Kang, N.; Maysinger, D.; Leroux, J. C. *Journal of controlled release : official journal of the Controlled Release Society* **2005**, *109*, 169.
15. Chen, H.; Kim, S.; He, W.; Wang, H.; Low, P. S.; Park, K.; Cheng, J. X. *Langmuir* **2008**, *24*, 5213.
16. Toncheva, V.; Schacht, E.; Ng, S. Y.; Barr, J.; Heller, J. *J. Drug Target.* **2003**, *11*, 345.
17. York, A. W.; Zablocki, K. R.; Lewis, D. R.; Gu, L.; Uhrich, K. E.; Prud'homme, R. K.; Moghe, P. V. *Adv. Mater.* **2012**, *24*, 733.
18. Lewis, D. R.; Petersen, L. K.; York, A. W.; Zablocki, K. R.; Joseph, L. B.; Kholodovych, V.; Prud'homme, R. K.; Uhrich, K. E.; Moghe, P. V. *Proceedings of the National Academy of Sciences* **2015**.
19. Gorelick, P. B.; Wong, K. S.; Bae, H.-J.; Pandey, D. K. *Stroke* **2008**, *39*, 2396.
20. Gil, E. S.; Li, J. S.; Xiao, H. N.; Lowe, T. L. *Biomacromolecules* **2009**, *10*, 505.
21. Sommer, H. Z.; Lipp, H. I.; Jackson, L. L. *The Journal of Organic Chemistry* **1971**, *36*, 824.

4.2. Cationic Amphiphilic Polymers for Antimicrobial Applications

Cationic amphiphiles have received widespread attention as antimicrobial agents that act via unique membrane-targeting mechanisms. These compounds interact with anionic bacterial membranes via a combination of electrostatic and hydrophobic interactions, and their bactericidal activity is often modulated by their hydrophobic-to-charge ratio.¹⁻⁴ In Chapter 3, two novel series of cationic amphiphiles, termed bola-like and gemini-like amphiphiles, were investigated for antimicrobial applications. Through a combination of biological and biophysical

assessments, two lead actives were identified (Figure 4.6) and it was determined that amphiphile charge location significantly influenced antibacterial activity.

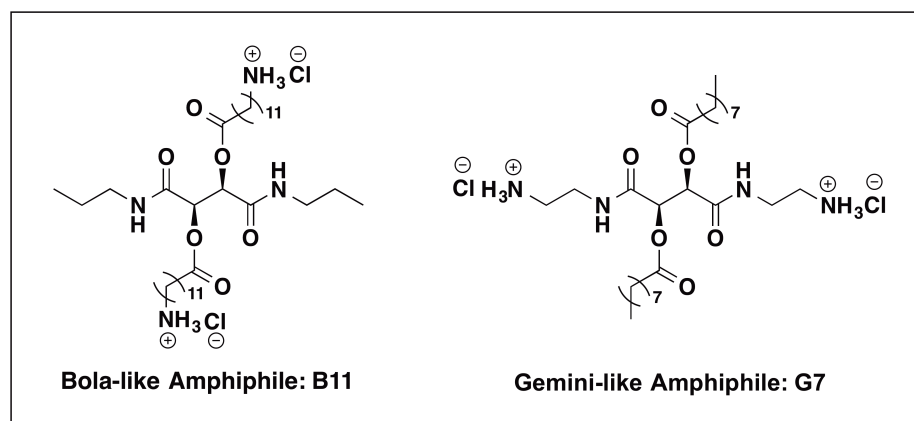


Figure 4.6. Lead antimicrobial amphiphiles, **B11** (left) and **G7** (right), identified in Chapter 3

While small molecular weight cationic amphiphiles have been investigated for a variety of antimicrobial applications, including food preservation, antibiotics, and water sterilization, they can suffer from environmental toxicity and short-term bioactivity.⁵ As an alternative, researchers have investigated cationic amphiphilic polymers for antimicrobial applications.^{3,4,6-9} Such polymers often exhibit improved stability in the presence of enzymes, higher local charge concentrations (beneficial for membrane interactions), and reduced toxicity,^{5,6,10} resulting in safer, more potent antimicrobials. Therefore, we hypothesized that incorporating lead cationic amphiphiles, identified in Chapter 3, into polymer backbones, would yield potent antimicrobial polymers that could be formulated

into different geometries for antimicrobial applications. Preliminary attempts to polymerize **B11**, the most efficacious bola-like amphiphile, are presented.

4.2.1. Results and Discussion

To synthesize a polymer whose repeat units were structurally similar to **B11**, synthetic methods were investigated to generate a polyamide with an ethylene diamine linker. Initial attempts employed a well-known activated ester polymerization,¹¹⁻¹³ reacting a pentachlorophenol- (PCP-) activated ester with ethylene diamine (Figure 4.7). To synthesize the PCP-activated ester, 12-Bocaminododecanoic acid was first coupled to a dibenzyl tartrate (DBT) backbone using carbodiimide coupling. The acylated DBT was deprotected via hydrogenolysis to yield an acylated tartaric acid (TA), which was subsequently coupled to PCP. ¹H NMR spectra confirmed DBT acylation and benzyl deprotection via the appearance (a and b in Figure 4.8A) and disappearance (Figure 4.8B) of aromatic and benzyl protons, respectively. To confirm PCP activation both ¹H and carbon (¹³C) NMR spectroscopy were used. The splitting of methyl protons alpha to carbonyl esters (d in Figure 4.8C), closely resembling the splitting of analogous methyl protons in the acylated DBT precursor (d in Figure 4.8A), suggested the formation of a diester. Furthermore, ¹³C NMR spectra revealed successful conjugation and that no PCP starting material remained.

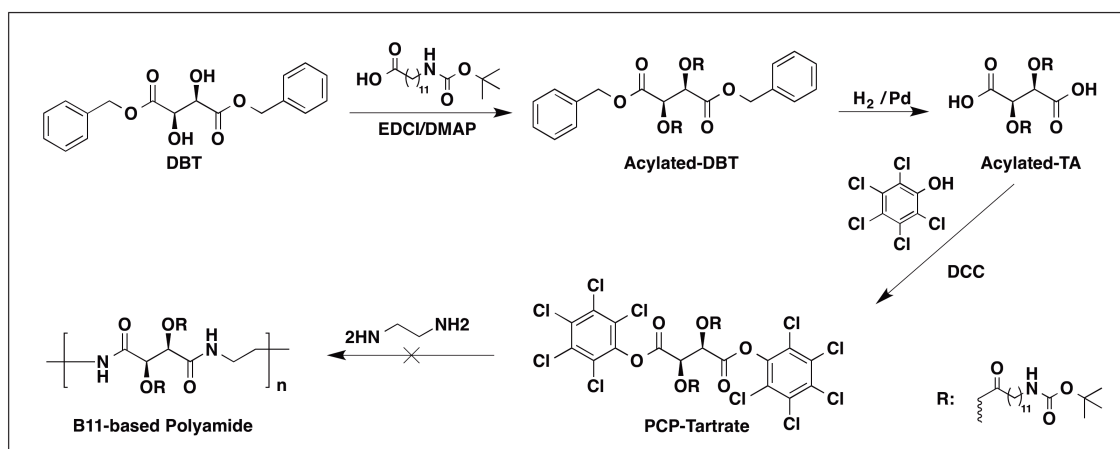


Figure 4.7. Synthetic scheme investigated to generate a **B11**-based polyamide via a PCP-activated ester intermediate

After confirming successful ester activation, the PCP-activated tartrate was reacted with stoichiometric amounts of ethylene diamine to generate a polyamide. While ¹H NMR spectroscopy and gel permeation chromatography (GPC) indicated some coupling took place, such that both oligomers and polymers of different molecular weights were generated, the reaction yield was very low and ester degradation occurred to yield free 12-Bocaminododecanoic acid.

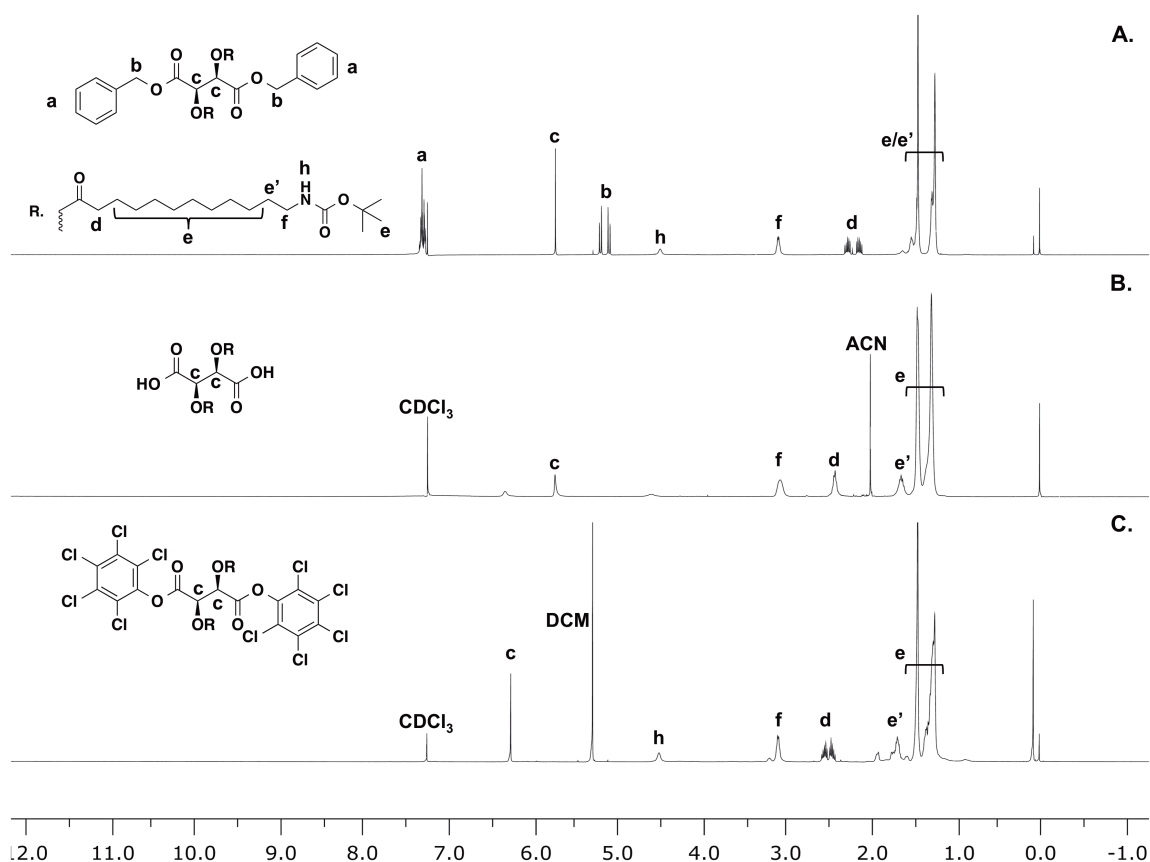


Figure 4.8. ^1H NMR spectra of 2,3-bis(12-Bocaminododecanoyl) -DBT (A), -TA (B), and -PCP (C)

As an alternate method, enzyme-catalyzed polymerization was investigated.¹⁴ To pursue this method, diethyl tartrate (ET) was first acylated with 12-Bocaminododecanoic acid, and the acylated product subsequently reacted with stoichiometric amounts of ethylene diamine in the presence of lipase (Novozyme 435, Figure 4.9), an inexpensive enzyme often used for polyester syntheses.¹⁴

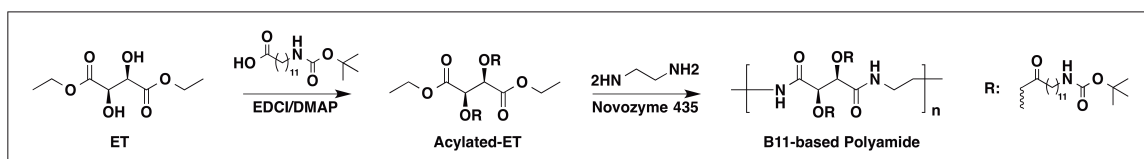


Figure 4.9. Synthetic scheme for lipase-catalyzed synthesis of **B11**-based polyamide

Polymerization product was precipitated from acetone and isolated as an off-white powder. The appearance of a new signal in the ^1H NMR spectrum (b in Figure 4.10) indicated coupling between diester and diamine, while GPC suggested the product was a pentamer of approximately 4.2 kDa. Differential scanning calorimetry (DSC) revealed a melting temperature (T_m) of $131\text{ }^\circ\text{C}$, suggesting oligomer crystallinity. Although the reaction yield was low, only unreacted starting material was present in the filtrate with no degradation products, suggesting the method was mild enough to preserve the acyl ester bonds. These preliminary findings suggest that lipase-catalyzed polymerizations could be used to generate a **B11**-based polyamide. Through optimizing reaction conditions (e.g., reaction time, temperature, percent lipase, volume solvent, and oligomerization conditions), yield could be improved. Once optimal polymerization conditions are identified, the product's Boc protecting groups can be selectively removed under acidic conditions¹⁵ to generate the final **B11** polyamide structure.

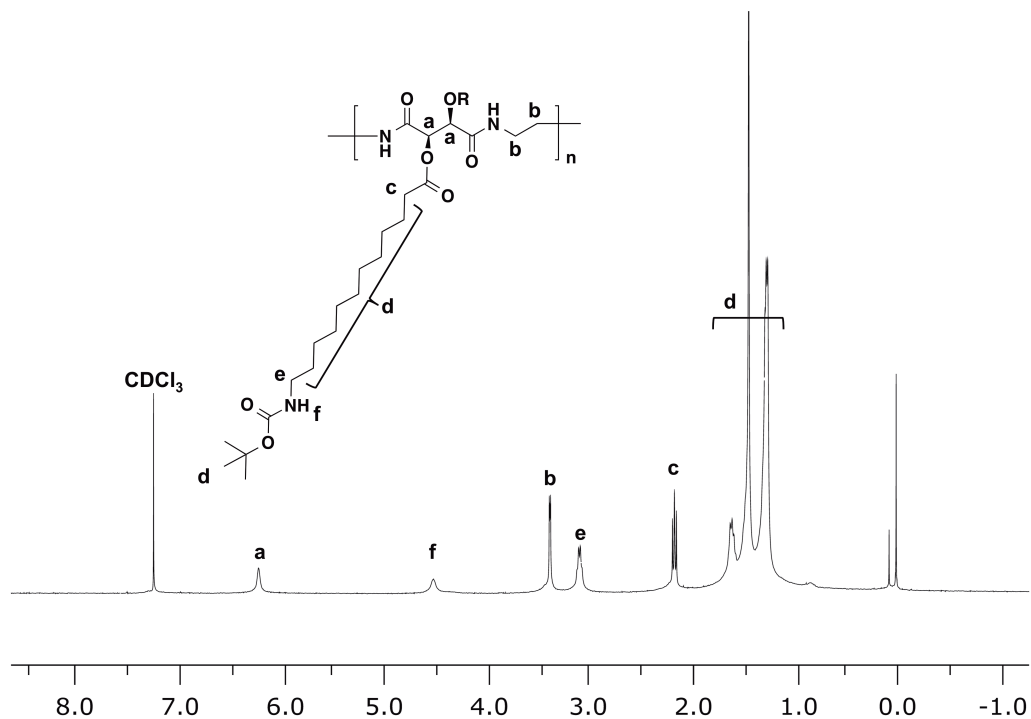


Figure 4.10. ^1H NMR spectrum of lipase-mediated polymerization product

4.2.2. Experimental

4.2.2.1. Synthesis of 2,3-bis(12-Bocaminododecanoyl) DBT

DBT (1.44 mmol), 12-Bocaminododecanoic acid (3.17 mmol), and catalytic DMAP (0.61 mmol) were dissolved in anhydrous DCM (25 mL) under argon. Upon dissolution, 1-ethyl-3-(3-dimethylaminopropyl)carbodiimide (EDCI, 6.05 mmol) was added as a coupling reagent and the reaction was stirred overnight under argon. The reaction mixture was diluted with DCM and washed with aqueous solutions of 10 % potassium bisulfite (3x) and saturated sodium

bicarbonate (NaHCO_3 , 3x) to remove the EDCI urea byproduct and unreacted 12-Bocaminododecanoic acid, respectively. The organic layer was washed with brine, dried over MgSO_4 and the product isolated *in vacuo*. Yield: 1.31 g, 98 % (pale yellow solid). $^1\text{H-NMR}$ (500 MHz, CDCl_3): δ 7.30 (m, 10H, Ar-H), 5.74 (s, 2H, CH), 5.16 (dd, 4H, ArCH_2), 4.49 (br, 2H, NH), 3.10 (m, 4H, CH_2N), 2.27 (quin, 2H, CH_2CO), 2.14 (quin, 2H, CH_2CO), 1.44 (m, 54H, Boc- CH_3 , CH_2).

4.2.2.2. Synthesis of 2,3-bis(12-Bocaminododecanoyl) TA

2,3-bis(12-Bocaminododecanoyl) DBT (1.41 mmol) was deprotected following modified literature procedures,^{16,17} using H_2 and a 10 % w/w Palladium on Carbon (Pd/C) catalyst in anhydrous DCM (10 mL). The reaction mixture was passed through a Celite filter using DCM (HPLC grade, 300 mL) to remove the catalyst and the filtrate concentrated *in vacuo*. Yield: 0.98 g, 93 % (sticky white solid). $^1\text{H-NMR}$ (400 MHz, CDCl_3): δ 5.75 (s, 2H, CH), 3.09 (m, 4H, CH_2N), 2.43 (m, 4H, CH_2CO), 1.65 (m, 4H, CH_2), 1.45 (m, 50H, Boc- CH_3 , CH_2).

4.2.2.3. Synthesis of 2,3-bis(12-Bocaminododecanoyl) PCP

PCP (2.82 mmol) was placed in a reaction flask under N_2 . 2,3-bis(12-Bocaminododecanoyl) TA (1.28 mmol) was dissolved in DCM (10 mL) and this solution added to the reaction flask. Upon complete dissolution of PCP, the reaction mixture was cooled to 0 °C, and DCC (2.82 mmol, 1 M in DCM) added

dropwise over 15 min. The reaction mixture was gradually warmed to room temperature and stirred 2 d. Product formation was monitored via TLC, using a combination of ultraviolet detection and ninhydrin staining to confirm the product contained aromatic rings and Boc groups, respectively. After 2 d, the reaction mixture was cooled to -20 °C for 2 h and vacuum filtered to remove the solid urea byproduct. The filtrate was then diluted with DCM, washed with aqueous solutions of 1 M HCl (3x), saturated NaHCO₃ (3x), and brine (1x), and dried over MgSO₄. Crude product was isolated *in vacuo*. Purification attempts could not remove residual DCC byproducts, thus product yield was not calculated. NMR, however, was used to understand the relative ratio of product to DCC byproduct for subsequent reaction steps. Product appearance: sticky orange solid. ¹H-NMR (500 MHz, CDCl₃): δ 6.27 (s, 2H, CH), 4.51 (br, 2H, NH), 3.10 (m, 4H, CH₂N), 2.53 (quin, 2H, CH₂CO), 2.47 (quin, 2H, CH₂CO), 1.68 (m, 4H, CH₂), 1.44 (m, 50H, Boc-CH₃, CH₂). ¹³C-NMR (500 MHz, CDCl₃, downfield region only): δ 171.11, 160.82, 154.95, 141.85, 131.54.

4.2.2.4. Polymerization of 2,3-bis(12-Bocaminododecanoyl) PCP

2,3-bis(12-Bocaminododecanoyl) PCP (0.56 mmol) was dissolved in DCM (1.5 or 15 mL) under N₂ and cooled to 0 °C. Separately, ethylene diamine was dissolved in DCM (100 µL into 1.5 mL DCM) to make a stock solution. An aliquot of stock solution (0.56 mmol) was added slowly to the reaction flask via syringe, and the reaction stirred 3 d. Diethyl ether was added to precipitate a white, gel-

like solid, which was isolated via vacuum filtration or centrifugation (1370 x *g*, 5 min). ¹H NMR spectra and GPC indicated that although coupling occurred, product was impure and further purification methods were not pursued given the minimal amount of final product generated.

4.2.2.5. Synthesis of 2,3-bis(12-Bocaminododecanoyl) ET

ET (0.43 mmol), 12-bocaminododecanoic acid (0.95 mmol), and DMAP (0.18 mmol) were dissolved in anhydrous DCM (8 mL) under N₂, and EDCI added. After stirring overnight, the reaction mixture was diluted with DCM and washed with aqueous solutions of 1 M HCl (3x), saturated NaHCO₃ (3x), and brine (1x). The organic layer was dried over MgSO₄ and concentrated *in vacuo* to give pure product. Yield: 0.30 g, 87 % (yellow oil). ¹H-NMR (400 MHz, CDCl₃): δ 5.57 (s, 2H, CH), 4.70 (br, 2H, NH), 4.09 (m, 4H, CH₂O), 2.96 (m, 4H, CH₂N), 2.28 (m, 4H, CH₂CO), 1.50 (m, 4H, CH₂), 1.30 (m, 56H, Boc-CH₃, CH₂).

4.2.2.6. Polymerization of 2,3-bis(12-Bocaminododecanoyl) ET

2,3-bis(12-Bocaminododecanoyl) ET (0.24 mmol) and ethylene diamine (0.24 mmol) were suspended in diphenyl ether (380 μL), and Novozyme 435 (20 mg, 10 wt %) added. The mixture was heated to 70 °C under N₂ and stirred overnight to promote oligomerization. After 15 h, the reaction mixture was placed under vacuum and heated to 90 °C to promote polymerization. The reaction was

stopped once solid formed (approximately 3 h), thereby preventing stirring. The crude product was dissolved in dilute chloroform and vacuum filtered to remove Novozyme 435. The filtrate was then concentrated *in vacuo* and acetone added, resulting in the precipitation of an off-white powder that was isolated via vacuum filtration. Yield: 25 mg, 13 % (off-white powder). $^1\text{H-NMR}$ (400 MHz, $\text{DMSO-}d_6$): δ 6.24 (s, 2H, CH), 4.53 (br, 2H, NH), 3.39 (d, 4H, CH_2N), 3.09 (m, 4H, CH_2N), 2.17 (m, 4H, CH_2CO), 1.60 (m, 8H, CH_2), 1.44 (m, 46H, Boc- CH_3 , CH_2). Weight-averaged molecular weight (M_w): 4.2 kDa; T_m : 131 °C.

4.2.3. References

1. Grenier, M. C.; Davis, R. W.; Wilson-Henjum, K. L.; LaDow, J. E.; Black, J. W.; Caran, K. L.; Seifert, K.; Minbiole, K. P. C. *Bioorganic & Medicinal Chemistry Letters* **2012**, 22, 4055.
2. LaDow, J. E.; Warnock, D. C.; Hamill, K. M.; Simmons, K. L.; Davis, R. W.; Schwantes, C. R.; Flaherty, D. C.; Willcox, J. A. L.; Wilson-Henjum, K.; Caran, K. L.; Minbiole, K. P. C.; Seifert, K. *European Journal of Medicinal Chemistry* **2011**, 46, 4219.
3. Gabriel, G. J.; Madkour, A. E.; Dabkowski, J. M.; Nelson, C. F.; Nusslein, K.; Tew, G. N. *Biomacromolecules* **2008**, 9, 2980.
4. Palermo, E. F.; Vemparala, S.; Kuroda, K. *Biomacromolecules* **2012**, 13, 1632.
5. Kenawy, E.-R.; Worley, S. D.; Broughton, R. *Biomacromolecules* **2007**, 8, 1359.
6. Scorciapino, M. A.; Pirri, G.; Vargiu, A. V.; Ruggerone, P.; Giuliani, A.; Casu, M.; Buerck, J.; Wadhwani, P.; Ulrich, A. S.; Rinaldi, A. C. *Biophys. J.* **2012**, 102, 1039.
7. Paslay, L. C.; Abel, B. A.; Brown, T. D.; Koul, V.; Choudhary, V.; McCormick, C. L.; Morgan, S. E. *Biomacromolecules* **2012**, 13, 2472.

8. Gabriel, G. J.; Pool, J. G.; Som, A.; Dabkowski, J. M.; Coughlin, E. B.; Muthukurnar, M.; Tew, G. N. *Langmuir* **2008**, *24*, 12489.
9. Bai, Y. X.; Liu, Y. B.; Li, Y. F.; Zhang, Q. *Polymers for Advanced Technologies* **2012**, *23*, 581.
10. Liu, D. H.; Choi, S.; Chen, B.; Doerksen, R. J.; Clements, D. J.; Winkler, J. D.; Klein, M. L.; DeGrado, W. F. *Angewandte Chemie-International Edition* **2004**, *43*, 1158.
11. Marques, M. S.; Regano, C.; Nyugen, J.; Aidanpa, L.; Munoz-Guerra, S. *Polymer* **2000**, *41*, 2765.
12. Garcia-Martin, M. D. G.; Hernandez, E. B.; Perez, R. R.; Alla, A.; Munoz-Guerra, S.; Galbis, J. A. *Macromolecules* **2004**, *37*, 5550.
13. Alla, A.; Oxelbark, J.; Rodriguez-Galan, A.; Munoz-Guerra, S. *Polymer* **2005**, *46*, 2854.
14. Ragupathy, L.; Ziener, U.; Dyllick-Brenzinger, R.; von Vacano, B.; Landfester, K. *Journal of Molecular Catalysis B-Enzymatic* **2012**, *76*, 94.
15. Han, G.; Tamaki, M.; Hruby, V. *Journal of Peptide Research* **2001**, *58*, 338.
16. Ihre, H.; De Jesus, O. L. P.; Frechet, J. M. J. *Journal of the American Chemical Society* **2001**, *123*, 5908.
17. Poree, D. E.; Zablocki, K.; Faig, A.; Moghe, P. V.; Uhrich, K. E. *Biomacromolecules* **2013**, *14*, 2463.

4.3. Screening Cationic Amphiphile Activity Against Clinically Relevant Pathogens

[These studies were conducted by the Nancy Connell laboratory in collaboration with the Joel Freundlich laboratory at Rutgers New Jersey Medical School]

The antimicrobial amphiphiles discussed in Chapter 3 were designed to mimic antimicrobial peptide (AMP) structural properties. Lead compounds from these series exhibited promising activity against representative gram-positive and gram-negative bacteria, likely through a membrane-targeted mechanism of action. While these studies are promising, multiple bacteria types are responsible for the pervasive increase in hospital-born infections and multidrug-resistant bacteria. The majority of resistance issues stem from a group of bacteria termed the ESKAPE pathogens (*Enterococcus faecium*, *Staphylococcus aureus*, *Klebsiella pneumoniae*, *Acinetobacter baumannii*, *Pseudomonas aeruginosa*, and *Enterobacter* species), which have been implicated in over 40 % of hospital-born intensive care unit infections.^{1,2} Therefore, we screened the clinical relevance and potential of the aforementioned bola- and gemini-like amphiphiles against other pathogens.

4.3.1. Results and Discussion

Bola- and gemini-like amphiphiles were screened against a series of bacteria, including five ESKAPE pathogens. Amphiphiles were incubated with different bacteria types and their minimum inhibitory concentration (MIC) determined, corresponding to the lowest amphiphile concentration that yielded no bacterial growth. Of all the amphiphiles tested, **G7** and **G9** – corresponding to gemini-like amphiphiles with 7 and 9 methylenes within their aliphatic arms – exhibited the lowest MIC values and therefore, the highest antimicrobial activity

(Table 4.1). Furthermore, these amphiphiles' lower cytotoxicity against Vero cells suggests **G7** and **G9** would be biocompatible if administered at their effective concentrations.

Table 4.1. Bola- and gemini-like amphiphiles MIC values ($\mu\text{g/mL}$) against various bacteria types; Assays with Vero cells demonstrate amphiphile cytocompatibility; ESKAPE pathogens are underlined; MICs highlighted in green and yellow depict very potent and potent treatments, respectively

	G11	G9	G7	B11	B9	B7
Vero Cell Cytotoxicity	25	50	> 50	50	50	50
<u>A. baumannii</u>	> 50	> 50	> 50	> 50	> 50	> 50
<u>B. cereus</u>	> 50	6.25	6.25	50	> 50	> 50
<u>B. cepacia</u>	> 50	> 50	> 50	> 50	> 50	> 50
<u>B. neotomae</u>	> 50	3.125	3.125	25	> 50	> 50
<u>E. faecium</u>	> 50	6.25	6.25	25	> 50	> 50
<u>K. pneumoniae</u>	> 50	> 50	50	> 50	> 50	> 50
<u>L. pneumophila</u>	> 50	25	12.5	> 50	> 50	> 50
<u>P. aeruginosa</u>	> 50	> 50	25	> 50	> 50	> 50
<u>S. aureus</u>	> 50	6.25	6.25	25	50	> 50
<u>Y. pseudotuberculosis</u>	> 50	6.25	12.5	> 50	> 50	> 50
<u>S. epidermidis</u>	50	6.25	12.5	25	> 50	> 50

Interestingly, both **G7** and **G9** demonstrated potent activity against two ESKAPE pathogens, *E. faecium* and *S. aureus*. These results are particularly significant given the abundance of infections connected to these pathogens. *E. faecium* exhibits resistance to vancomycin and ampicillin¹ and is the third leading cause of blood stream infections in US hospitals,² while methicillin-resistant *S. aureus* currently causes more hospital deaths in the US than HIV and tuberculosis combined.² Additionally, **G9** exhibited strong activity against *S. epidermidis*, a skin-colonizing, gram-positive bacterium closely related to *S.*

aureus.³ As *S. epidermidis* is the primary cause of medical device-related infections, this strain is another valuable target for preventing hospital-born infections. These combined results indicate that **G7** and **G9** possess antimicrobial activity against clinically relevant bacterial strains. Given their cytocompatibility, these compounds should be further explored in antibiotic applications.

4.3.2. References

1. Rice, L. B. *Infection Control and Hospital Epidemiology* **2010**, 31, S7.
2. Boucher, H. W.; Talbot, G. H.; Bradley, J. S.; Edwards, J. E., Jr.; Gilbert, D.; Rice, L. B.; Scheld, M.; Spellberg, B.; Bartlett, J. *Clinical Infectious Diseases* **2009**, 48, 1.
3. Otto, M. *Nature Reviews Microbiology* **2009**, 7, 555.

4.4. Investigation into Antimicrobial Amphiphile Critical Micelle Concentrations

Cationic amphiphiles have received widespread attention as antimicrobial agents given their ability to disrupt bacterial membranes. This unique mechanism of action often reduces the development of bacterial resistance, rendering antimicrobial amphiphiles promising antibiotics.^{1,2} To disrupt bacterial membranes, amphiphiles may act via different mechanisms, including pore-

forming mechanisms and detergent-like mechanisms.²⁻⁴ The carpet model, for instance, describes a detergent-like mechanism in which amphiphiles accumulate on the bacterial membrane until reaching their critical micelle concentration (CMC), at which time micelles form and solubilize membrane components.²⁻⁴ Given that the cationic amphiphiles designed in Chapter 3 demonstrated antimicrobial activity and membrane-targeting activity, it is plausible that they act through a similar mechanism. To understand whether micellization is important for bola-like and gemini-like amphiphiles' antimicrobial activity, preliminary studies were conducted to assess amphiphile aggregation behavior.

4.4.1. Results and Discussion

As preliminary dynamic light scattering measurements indicated that **B11** forms nanoscale assemblies, surface pressure measurements were used to investigate **B11**'s critical micelle concentration. These studies indicated that **B11** underwent an aggregation event at approximately 28 μM (Figure 4.11), close to **B11**'s MIC value against *S. aureus*. While this result could suggest that micellization influences **B11**'s activity against *S. aureus*, further studies need to be conducted to ascertain whether membrane solubilization is observed *in vitro*. Similar studies can be conducted for both **G7** and **G9**, as they showed promising activity against a range of bacteria.

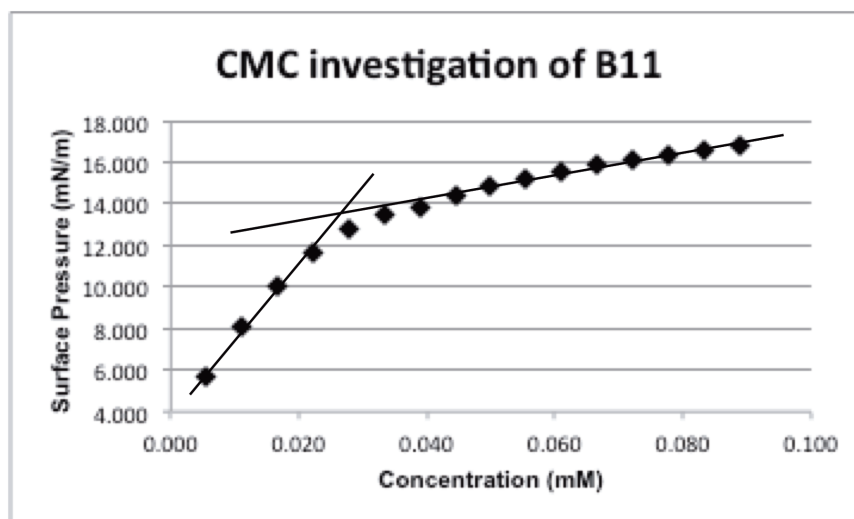


Figure 4.11. Surface pressure increase as a function of **B11** concentration; The inflection point corresponds to **B11**'s CMC

4.4.2. Experimental

Surface pressure was monitored using a Langmuir surface balance equipped with a custom-built microtrough from KSV-Nima (Biolin Scientific, Espoo, Finland). The trough was filled with 4-(2-hydroxyethyl)-1-piperazineethanesulfonic acid (HEPES) buffer (9 mL, 10 mM HEPES, pH 7.4) and surface pressure allowed to equilibrate. **B11** was dissolved in buffer at a concentration of 10 mM, injected into the trough via a side port (5 μ L injection volume), and surface pressure increase monitored. Upon surface pressure equilibration, a subsequent injection was made. This process was repeated until surface pressure increase appeared uniform. Data were collected and processed using KSV Nima and Microsoft Excel.

4.4.3. References

1. Grenier, M. C.; Davis, R. W.; Wilson-Henjum, K. L.; LaDow, J. E.; Black, J. W.; Caran, K. L.; Seifert, K.; Minbiole, K. P. C. *Bioorganic & Medicinal Chemistry Letters* **2012**, 22, 4055.
2. Lavery, G.; Gorman, S. P.; Gilmore, B. F. *International Journal of Molecular Sciences* **2011**, 12, 6566.
3. Park, S. C.; Park, Y.; Hahm, K. S. *International Journal of Molecular Sciences* **2011**, 12, 5971.
4. Brogden, K. A. *Nature Reviews Microbiology* **2005**, 3, 238.

4.5. Optimized Purification of NHS-Activated Hydrophobe

AMs, comprised of an acylated sugar-based hydrophobic domain conjugated to a PEG tail, have demonstrated promise as cardiovascular therapies.¹⁻⁶ To synthesize various AM derivatives, NHS ester activation is often employed.^{6,7} One such activated intermediate is **NHS-M12**, a linear, sugar-based hydrophobe modified with NHS-esters (Figure 4.12). As this activated hydrophobe is commonly used for AM derivatization, an efficient method to obtain pure **NHS-M12** is necessary. While published reaction conditions are capable of producing **NHS-M12**, conventional purification methods require

optimization in order to consistently isolate pure **NHS-M12**. An alternate purification method was investigated.

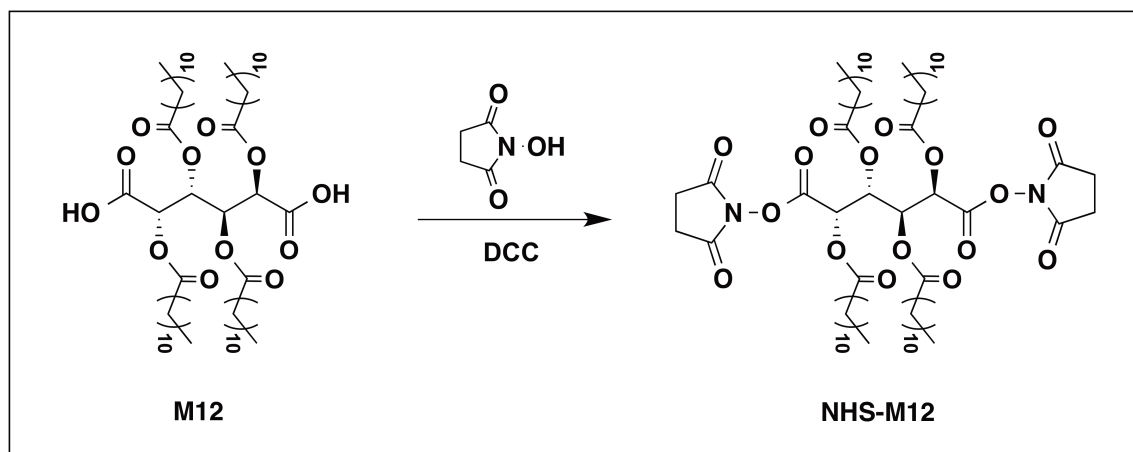


Figure 4.12. Synthetic scheme for **NHS-M12**

4.5.1. Results and Discussion

Previously outlined reaction conditions were employed to synthesize **NHS-M12**, using a carbodiimide coupling reagent.⁷ To isolate pure **NHS-M12** product, the reaction mixture was first filtered to remove urea byproduct and extracted to remove residual NHS and DCC. Established protocols indicated that pure product could be obtained by drying the resulting organic layer *in vacuo*. This methodology, however, yielded impurities (Figure 4.13A). As an alternative, pure product was precipitated multiple times from minimal DCM at -20 °C after extraction. The improvement in product purity was apparent when comparing the

^1H NMR spectra from each purification method (Figure 4.13). Furthermore, the new purification procedure enabled isolation of **NHS-M12** in high yields (85 %).

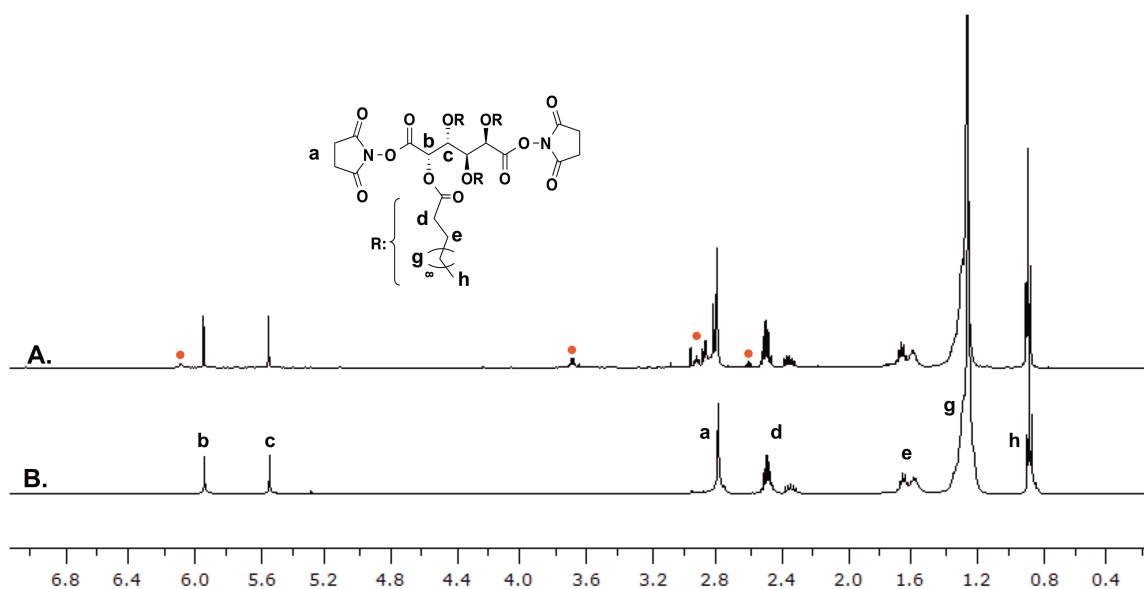


Figure 4.13. ^1H NMR spectra of product obtained from conventional (A) and optimized (B) purification methods; Impurities are denoted by red circles

4.5.2. Experimental

4.5.2.1. Synthesis of NHS-M12

NHS-M12 was synthesized according to modified literature procedures.⁷ In brief, **M12** (2.13 mmol) and NHS (19.28 mmol) were dissolved in anhydrous DCM (30 mL) and DMF (14 mL) under Argon and DCC (6.77 mmol, 1 M in DCM) added dropwise over 30 min. The reaction was stirred 24 h, cooled to $-20\text{ }^{\circ}\text{C}$ for 1 h, and vacuum filtered to remove the solid urea byproduct. The filtrate was

then washed with 0.1 M HCl (2x), brine (2x), and 50:50 brine:water (1x), dried over MgSO₄, and concentrated *in vacuo*. The resulting crude mixture was dissolved in minimal DCM, cooled to -20 °C, and the precipitate isolated via vacuum filtration. This precipitation process was repeated three times. Initial precipitation yielded pure urea byproduct, while the latter two precipitations yielded pure product. Yield: 2.06 g, 85 % (white powder). ¹H-NMR (500 MHz, CDCl₃): δ 5.95 (s, 2H, CH), 5.55 (s, 2H, CH), 2.79 (s, 8H, CH₂CO), 2.41 (m, 8H, CH₂CO), 1.61 (m, 8H, CH₂), 1.25 (br, 64H, CH₂), 0.87 (t, 12H, CH₃).

4.5.3. References

1. Chnari, E.; Nikitzuk, J. S.; Uhrich, K. E.; Moghe, P. V. *Biomacromolecules* **2006**, 7, 597.
2. Chnari, E.; Nikitzuk, J. S.; Wang, J.; Uhrich, K. E.; Moghe, P. V. *Biomacromolecules* **2006**, 7, 1796.
3. Wang, J.; Plourde, N. M.; Iverson, N.; Moghe, P.; Uhrich, K. E. *Int. J. Nanomed.* **2007**, 2, 697.
4. Iverson, N. M.; Sparks, S. M.; Demirdirek, B.; Uhrich, K. E.; Moghe, P. V. *Acta Biomaterialia* **2010**, 6, 3081.
5. Hehir, S.; Plourde, N. M.; Gu, L.; Poree, D. E.; Welsh, W. J.; Moghe, P. V.; Uhrich, K. E. *Acta Biomaterialia* **2012**, 8, 3956.
6. Poree, D. E.; Zablocki, K.; Faig, A.; Moghe, P. V.; Uhrich, K. E. *Biomacromolecules* **2013**, 14, 2463.
7. Sparks, S. M.; Waite, C. L.; Harmon, A. M.; Nusblat, L. M.; Roth, C. M.; Uhrich, K. E. *Macromolecular bioscience* **2011**, 11, 1192.

4.6. Synthesis of Di-*tert*-Butyl 5-Aminoisophthalate

Previous research has indicated that AMs possessing a rigid presentation of charged moieties in the hydrophobic domain exhibit promising anti-atherogenic bioactivity.^{1,2} One such AM, **2cbM**, contains two aromatic carboxylic acids conjugated to a mucic acid-based hydrophobic domain (Figure 4.14). While **2cbM** is a promising active, the methodologies employed for its synthesis are often unreliable, and the presence of multiple carboxylic acid moieties can yield unwanted byproducts during further modification attempts (e.g., conjugation to fluorophors). Consequently, it would be beneficial if **2cbM**'s precursor, 5-aminoisophthalic acid, were protected prior to **2cbM** synthesis, enabling new synthetic methodologies to be investigated and limiting **2cbM** side reactions. Di-*tert*-butyl 5-aminoisophthalate synthesis was therefore investigated to generate a protected **2cbM** precursor.

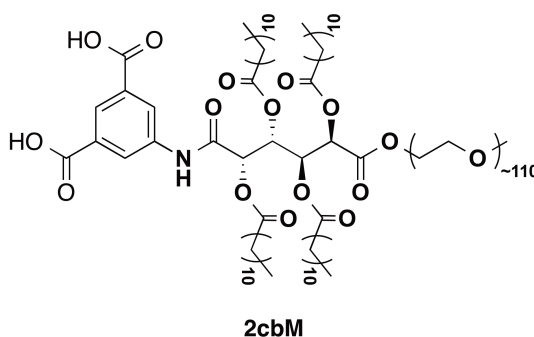


Figure 4.14. Chemical structure of **2cbM**

4.6.1. Results and Discussion

Initial attempts to synthesize di-*tert*-butyl 5-aminoisophthalate focused on acid catalyzed protections using *tert*-butanol (t-BuOH) and sulfuric acid (H₂SO₄) or *para*-toluenesulfonic acid. When these conditions yielded no product, 5-nitroisophthalate was investigated as alternate starting material, as research has suggested this compound can be *tert*-butyl ester protected and subsequently reduced to yield di-*tert*-butyl 5-aminoisophthalate. Following literature procedures,^{3,4} a DCC coupling reaction was investigated to generate the *tert*-butyl protected nitroisophthalate intermediate. ¹H and ¹³C NMR spectroscopy indicated pure product could be obtained after column chromatography. However, the presence of various impurities prior to chromatography (observed via TLC and NMR spectroscopy) suggested that the coupling procedure could be improved. Wentworth *et al.* indicated that *tert*-butyl protected nitroisophthalate could be synthesized by chlorination with oxalyl chloride followed by reaction with t-BuOH.⁵ These conditions were modified and optimized to obtain di-*tert*-butyl 5-nitroisophthalate in 62 % yield (Figure 4.15). This intermediate was subsequently reduced to di-*tert*-butyl 5-aminoisophthalate via hydrogenolysis.

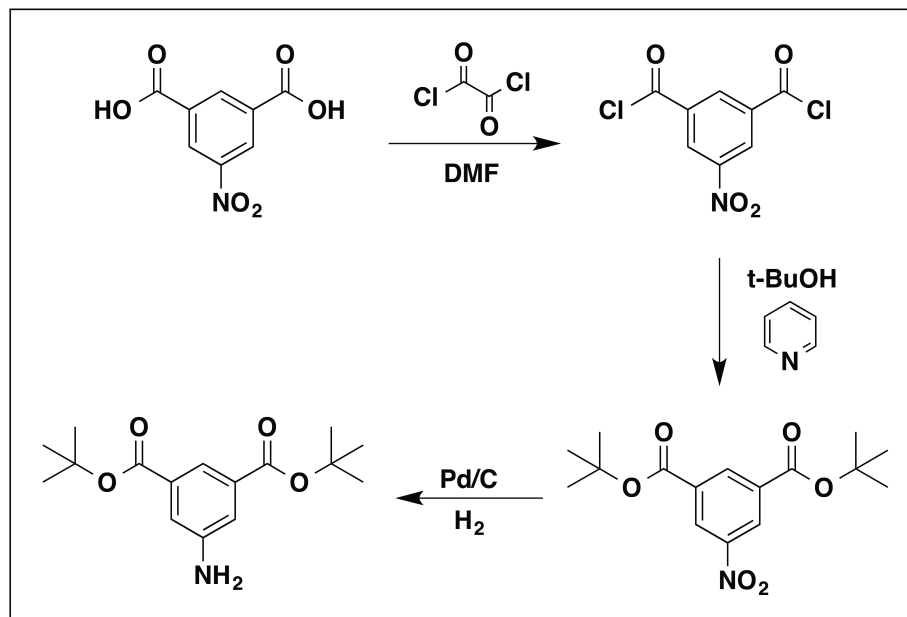


Figure 4.15. Synthetic scheme for di-*tert*-butyl 5-aminoisophthalate

NMR spectroscopy was used to confirm the synthesis of di-*tert*-butyl 5-nitroisophthalate and di-*tert*-butyl 5-aminoisophthalate. The appearance of a large singlet at 1.64 ppm (b in Figure 4.16A) indicated the successful *tert*-butyl protection of 5-nitroisophthalic acid, while the appearance of a broad signal at 3.92 ppm (c in Figure 4.16B) and the altered splitting of aromatic protons suggested successful reduction of the nitro group to yield di-*tert*-butyl 5-aminoisophthalate.

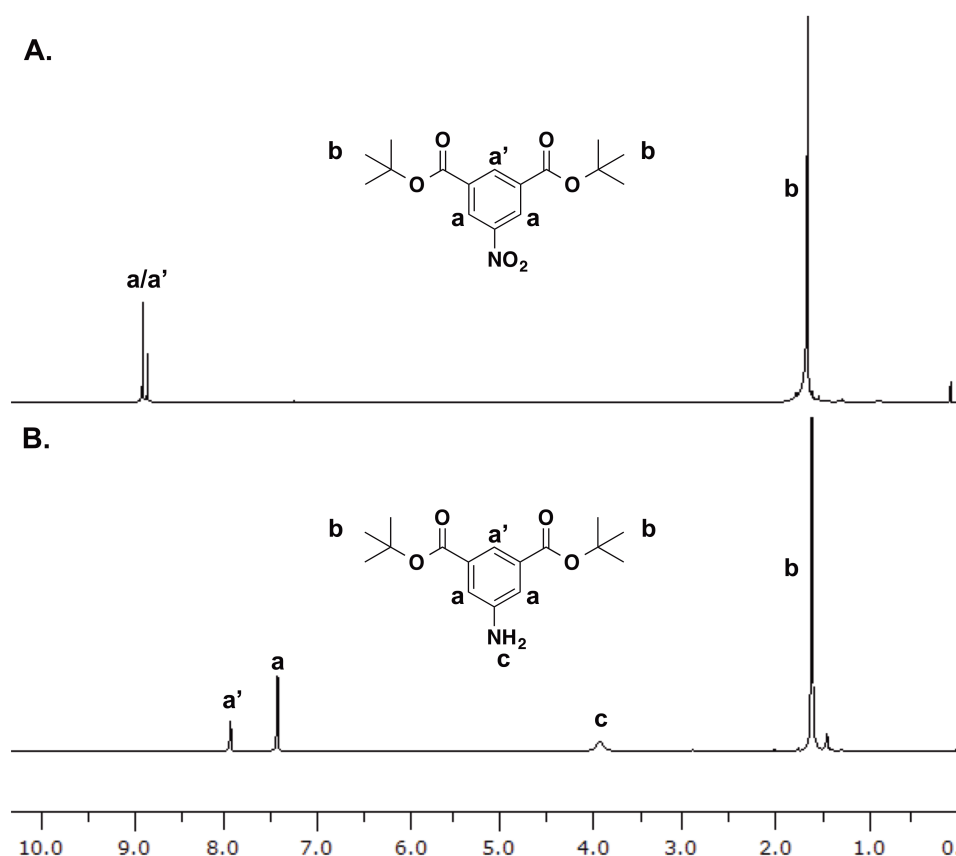


Figure 4.16. ^1H NMR spectra of di-*tert*-butyl 5-nitroisophthalate (A) and di-*tert*-butyl 5-aminoisophthalate (B)

4.6.2. Experimental

4.6.2.1. Synthesis of di-*tert*-butyl 5-nitroisophthalate

5-nitroisophthalic acid (0.47 mmol) was dissolved in anhydrous DCM (5 mL) and catalytic anhydrous DMF (0.20 mL). Upon complete dissolution of starting material, oxalyl chloride (2.37 mmol) was added slowly via syringe and

the reaction stirred 3 h. The reaction mixture was concentrated *in vacuo* to remove excess oxalyl chloride and placed under high vacuum for 1-2 h. The resulting chlorinated intermediate was then suspended in anhydrous pyridine under Argon, *t*-BuOH (4.74 mmol) added, and the reaction stirred 2 d. The reaction mixture was transferred to a separatory funnel, diluted with DCM, and washed with 1 M HCl to remove pyridine. The DCM layer was dried over MgSO₄, concentrated, and pure product isolated via flash chromatography (99:1 hexanes:ethylacetate). Yield: 0.47 g, 62 % (off-white solid). ¹H-NMR (500 MHz, CDCl₃): δ 8.92 (m, 3H, Ar-H), 1.64 (s, 18H, CH₃). ¹³C-NMR (500 MHz, CDCl₃): δ 163.08, 148.49, 135.83, 134.31, 127.80, 83.35, 28.31.

4.6.2.2. Synthesis of di-*tert*-butyl 5-aminoisophthalate

Di-*tert*-butyl 5-nitroisophthalate (0.37 mmol) was dissolved in methanol (5 mL) and minimal DCM (0.50 mL), and a 10 % w/w Pd/C catalyst added. The reaction flask was evacuated, filled with H₂, and stirred under H₂. After 24 h, the reaction mixture was passed through a Celite filter using DCM to remove the Pd/C catalyst and the filtrate concentrated *in vacuo* to yield pure product. Yield: 56 mg, 52 % (pale yellow solid). ¹H-NMR (400 MHz, CDCl₃): δ 7.96 (s, 1H, Ar-H), 7.44 (s, 2H, Ar-H), 3.92 (br, 2H, NH₂), 1.59 (s, 18H, CH₃). ¹³C-NMR (500 MHz, CDCl₃): δ 165.51, 146.60, 133.36, 120.78, 119.57, 81.43, 28.32.

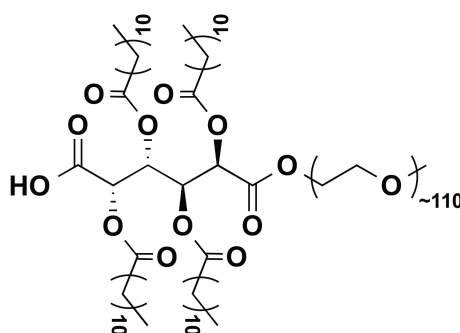
4.6.3. References

1. Iverson, N. M.; Sparks, S. M.; Demirdirek, B.; Uhrich, K. E.; Moghe, P. V. *Acta Biomaterialia* **2010**, *6*, 3081.
2. Hehir, S.; Plourde, N. M.; Gu, L.; Poree, D. E.; Welsh, W. J.; Moghe, P. V.; Uhrich, K. E. *Acta Biomaterialia* **2012**, *8*, 3956.
3. Roberts, J. M.; Fini, B. M.; Sarjeant, A. A.; Farha, O. K.; Hupp, J. T.; Scheidt, K. A. *Journal of the American Chemical Society* **2012**, *134*, 3334.
4. Drewe, W. C.; Nanjunda, R.; Gunaratnam, M.; Beltran, M.; Parkinson, G. N.; Reszka, A. P.; Wilson, W. D.; Neidle, S. *J. Med. Chem.* **2008**, *51*, 7751.
5. Wentworth, P.; Datta, A.; Smith, S.; Marshall, A.; Partridge, L. J.; Blackburn, G. M. *Journal of the American Chemical Society* **1997**, *119*, 2315.

4.7. Carboxylic Acid Protection of Mucic Acid

Mucic acid-based AMs (Figure 4.17), comprised of an acylated mucic acid backbone conjugated to a PEG tail, have exhibited promise as anti-atherogenic therapies.¹⁻³ Past studies have indicated that the presentation of aliphatic arms, dictated by mucic acid's meso stereochemistry, largely influences this bioactivity.^{4,5} As such, it would be beneficial to investigate other AM derivatives based on the mucic acid backbone. Given that mucic acid contains six functional groups (i.e., two carboxylic acids and four hydroxyls, Figure 4.18), chemical conjugation methods are limited as they may result in unwanted byproducts. Consequently, fewer mucic acid-based derivatives have been explored. Through

protecting mucic acid's carboxylic acid groups, a number of chemical coupling reactions could be employed, enabling the investigation of new modifications to mucic acid-based AMs' hydrophobic domain. This protection may also improve the organic solubility of the resulting mucate, enhancing the compound's reactivity and increasing product yields. Different methods were therefore investigated to protect mucic acid's carboxylic acids.



Mucic Acid-based AM

Figure 4.17. Chemical structure of conventional mucic acid-based AM (**M12P5**)

4.7.1. Results and Discussion

To synthesize a protected mucic acid backbone, reaction conditions were investigated that would either yield *tert*-butyl ester or benzyl ester protecting groups. These groups were chosen as they could be selectively cleaved without influencing alkyl ester moieties: *tert*-butyl esters could be cleaved via an acid catalyzed trifluoroacetic acid reaction, while benzyl esters could be cleaved using palladium-catalyzed hydrogenolysis.^{6,7} Reactions were conducted neat in

alcohol or dispersed in DMF at multiple temperatures. Reaction times ranged from 24 h to multiple days, with reaction progress monitored via TLC or NMR spectroscopy.

To generate di-*tert*-butyl mucate, the Steglich esterification was first investigated, using DCC or EDCI in the presence of a DMAP catalyst to couple of *t*-BuOH with mucic acid.⁸ This method has been previously used to generate *tert*-butyl esters,⁸ however, no discernible products were yielded under the conditions employed. Although mucic acid's hydroxyl moieties are sterically confined, it is plausible that they interfered with the coupling. Additionally, mucic acid's poor solubility may have hindered effective coupling. As an alternative, mucic acid was dispersed in *t*-BuOH in the presence of a Dowex catalyst⁹ or catalytic H₂SO₄.¹⁰ Within these reactions, the catalysts will donate protons to mucic acid's carboxylic acid moiety,¹¹ making nucleophilic attack by *t*-BuOH more favorable. Neither reaction yielded product.

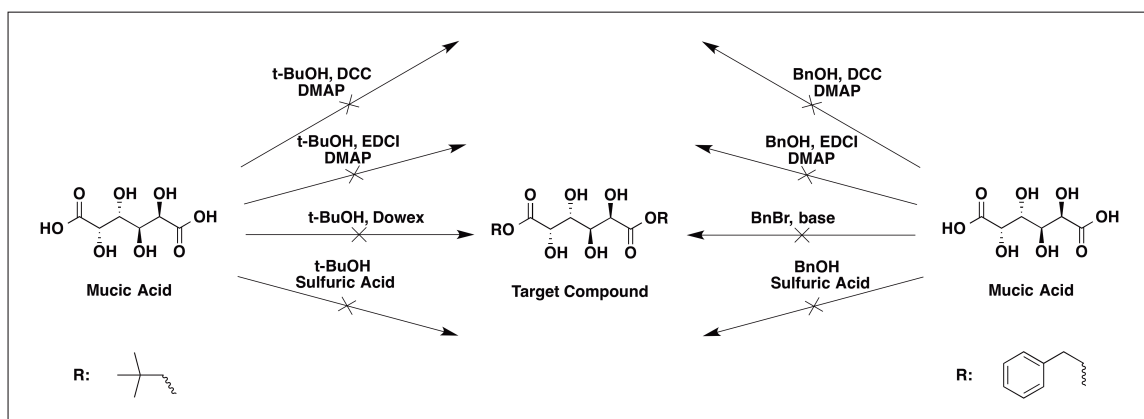


Figure 4.18. Reaction conditions attempted to generate *tert*-butyl (left) or benzyl (right) protected mucic acid; The reaction conditions attempted did not result in product formation

A series of reaction conditions was similarly explored to generate dibenzyl mucate. The aforementioned EDCI coupling, DCC coupling, and H_2SO_4 catalyzed esterifications were attempted using benzyl alcohol (BnOH). Additionally, mucic acid was reacted with benzyl bromide (BnBr) in the presence of various bases (e.g., imidazole, K_2CO_3 , sodium carbonate) to deprotonate mucic acid's carboxylic acids and promote nucleophilic attack.¹² The various conditions attempted to benzyl protect mucic acid also yielded no product.

Mucic acid protection was not possible using the aforementioned methods, as mucic acid's poor solubility likely hindered protection attempts. If a suitable solvent can be identified to solubilize mucic acid, protection attempts could be revisited. As an alternative, dendrimer branch points could be grown from a DBT backbone to achieve similar hydroxyl group presentation with potential for various chemical modifications (Figure 4.19).¹³

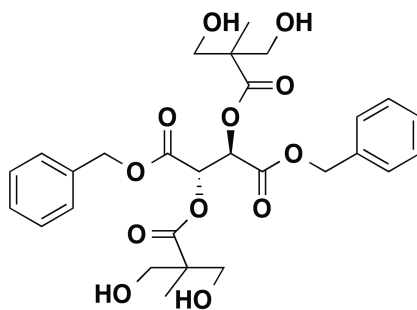


Figure 4.19. Meso DBT backbone modified with dendrimer branch points to enable conjugation to four hydrophobic arms

4.7.2. Experimental

4.7.2.1. Carbodiimide coupling

Mucic acid (1 eq), alcohol (2.05-2.2 eq), and DMAP (0.2-0.4 eq), were suspended in DMF. Carbodiimide (2.2 – 4.1 eq.) was added and the reaction stirred at temperatures ranging from 30 °C to 80 °C for a minimum of 24 h and a maximum of 10 d.

4.7.2.2. Dowex-catalyzed esterification

Mucic acid (1 eq) and catalytic Dowex 50wx2-200 were suspended in excess t-BuOH at 30 °C and the reaction stirred for 48 h.

4.7.2.3. Sulfuric acid-catalyzed esterification

Mucic acid (1 eq) was suspended in excess alcohol, catalytic H₂SO₄ added, and the reaction stirred at temperatures ranging from 90 °C to 120 °C for a minimum of 48 h and a maximum of 7 d.

4.7.2.4. Benzyl bromide protection

Mucic acid (1 eq) and base (2.05 – 2.2 eq) were suspended in DMF, BnBr (2.05 – 2.5 eq) added, and the reaction stirred at 60-70 °C for a minimum of 7 d and a maximum of 14 d.

4.7.2.5. Reaction purification

For the reactions explored, various reaction workup conditions were investigated, including extractions, filtrations, triturations, precipitations, and column chromatography.

4.7.3. References

1. Iverson, N. M.; Sparks, S. M.; Demirdirek, B.; Uhrich, K. E.; Moghe, P. V. *Acta Biomaterialia* **2010**, 6, 3081.

2. Chnari, E.; Nikitzuk, J. S.; Uhrich, K. E.; Moghe, P. V. *Biomacromolecules* **2006**, 7, 597.
3. Chnari, E.; Nikitzuk, J. S.; Wang, J.; Uhrich, K. E.; Moghe, P. V. *Biomacromolecules* **2006**, 7, 1796.
4. Hehir, S.; Plourde, N. M.; Gu, L.; Poree, D. E.; Welsh, W. J.; Moghe, P. V.; Uhrich, K. E. *Acta Biomaterialia* **2012**, 8, 3956.
5. Lewis, D. R.; Kholodovych, V.; Tomasini, M. D.; Abdelhamid, D.; Petersen, L. K.; Welsh, W. J.; Uhrich, K. E.; Moghe, P. V. *Biomaterials* **2013**, 34, 7950.
6. Craley, C. R.; Zhang, R.; Kowalewski, T.; McCullough, R. D.; Stefan, M. C. *Macromol. Rapid Commun.* **2009**, 30, 11.
7. Ihre, H.; De Jesus, O. L. P.; Frechet, J. M. J. *Journal of the American Chemical Society* **2001**, 123, 5908.
8. Neises, B.; Steglich, W. *Angewandte Chemie International Edition in English* **1978**, 17, 522.
9. Yadav, G. D.; Rahuman, M. *Org. Process Res. Dev.* **2002**, 6, 706.
10. Amslinger, S.; Hirsch, A.; Hampel, F. *Tetrahedron* **2004**, 60, 11565.
11. Zeng, Z.; Cui, L.; Xue, W.; Chen, J.; Che, Y. In *Chemical Kinetics*; Patel, V., Ed. 2012.
12. Katritzky, A. R.; Zhang, S.; Soares, A.; Wang, M. *Arkivoc* **2001**, 10, 54.
13. Poree, D. E.; Zablocki, K.; Faig, A.; Moghe, P. V.; Uhrich, K. E. *Biomacromolecules* **2013**, 14, 2463.

4.8. General Materials and Methods

DBT, 1 M HCl, and polytetrafluoroethylene (PTFE) syringe filters were purchased from Fisher Scientific (Fair Lawn, NJ). Silica gel was purchased from

VWR (Radnor, PA). All other reagents and solvents were purchased from Sigma-Aldrich (Milwaukee, WI) and used as received. **M12** and **M12P5** were prepared according to previously published procedures.¹ The synthesis of 12-Bocaminododecanoic acid is provided in Chapter 3.

NMR spectra were obtained using a Varian 400 or 500 MHz spectrophotometer. Samples were dissolved in deuterated chloroform (CDCl_3) with trimethylsilane as an internal reference or deuterated dimethyl sulfoxide ($\text{DMSO}-d_6$) as solvent and internal reference. Fourier transform infrared (FT-IR) spectra were recorded on a Thermo Scientific Nicolet iS10 spectrophotometer using OMNIC software with an average of 32 scans. FT-IR samples were pressed into potassium bromide discs (1 wt % sample).

Small molecule molecular weights were determined using a ThermoQuest Finnigan LCQ-DUO system equipped with a syringe pump, an optional divert/inject valve, an atmospheric pressure ionization source, a mass spectrometer detector, and the Xcalibur data system. Samples were prepared at a concentration of 10 $\mu\text{g/mL}$ in methanol. Polymer M_w data were determined by GPC, using a Waters LC system (Milford, MA), equipped with a 2414 refractive index detector, 1515 isocratic HPLC pump, 717plus autosampler, and two PL gel columns 103 and 105 Å (Polymer Laboratories) in series. Samples were prepared at 10 mg/mL in DMF and filtered with 0.45 μm PTFE syringe filters prior to autoinjection. DMF with 0.1 % TFA was used as eluent at a flow rate 0.8 mL/min . Empower software was used for data collection and processing, with M_w calibrated against narrow polystyrene standards.

DSC measurements were conducted on TA Instrument Q200. Samples (4-5 mg) were heated under nitrogen from $-10\text{ }^{\circ}\text{C}$ to $150\text{ }^{\circ}\text{C}$ at a heating rate of $10\text{ }^{\circ}\text{C}/\text{min}$ and cooled to $-10\text{ }^{\circ}\text{C}$ at a rate of $10\text{ }^{\circ}\text{C}/\text{min}$ with a two-cycle minimum. TA Instruments Universal Analysis 2000 software was used for data analysis.

4.8.1. References

1. Tian, L.; Yam, L.; Zhou, N.; Tat, H.; Urich, K. E. *Macromolecules* **2004**, *37*, 538.

5. FUTURE WORK SUGGESTIONS

In addition to continuing the work outlined in the Chapter 4, many future avenues can be investigated for the research presented herein. The antibacterial work represents a novel area that will benefit from further studies. As demonstrated in Chapter 3, both charge location and hydrophobic-to-charge ratio influence the antimicrobial activity of biscationic tartaric acid-based amphiphiles. When screening these compounds against a broader spectrum of bacteria (Appendix, Section 4.3), two gemini-like compounds – **G7** and **G9** – exhibited potent bioactivity against clinically relevant pathogens. To understand what chemical features influenced this activity and potentially enhance these gemini-like amphiphiles' bioactivity, a series of systematic chemical modifications can be investigated.

While **G7** and **G9** exhibit promising antimicrobial activity, a more hydrophobic analog, **G11**, exhibits no activity. This finding indicates that gemini-like amphiphiles' relative hydrophobicity and/or aliphatic chain lengths modulate bioactivity. To determine whether there is an optimal influence of hydrophobic chain length on antibacterial activity, gemini-like amphiphiles with shorter aliphatic chains can be investigated, generating amphiphiles such as **G3** and **G5**, which would contain 3 and 5 methylene units within their acyl chains, respectively (Figure 5.1). If necessary, chains containing even number of methylenes can also be explored to determine the optimal hydrophobic domain.

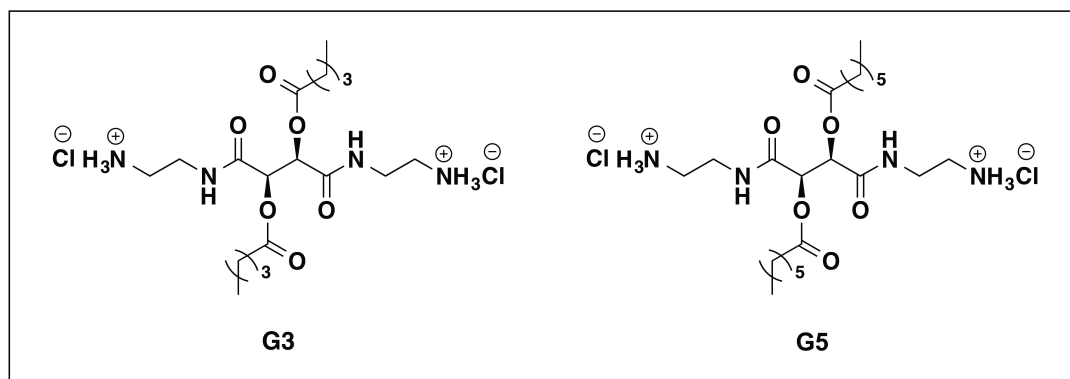


Figure 5.1. Chemical structures of two potential gemini-like amphiphiles possessing shorter aliphatic arms

In addition to modifying gemini-like amphiphiles' hydrophobic domain, different cationic charge structures can be investigated. Chapter 3 demonstrated that gemini-like amphiphiles interact with anionic biomimetic vesicles via electrostatic interactions, indicating the importance of charge in antibacterial activity and the significance of gemini-like amphiphiles' cationic moieties. By changing these compounds' primary amine moieties to a variety of secondary, tertiary, quaternary, and/or guanidinylated amines (Figure 5.2), gemini-like amphiphiles' bioactivity can be further tuned and an understanding of charge structure obtained. These modifications may include linear, cyclic, and aromatic amine groups. While these modifications have been presented in the context of **G7** and **G9**, similar changes in charge structure can be investigated for **B11**, the most potent bola-like amphiphile.

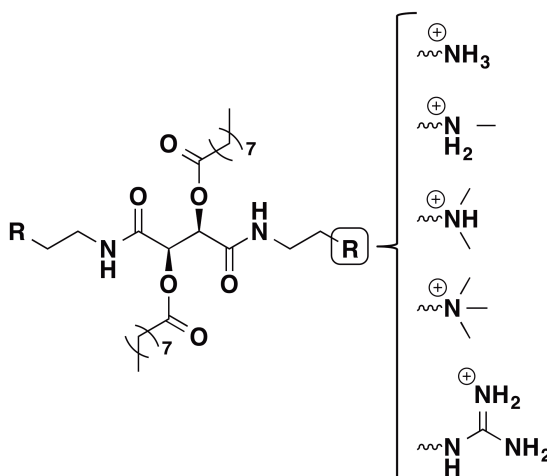


Figure 5.2. Depiction of different amine moieties that can be investigated, using **G7**'s amphiphile structure as an example; Counterions (not shown) will depend on the synthetic methodologies used to synthesize the final structure

While these modifications will provide insight as to what structural elements yield the most potent antimicrobials, future work can also focus on identifying the potential applications of these compounds. Given **G7** and **G9**'s biocompatibility at therapeutic levels, these compounds could be investigated in different antibiotic applications, whether administered alone or as an additive to existing drugs. Research has indicated that synergies often exist between commercial drugs and cationic amphiphiles, as amphiphiles will weaken the bacterial membrane and promote interaction between drug and bacteria. Therefore, *in vitro* studies could investigate whether such synergies exist.^{1,2}

In addition to using the amphiphiles as antibiotics, these compounds can be investigated for topical applications, as antibacterial soap additives and topical treatments, or as coatings, as medical device coatings and hospital surface




coatings. Depending on the particular application, different studies can be conducted to assess amphiphile potential. For soap applications, amphiphiles' foamability may be explored, whereas for topical treatment applications, amphiphiles' transdermal diffusion may be investigated. For coating applications, studies may investigate amphiphiles ability to form films on different implant materials or their miscibility with commercial paints. The variety of applications for such cationic amphiphiles, in conjunction with the broad array of chemical modifications that can be used to tune amphiphile properties, highlight the relevance and potential of bola- and gemini-like amphiphiles.

5.1. References

1. Park, S. C.; Park, Y.; Hahm, K. S. *International Journal of Molecular Sciences* **2011**, *12*, 5971.
2. Lavery, G.; Gorman, S. P.; Gilmore, B. F. *International Journal of Molecular Sciences* **2011**, *12*, 6566.

6. COPYRIGHT PERMISSION

6.1. Biomacromolecules

				Home	Create Account	Help
 ACS Publications <small>Most Trusted. Most Cited. Most Read.</small>		Title:	Impact of Hydrophobic Chain Composition on Amphiphilic Macromolecule Antiatherogenic Bioactivity			
		Author:	Allison Faig, Latrisha K. Petersen, Prabhas V. Moghe, et al			
		Publication:	Biomacromolecules			
		Publisher:	American Chemical Society			
		Date:	Sep 1, 2014			
Copyright © 2014, American Chemical Society						

[LOGIN](#)

If you're a **copyright.com user**, you can login to RightsLink using your copyright.com credentials. Already a **RightsLink user** or want to [learn more?](#)

PERMISSION/LICENSE IS GRANTED FOR YOUR ORDER AT NO CHARGE

This type of permission/license, instead of the standard Terms & Conditions, is sent to you because no fee is being charged for your order. Please note the following:

- Permission is granted for your request in both print and electronic formats, and translations.
- If figures and/or tables were requested, they may be adapted or used in part.
- Please print this page for your records and send a copy of it to your publisher/graduate school.
- Appropriate credit for the requested material should be given as follows: "Reprinted (adapted) with permission from (COMPLETE REFERENCE CITATION). Copyright (YEAR) American Chemical Society." Insert appropriate information in place of the capitalized words.
- One-time permission is granted only for the use specified in your request. No additional uses are granted (such as derivative works or other editions). For any other uses, please submit a new request.

[BACK](#)
[CLOSE WINDOW](#)